2016

Green cooperative spectrum sensing and scheduling in heterogeneous cognitive radio networks

Abdulkadir Celik
Iowa State University

Green cooperative spectrum sensing and scheduling in heterogeneous cognitive radio networks

by

Abdulkadir Celik

A dissertation submitted to the graduate faculty

in partial fulfillment of the requirements for the degree of

DOCTOR OF PHILOSOPHY

Co-majors: Electrical Engineering; Computer Engineering

Program of Study Committee:

Ahmed E. Kamal, Major Professor

Morris Chang

Sang W. Kim

Daji Qiao

Zhengdao Wang

Iowa State University

Ames, Iowa

2016

TABLE OF CONTENTS

LIST OF TABLES vi

LIST OF FIGURES vii

LIST OF ABBREVIATIONS x

LIST OF NOTATIONS xiii

ABSTRACT xix

1. INTRODUCTION 1

1.1 Cognitive Radio Networks: Motivation 1

1.1.1 Spectrum Efficiency 2

1.1.2 Energy Efficiency 6

1.1.3 Energy Harvesting 7

1.2 Main Contributions 10

1.3 Thesis Organization 13

2. BACKGROUND ON SPECTRUM SENSING 15

2.1 Sensing Regulations 15

2.2 Sensing Challenges 16

2.3 Local Spectrum Sensing 17

2.3.1 General Signal Model 18

2.3.2 Energy Detector (ED) 19

2.3.3 Feature Detector (FD) 21

2.3.4 Other Techniques . . . 22
2.3.5 Summary . . . 24
2.4 Cooperative Spectrum Sensing (CSS) . . . 25
2.4.1 Categorization of CSS . . . 25
2.4.2 Data Fusion Methods . . . 27
2.4.3 Chapter Summary . . . 29

3. MULTI-OBJECTIVE CLUSTERING FOR MULTI-CHANNEL CSS 30

3.1 Overview . . . 30
3.1.1 Chapter Contributions and Novelty . . . 31
3.1.2 Chapter Organization . . . 33
3.2 Related Work . . . 33
3.3 Cluster Head Assignment and multihop Path Selection . . . 35
3.3.1 Cluster Topology and Path Characterization . . . 36
3.3.2 The Best Cluster Head Selection . . . 38
3.4 Multi-Objective Clustering Optimization . . . 38
3.4.1 Micro Perspective: Intra-Cluster Optimization . . . 38
3.4.2 Macro Perspective: Inter-Cluster Optimization . . . 45
3.5 Results and Analysis . . . 50
3.5.1 Cluster Head Selection . . . 50
3.5.2 CSS with Hard Decision Fusion . . . 52
3.5.3 CSS with Soft Decision Fusion . . . 55
3.5.4 Multi-Objective Clustering Optimization . . . 57
3.6 Chapter Summary . . . 59

4. ENERGY & SPECTRUM EFFICIENT CSS SCHEDULING 61

4.1 Overview . . . 61
4.1.1 Chapter Contributions and Novelty . . . 62
4.1.2 Chapter Organization . . . 62
4.2 Related Work . . . 63

4.3 System Model . . . 64
4.4 CSS model . . . 66
4.4.1 Heterogeneous Mode . . . 66
4.4.2 Homogeneous Mode . . . 67
4.5 CSS Scheduling Optimization . . . 67
4.5.1 Energy and Spectrum Efficiency . . . 68
4.5.2 Problem Formulation . . . 70
4.6 Energy & Spectrum Efficient Heuristics . . . 74
4.6.1 Prioritized Ordering Heuristic . . . 75
4.6.2 Scheduling and Assignment Heuristic . . . 76
4.7 Results and Analysis . . . 77
4.7.1 Relationship among Cluster Size, Energy, $P_f^\star$, and $P_d^\star$ . . . 77
4.7.2 Comparison Between Optimal and Heuristic Solutions . . . 78
4.7.3 Numerical Results for SAH . . . 81
4.8 Chapter Summary . . . 83

5. FULL-DUPLEX HYBRID ENERGY HARVESTING CSS **84**

5.1 Overview . . . 84
5.1.1 Chapter Contributions and Novelty . . . 86
5.1.2 Chapter Organization . . . 87
5.2 Related Work . . . 87
5.3 System Model . . . 89
5.3.1 Time-slotted Operation for Half-Duplex System . . . 92
5.3.2 Time-slotted Operation for Full-Duplex Systems . . . 92
5.4 CSS Model . . . 92
5.5 Energy State Evolution and Myopic Policy Optimization . . . 94
5.6 Results and Analysis . . . 99
5.7 Chapter Summary . . . 102

6. CONCLUSIONS AND FUTURE WORK **104**

6.1 Conclusions and Summary of Contributions 104

6.2 Future Work 107

A. CHAPTER 3 PROOFS **109**

A.1 Convexity Analysis of Hard Decision Case 109

A.1.1 Concavity / convexity of $P^d_{m,n}(S^n_m, \varepsilon^n_m, \rho^n_m)$ / $P^f_{m,n}(S^n_m, \varepsilon^n_m)$ 110

A.1.2 Log-concavity of $Q^d_m(\tilde{P}^d_{m,n})$ and $Q^f_m(\tilde{P}^f_{m,n})$ 111

B. CHAPTER 4 PROOFS **114**

B.1 Convexity Analysis of CSSS 114

B.2 Monotonicity and Convexity Analysis of η 115

BIBLIOGRAPHY **117**

LIST OF TABLES

Table 3.1 A random chromosome representation for solution **s** 50

Table 3.2 Default parameters used for obtaining results 50

Table 4.1 Default parameters used for obtaining results 78

Table 5.1 Energy States at the beginning of timeslot t, B_n^t. 96

Table 5.2 Default parameters used for obtaining results 100

LIST OF FIGURES

Figure 1.1 Demonstration of spectrum hole in the dimensions of power, time, and frequency. 3

Figure 2.1 Demonstration of channel impairments: hidden terminal, multipath fading, shadowing, and receiver uncertainty 17

Figure 2.2 Categorization of CSS: (a) centralized, (b) distributed, and (c) relay-assisted. 26

Figure 3.1 Demonstration of a large scale CRN with $M = 9$ PCs and $N = 90$ SUs. SUs assigned to a cluster have a diamond shape with the color of the PU which is sensed by the cluster. The cluster heads are shown in hexagonal shapes. An example of the multihop reporting is also illustrated for cluster 2. 30

Figure 3.2 Multihop Reporting of SU n within cluster m 36

Figure 3.3 Non-dominated Sorting Genetic Algorithm-II procedure 48

Figure 3.4 Comparison between singlehop and multihop approaches 51

Figure 3.5 A simple heterogeneous cluster instance to compare traditional and proposed HDF-based CSS. 52

Figure 3.6 Total error rate vs different voting rules and cluster sizes 53

Figure 3.7 Comparison of energy loss caused from traditional and proposed HDF-based schemes using singlehop reporting. 54

Figure 3.8 Comparison of energy loss caused from traditional and proposed HDF-based schemes using proposed multihop reporting and CH selection method. 55

Figure 3.9 Comparison of energy loss caused from traditional and proposed quantized SDF-based schemes using singlehop reporting. 56

Figure 3.10 Comparison of energy loss caused from traditional and proposed quantized SDF-based schemes using proposed multihop reporting and CH selection method. 56

Figure 3.11 MOCO Results for coarse micro perspective. 57

Figure 3.12 Clustered network topology based on results in Figure 3.11. Numbers next to the SUs show the SNR values of SUs for the PU 1. SUs selected to a cluster have a diamond shape with the color of the PU which is sensed by the cluster. The cluster heads of clusters are shown in hexagonal shapes. 58

Figure 3.13 MOCO results for $\mathbf{F}$ and H_1 for different CSS schemes. 59

Figure 3.14 MOCO results for $\mathbf{G}$ and H_2 for different CSS schemes. 60

Figure 4.1 Demonstration of a scheduling timeslot consisting of switching-sensing-reporting cycles and secondary data transmission. 64

Figure 4.2 Total number of samples, $\tilde{P}_f^\star$, and $\tilde{P}_d^\star$ vs. cluster size. 78

Figure 4.3 Comparison between the optimal and heuristic solutions for an average of 30 CRN scenarios with 4 PCs and 8 SUs with SNRs randomly selected between 0 and -30 dB. 79

Figure 4.4 Comparison of optimal and heuristic solutions for an average of 30 CRN scenarios with 8 PCs and 4 SUs with SNRs randomly selected between 0 and -10 dB. 80

Figure 4.5 SAH results over 100 CRN scenarios with $M = 20$, $N = 100$, SNRs range from -30 to 0 dB and $\delta = 8$. Behaviors of η, E and R under different regimes with respect to (a) number of SUs, (b) number of PUs and (c) mean SNRs. 81

Figure 5.1 Full-Duplex Hybrid Energy Harvesting Model 90

Figure 5.2 Time-slot Representation of (a) Half and (b) Full Duplex Energy Harvesting CRs 91

Figure 5.3 Comparison of Binomial and Poisson-Binomial based fusion rules: Optimal timeslots for Binomial (a) and (b) Poisson-Binomial, number of samples, detection and false alarm probabilities for Binomial (c) and (d) Poisson-Binomial. 100

Figure 5.4 Horizontal energy levels and throughput for $\pi_0 = 0.4$. 101

Figure 5.5 Horizontal energy levels and throughput for $\pi_0 = 0.8$ 102

Figure B.1 η with respect to sensing durations a and b along with the contour plot under the three-dimensional shaded surface which shows the polyhedron shaped convex sub-level sets for $\alpha = 5, 10, 15, 20$. 116

LIST OF ABBREVIATIONS

AWGN	Additive White Gaussian Noise
BEP	Bit Error Probability
CBS	Cognitive Base Station
CCC	Common Control Channel
CFD	Cyclostationary Feature Detector
CH	Cluster Head
CLT	Central Limit Theorem
CP	Cyclic Prefix
CR	Cognitive Radio
CRN	Cognitive Radio Network
CSCG	Circularly Symmetric Complex Gaussian
CSS	Cooperative Spectrum Sensing
CSSS	Cooperative Spectrum Sensing Scheduling
DC	Direct Current
DSA	Dynamic Spectrum Access
EA	Evolutionary Algorithm
ED	Energy Detector
EE	Energy Efficient
EE-CRN	Energy Efficient Cognitive Radio Network
EE-CSS	Energy Efficient Cooperative Spectrum Sensing
EEH	Energy Efficient and Energy Harvesting

EEH-CRN	Energy Efficient and Energy Harvesting CRN
EEH-CSS	Energy Efficient and Energy Harvesting CSS
EH	Energy Harvesting
EH-CRN	Energy Harvesting Cognitive Radio Network
EH-CSS	Energy Harvesting Cooperative Spectrum Sensing
EH-SU	Energy Harvesting Secondary User
ELR	Energy Limited Regime
ESLR	Energy & Spectrum Limited Regime
FC	Fusion Center
FCC	Federal Communications Commission
FD	Feature Detector
FDS	Full-Duplex System
FSST	Fixed Sample Size Test
HD-GP	Hard Decision based General Problem
HDF	Hard Decision Fusion
HDS	Half-Duplex System
ICT	Information and Communications Technologies
IoT	Internet of Things
LLP	Lower Level Problem
LLR	Log-Likelihood Ratio
LM	Lloyd-Max
LoS	Line of Sight
MINLP	Mixed Integer Non-Linear Programming
MO	Multi-Objective Optimization
MOCO	Multi-Objective Clustering Optimization
MOE	Maximum Output Entropy

MOGA	Multi-Objective Genetic Algorithm
NP	Non-Deterministic Polynomial-Time
NSGA-II	Non-dominated Sorting Genetic Algorithm-II
OFDM	Orthogonal Frequency-Division Modulation
OSA	Opportunistic Spectrum Access
PB	Primary Battery
PC	Primary Channel
POH	Prioritized Ordering Heuristic
POMDP	Partially Observable Markov Decision Process
PSD	Power Spectral Density
PU	Primary User
QoS	Quality of Service
RF	Radio Frequency
SAH	Scheduling and Assignment Heuristic
SB	Secondary Battery
SD-GP	Soft Decision based General Problem
SDF	Soft Decision Fusion
SDR	Software Defined Radio
SIR	Signal-to-Interference-Ratio
SLR	Spectrum Limited Regime
SNR	Signal-to-Noise-Ratio
SSP	Symbol Success Probability
SU	Secondary User
ULP	Upper Level Problem
WSST	Weighted Sample Size Test

LIST OF NOTATIONS

$\in$	Set membership operator
$\cup$	Union operator
$\cap$	Intersection operator
$\times$	Cartesian Product
$\circ$	Schur Product
$\boldsymbol{a} \in \mathbb{D}^M$	$M \times 1$ vector with domain $\mathbb{D}$
$\boldsymbol{A} \in \mathbb{D}^{M \times N}$	$M \times N$ matrix with domain $\mathbb{D}$
$(\cdot)^T$	Transpose
$(\cdot)^H$	Hermitian transpose
$\{\cdot\}^N$	N-tuple Set
$\mathcal{P}[A]$	Probability of event A
$\mathcal{P}[A\|B]$	Conditional probability of event A given event B
$\mathbb{E}[\cdot]$	Expectation
$\mathcal{CN}(\mu, \sigma^2)$	CSCG distribution with mean μ and variance σ^2
χ^2_a	Central chi-squared distribution with a degrees of freedom
$\chi^2_a(b)$	Non-central chi-squared distribution with a degrees of freedom and non-centrality parameter b
!	Factorial
$\lfloor\cdot\rfloor$	Floor function
$\lceil\cdot\rceil$	Ceiling function

$\lvert\cdot\rvert$	Absolute value of a function or cardinality of a set
$\mathbb{I}(\cdot)$	Indicator function
$e^{(\cdot)}$	Exponential function
$\log(\cdot)$	Logarithm
$\min_a(\cdot)$	Minimum of a set or function with respect to a
$\max_a(\cdot)$	Maximum of a set or function with respect to a
$\operatorname{argmin}(\cdot)$	The argument of minimum
$\operatorname{argmax}(\cdot)$	The argument of maximum
$\operatorname{erfc}(\cdot)$	Complementary error function
$\Gamma(\cdot)$	Gamma function
$\Gamma(a,b)$	Incomplete gamma function
$\mathcal{Q}(\cdot)$	Q-function
$\mathcal{Q}_a(b,c)$	Generalized Marcum-Q function
$\mathcal{O}(\cdot)$	Big O notation
M	Number of clusters or PCs with indices $1 \leq m \leq M$
$\mathcal{M}$	Set of scheduled PCs
N	Number of SUs with indices $1 \leq n \leq N$
$\mathcal{N}$	Set of assigned SUs
$\mathcal{H}_m^0$	Binary hypotheses for PU absence on PC m
$\mathcal{H}_m^1$	Binary hypotheses for PU presence on PC m
π_m^0	Apriori probability of being idle for PC m, ie. $\mathcal{P}\left[\mathcal{H}_m^0\right]$
π_m^1	Apriori probability of being busy for PC m, ie. $\mathcal{P}\left[\mathcal{H}_m^1\right]$
r_m^n	Received signal by SU n on PC m
p_m	Transmitted primary signal on PC m
h_m^n	Composite channel gain between SU n and PU m
z_m^n	AWGN noise of SU n on PC m

S_m^n	Number of samples taken by SU n on PC m
$\bar{S}$	Upper bound on S_m^n
ε_m^n	Local detection threshold of SU n on PC m
γ_m^n	SNR of SU n on PC m
$\bar{\gamma}_m^n$	Average SNR of SU n on PC m
T	Timeslot duration
T_c	Cyclic prefix block of OFDM
T_d	Data block of OFDM
ρ_m^n	Auto-correlation coefficient of SU n on PC m
$\mathcal{C}_m$	SU set of cluster m with cardinality C_m
L_m	Number of quantization levels of SUs in CH m
$\ell_{m,n}^j$	j^{th} quantization level of SU n in cluster m on PC m, $1 \leq j \leq L_m$
Λ_m^n	Log-likelihood ratio of SU n on PC m
$\hat{\Lambda}_m^n$	Corresponding quantization level to Λ_m^n
H_m^n	Number of hops between SU n and CH m with indices $1 \leq h \leq H_m^n$
$c_{m,n}^h$	Transmitted codeword in h^{th} hop
$n \rightsquigarrow n'$	An arbitrary multi-hop path from SU n to SU n'
$n \rightarrow n'$	The shortest multi-hop path from SU n to SU n'
$\boldsymbol{T}_h$	Channel transition matrix for h^{th} hop
$\boldsymbol{T}_{n \rightsquigarrow n'}$	End-to-end channel transition matrix for $n \rightsquigarrow n'$
$\boldsymbol{T}_{n \rightarrow n'}$	End-to-end channel transition matrix for $n \rightarrow n'$
$\tilde{\Lambda}_m^n$	Reconstructed quantization level by CH m
$P_{m,n}^f$	Local false alarm probability of SU n on PC m
$P_{m,n}^d$	Local detection probability of SU n on PC m

u_m^n	Local hard decision of SU n on PC m
$\tilde{P}_{m,n}^f$	Received $P_{m,n}^f$ by CH m
$\tilde{P}_{m,n}^d$	Received $P_{m,n}^d$ by CH m
$\tilde{u}_m^n$	Received u_m^n by CH m
$\mathcal{K}_m^{ide}$	Global test statistic of ideal CSS
$\mathcal{K}_m^{hd}$	Global test statistic of HDF-based CSS
$\mathcal{K}_m^{sd}$	Global test statistic of SDF-based CSS
κ_m^{ide}	Global threshold of ideal CSS
κ_m^{hd}	Global threshold of HDF-based CSS
κ_m^{sd}	Global threshold of SDF-based CSS
Q_m^f	Global false alarm probability of CH m
Q_m^d	Global detection probability of CH m
Q_{th}^f	Global spectrum utilization constraint
Q_{th}^d	Global collision constraint
E_m^{ide}	Energy consumption of ideal CSS
E_m^{hd}	Energy consumption of HDF-based CSS
E_m^{sd}	Energy consumption of SDF-base CSS
$\boldsymbol{F} \in \mathbb{R}^M$	Intra-cluster energy minimization objectives
$\boldsymbol{G} \in \mathbb{R}^M$	Intra-cluster throughput maximization objectives
$\boldsymbol{H} \in \mathbb{R}^2$	Inter-cluster energy and throughput fairness objectives
$\boldsymbol{y} \in \{0,1\}^M$	PC scheduling vector with binary elements $y_m \in \{0,1\}$
$\bar{\boldsymbol{y}} \in \{0,1\}^M$	A specific instance of $\boldsymbol{y}$
$\boldsymbol{X} \in \{0,1\}^{M \times N}$	SU↔PC assignment vector with elements $x_m^n \in \{0,1\}$
$\bar{\boldsymbol{X}} \in \{0,1\}^M$	A specific instance of $\boldsymbol{X}$
$\boldsymbol{S} \in \mathbb{R}^{+^{M \times N}}$	Number of samples matrix with positive real elements S_m^n
$\boldsymbol{\mathcal{E}} \in \mathbb{R}^{M \times N}$	Detection threshold matrix with real elements ε_m^n

$\boldsymbol{\Gamma} \in \mathbb{R}^{+^{M \times N}}$	SNR matrix with real elements γ_m^n
$\boldsymbol{P} \in \mathbb{R}^{M \times N}$	BEP matrix with elements $p_m^n \in [0, 1]$
$\boldsymbol{f} \in \mathbb{R}^{M}$	Operating frequency vector of PCs with elements f_m^c
T_s^n	Sum of sensing cycle durations of SU n
T_s	Channel searching stage duration, i.e. $T_s = \max_{n \in \mathcal{N}} T_s^n$
β	Channel switching delay factor
P_{sw}	Channel switching power
E_{SW}	Total channel switching energy cost of assigned SUs
P_r	Power consumed per report
τ_r	Time spent per report
E_r	Energy spent per report
E_R	Total reporting energy cost of assigned SUs
P_s	Power consumed per sample
τ_s	Time spent per sample
E_s	Energy spent per sample
E_S	Total sensing energy cost of assigned SUs
E	Opportunity Cost, ie. $E = E_{SW} + E_S + E_R$
R	Opportunity, ie. the achievable total data rate, R
η	Spectrum & energy efficiency objective, ie. $\eta = E/R$
$\boldsymbol{c_E}$	Sorted PCs wrt. E under the ELR
$\boldsymbol{c_R}$	Sorted PCs wrt. R under the SLR
$\boldsymbol{c_\eta}$	Sorted PCs wrt. η under the ESLR
$\mathcal{S}^\star$	Heuristic solution to the CSSS problem
B_n^1	PB capacity of SU n
B_n^2	SB capacity of SU n
$B_n^{1,t}$	PB storage level of SU n at the beginning of timeslot t

$B_n^{2,t}$	SB storage level of SU n at the beginning of timeslot t
ζ_n^1	PB storing efficiency of SU n
ζ_n^2	SB storing efficiency of SU n
ζ_n^{rf}	RF harvesting efficiency of SU n
ϱ_n	Harvesting Ratio of SU n
Θ_n^{hd}	Maximum time spent for harvesting+sensing in HDS
Θ_n^{fd}	Maximum time spent for harvesting+sensing in FDS
Δ_n^{hd}	Net gained energy during Θ_n^{hd} in HDS
Δ_n^{fd}	Net gained energy during Θ_n^{fd} in FDS
$\Delta_n^{rf,hd}$	Harvested RF energy in HDS
$\Delta_n^{rf,fd}$	Harvested RF energy in FDS
Υ_n	Total harvested energy from renewable source in FDS
R_n^{hd}	Achievable data rate of SU n in HDS
R_n^{fd}	Achievable data rate of SU n in FDS

ABSTRACT

The motivation behind the cognitive radio networks (CRNs) is rooted in scarcity of the radio spectrum and inefficiency of its management to meet the ever increasing high quality of service demands. Furthermore, information and communication technologies have limited and/or expensive energy resources and contribute significantly to the global carbon footprint. To alleviate these issues, energy efficient and energy harvesting (EEH) CRNs can harvest the required energy from ambient renewable sources while collecting the necessary bandwidth by discovering free spectrum for a minimized energy cost. Therefore, EEH-CRNs have potential to achieve *green* communications by enabling spectrum and energy self-sustaining networks. In this thesis, green *cooperative spectrum sensing* (CSS) policies are considered for large scale heterogeneous CRNs which consist of multiple *primary channels* (PCs) and a large number of *secondary users* (SUs) with heterogeneous sensing and reporting channel qualities.

Firstly, a multi-objective clustering optimization (MOCO) problem is formulated from macro and micro perspectives; *Macro perspective* partitions SUs into clusters with the objectives: 1) Intra-cluster energy minimization of each cluster, 2) Intra-cluster throughput maximization of each cluster, and 3) Inter-cluster energy and throughput fairness. A multi-objective genetic algorithm, Non-dominated Sorting Genetic Algorithm-II (NSGA-II), is adopted and demonstrated how to solve the MOCO. *The micro perspective*, on the other hand, works as a sub-procedure on cluster formations given by macro perspective. For the micro perspective, a multihop reporting based CH selection procedure is proposed to find: 1) The best CH which gives the minimum total multi-hop error rate, and 2) the optimal routing paths from SUs to the CHs using *Dijkstra's algorithm*. Using *Poisson-Binomial* distribution, a novel and generalized K-out-of-N voting rule is developed for heterogeneous CRNs to allow SUs to have different levels of local detection performance. Then, a convex optimization framework is established to minimize the intra-cluster energy cost subject to collision and spectrum utilization constraints.

Likewise, instead of a common fixed sample size test, a weighted sample size test is considered for quantized soft decision fusion to obtain a more EE regime under heterogeneity.

Secondly, an energy and spectrum efficient CSS scheduling (CSSS) problem is investigated to minimize the energy cost per achieved data rate subject to collision and spectrum utilization constraints. The total energy cost is calculated as the sum of energy expenditures resulting from *sensing*, *reporting* and *channel switching* operations. Then, a mixed integer non-linear programming problem is formulated to determine: 1) The optimal scheduling subset of a large number of PCs which cannot be sensed at the same time, 2) The SU assignment set for each scheduled PC, and 3) Optimal sensing parameters of SUs on each PC. Thereafter, an equivalent convex framework is developed for specific instances of above combinatorial problem. For the comparison, optimal detection and sensing thresholds are also derived analytically under the homogeneity assumption. Based on these, a prioritized ordering heuristic is developed to order channels under the spectrum, energy and spectrum-energy limited regimes. After that, a scheduling and assignment heuristic is proposed and shown to have a very close performance to the exhaustive optimal solution. Finally, the behavior of the CRN is numerically analyzed under these regimes with respect to different numbers of SUs, PCs and sensing qualities.

Lastly, a single channel energy harvesting CSS scheme is considered with SUs experiencing different energy arrival rates, sensing, and reporting qualities. In order to alleviate the *half-duplex* EH constraint, which precludes from charging and discharging at the same time, and to harvest energy from both renewable sources and ambient radio signals, a *full-duplex hybrid energy harvesting* (EH) model is developed. After formulating the energy state evolution of half and full duplex systems under stochastic energy arrivals, a convex optimization framework is established to jointly obtain the optimal harvesting ratio, sensing duration and detection threshold of each SU to find an optimal myopic EH policy subject to *collision and energy-causality* constraints.

CHAPTER 1. INTRODUCTION

1.1 Cognitive Radio Networks: Motivation

The motivation behind the cognitive radio technology is rooted in the deficiency of the current rigid spectrum management approaches to meet the ever increasing high *quality of service* (QoS) requirements of today's wireless communication systems. Prospective demands of next-generation wireless networks are ambitious and compel the telecommunications systems to support 1000 times heavier data traffic, 100 times less energy consumption per transmitted bit, and 10 times lower round-trip latency [1]. While this data deluge is a natural outcome of the increasing number of mobile devices with data hungry applications and the Internet of Things (IoT), low latency demand is required by the future interactive applications such as "tactile internet", virtual and enhanced reality, and online internet gaming, etc. Bearing in mind that the mobile devices are battery limited and thirty percent of their energy sources are expended by wireless networking modules [2], energy efficiency lend itself to being an inevitable design consideration.

Accordingly, wireless researchers in both academic and industrial communities focus on boosting the achievable data rate per unit of time and per unit of spectrum, and substantially shrinking the induced energy cost at the same time. Nonetheless, such a goal inherently requires revolutionary spectrum and energy efficient solutions, the performance of which are fundamentally limited by accessible radio spectrum and energy resources. Furthermore, it has been shown that two to three percent of the global carbon footprint are generated by the information and communications technologies (ICT) and is expected to grow in the near future [3]. Hence, energy harvesting communication has come into prominence to provide the mankind with a *green* ICT by harnessing the energy from ambient resources (e.g., solar, wind, thermoelectric,

electromagnetic, RF signals, etc.), and thereby establish the basis of energy self-sustained and energy self-maintained communication networks. As a an enabler of spectrum and energy self-sustaining communications, *energy efficient* (EE) and *energy harvesting* (EH) cognitive radio networks (CRNs) will be introduced in an order which exhibits both the relevance and the complexity of the objectives: *Spectrum efficiency*, *energy efficiency*, and *energy harvesting*.

1.1.1 Spectrum Efficiency

The radio spectrum is a limited natural resource and its accessibility is directly regulated and licensed by the governmental institutions such as the Federal Communications Commission (FCC) in the United States. With the conventional spectrum allocation policies, radio spectrum is exclusively allocated to operators for long time periods and each operator is restricted to communicate within its licensed bands. However, the studies and measurements conducted by the Spectrum-Policy Task Force of the FCC have revealed the fact that efficiency of the spectrum access policies is a more significant problem than the spectrum scarcity since the spatio-temporal spectrum utilization of the licensed bands ranges from 15% to 85% [4]. The limited availability and under-utilization of the radio frequency (RF) spectrum has therefore led the FCC to propose the opening of licensed bands to the public. Unlike current *static spectrum access* policies, this necessitates a *dynamic spectrum access* (DSA) strategy where unlicensed users, a.k.a *secondary users* (SUs), utilize the incumbent licensees' spectrum insomuch that they do not cause performance degradation for the licensed users, a.k.a *primary users* (PUs) [5]. Thus, primary and secondary networks refer to the networks comprised of the set of transceiving PUs and SUs, respectively. Based on the hierarchical relationship between the primary and secondary networks, there are two essential DSA approaches: *Spectrum underlay* and *spectrum overlay*.

The spectrum underlay approach enforces rigorous restrictions on the power spectral density of SUs to make them operate under a noise floor in order to protect PUs from the potential harm of the secondary network. Therefore, SUs operating in the spectrum underlay approach endeavor to achieve high data rates by spreading the transmitted signals over a wide frequency band (UWB). However, the stringent transmission power levels restrain the spectrum underlay

approach to very short ranges [6]. In contrast, the spectrum overlay approach, which is also known as the *opportunistic spectrum access* (OSA), allows SUs to access licensed spectra in a non-intrusive and opportunistic manner such that SUs detect and utilize unused licensed bands at a given particular time and location, a.k.a *spectrum holes* or *white space* as depicted in Figure 1.1 where PU activity is shown in power, frequency and time axes. A SU should detect, utilize and vacate the spectrum holes as shown with arrows in Figure 1.1. To protect the PUs from secondary network interference, SUs are required to sense the primary channels (PCs) periodically and evacuate the channel if a PU emerge, that brings in the periodic nature of sensing and the commonly made assumption of time-slotted operation of SUs.

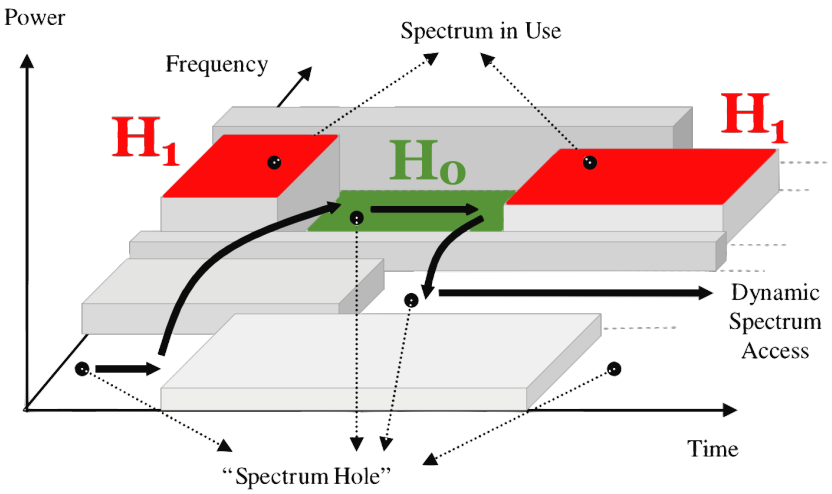

Figure 1.1: Demonstration of spectrum hole in the dimensions of power, time, and frequency [5].

As a key technology, *Cognitive radios* (CRs) [7], [8], have been introduced to discover and utilize the spectrum holes. As an inclusive of software defined radios (SDRs) and an exclusive of the traditional radios, distinctive features of CRs can be grouped into two main aspects: *cognitive capability* and *reconfigurability*. Cognition is the capability of learning how to interact with the surrounding radio environment by gathering information via spectrum sensing. On the other hand, reconfigurability is the ability of changing the radio parameters (e.g., operating frequency, modulation type, transmission power, etc.) to take intelligent actions according to

the perceived cognition through the sensing and learning process in order to achieve the optimal performance [9].

Spectrum sensing is one of the most critical CRN functions since the performance of spectrum hole detection directly affects the primary and secondary network performance. Denoting the absence and the presence of the PU activity by the binary hypotheses $\mathcal{H}_0$ and $\mathcal{H}_1$, respectively, detection performance is subject to two types of error probabilities: false alarm ($P_f = \mathcal{P}[\mathcal{H}_1|\mathcal{H}_0]$) and misdetection ($P_m = \mathcal{P}[\mathcal{H}_0|\mathcal{H}_1]$). While higher P_f results in reduced spectral efficiency, higher P_m causes more interference with the primary network. Since the detection performance of individual SUs is severely affected by propagation channel impairments and hardware limitations (e.g., path loss, shadowing, multipath fading, hidden terminal problem, noise estimation errors, and receiver uncertainty etc.) *cooperative spectrum sensing* (CSS) has been proposed to achieve a *cooperative gain* by taking advantage of the spatial and multi-user diversity [10], [11]. Cooperative gain can be defined as the acquired more reliable detection probability to protect primary network from the SU interference and less false alarm probability to utilize the spectrum more efficiently. Unfortunately, cooperative gain is not free of cooperation overhead which can be defined as any extra design complexity, energy consumption, sensing duration, and communication among SUs induced from cooperation compared to the individual spectrum sensing [12].

CSS can be divided into two categories based on data sharing methods within the network: *centralized* and *distributed*. In the centralized CSS, SUs report sensing results over a dedicated *common control channel* (CCC) to a *fusion center* (FC) which combines and diffuses the final decisions back to SUs via the CCC. Unlike the centralized CSS, SUs communicate among themselves over the CCC and conclude in a unified decision under the distributed CSS. Furthermore, CSS can be classified into two subcategories based on the fusion methods: *soft decision fusion* (SDF) and *hard decision fusion* (HDF). In the SDF, SUs share all observations data which are then fused with a signal combining technique while in HDF, SUs share their binary decisions which are combined by a decision fusion rule. Albeit SDF's superior performance, sharing that massive amount of observation data results in high energy consumption and communication overhead which cannot be sustained by SUs with limited energy resources and by the CCC due

to limited bandwidth availability. In this respect, *quantized SDF* has become prominent as it does not only have a reasonable communication overhead but also have a satisfactory detection performance [13].

In the most primitive sense, the CSS schemes can be divided into the following tasks:

1. ***Spectrum Sensing Scheduling*** appoints the best set of PCs to be sensed in order to maximize the utilization of the secondary network based on the statistical information of the PU activity obtained from past observations.

2. ***Spectrum Sensing and SU Assignment*** attains the optimal assignment of SUs to sense the scheduled PCs and determines the optimal sensing parameters for each of them by taking the sensing and reporting quality of different SUs on scheduled PCs into account. Based on the local decision reports of cooperating SUs, it also selects the optimal fusion rule and makes decisions about the PC states.

3. ***Spectrum Access and Sharing*** decides on the appropriate spectrum access protocols and the optimal resource allocation policies among the SUs if the global decision is in favor of the PU absence.

4. ***Spectrum Handoff and Mobility*** enforces SUs to evacuate the occupied PCs in the case of a decision in favor of the PU presence. If it is necessary to find more spectrum holes to sustain the QoS requirements of the secondary network, it refers to task 1 to find a new set of PCs to sense for maintaining seamless communication.

However, considering certain objectives and constraints, carrying out the tasks 1, 2, and 4 is non-trivial due to the combinatorial nature of the channel scheduling and SU assignment problems, and requires high computational power and time complexity even for moderate size primary and secondary networks. Moreover, for secondary networks with large size of SUs spreaded over a large geographical area, treating all SUs as a single cooperating entity may incur high CCC bandwidth, energy and delay overhead. Therefore, grouping SUs into clusters was shown to be an effective method to alleviate the communication range and energy overhead problems [14]. Accordingly, a cluster-based CSS scheme should take care of followings: 1)

Formation of SU clusters to minimize/maximize a certain objective, 2) Determination of the optimal sensing and reporting parameters of cluster members, 3) Selection of the best *cluster head* (CH) which undertakes the role of the FC to coordinate cluster members and make global decisions, and 4) Scheduling of PCs to be sensed subject to necessary primary network protection regulations.

1.1.2 Energy Efficiency

To fulfill the appeal of emerging technologies for higher data rates, early research attempts in CRNs have mainly focused on enhancing the spectral efficiency by maximizing the discovered free spectrum without considering the energy restrictions of the CRs. However, a substantial proportion of mobile and wireless network devices have limited energy resources. Indeed, considering the fact that 30% of the energy expenditure of mobile devices is caused by wireless networking and computing hardware [15], EE-CRNs can play a vital role to provide portable devices with more spectrum for less energy consumption.

Nevertheless, achieving an EE-CRN setting is a formidable task because of the following practical concerns: 1) Hierarchical structure between primary and secondary networks with their competing demands, 2) Negative impacts of imperfect sensing and reporting schemes, 3) Ramifications of tackling the SUs' heterogeneous sensing and reporting qualities, 4) QoS thresholds and fairness requirement of SUs, and 5) Network architecture complexity and cooperation overhead to acquire a satisfactory solution which addresses these multifaceted technical challenges.

For instance, high QoS benefit for low energy cost expectation of the secondary network is mainly constrained by regulations to protect the PUs from the SU interference. Hence, there is need for a CSS scheme which maximizes the secondary network utilization by minimizing the false alarm rate while providing mandatory protection levels by keeping the misdetection rate below a certain threshold. Since the signal-to-noise ratios (SNRs) of SUs on the PCs are mostly given parameters and out of control of the network management, increasing the number of samples (i.e., increasing the sensing duration) is the only practical way to obtain targeted false alarm and misdetection rates. However, increasing the number of samples incurs more

sensing energy consumption and less available time to utilize the PCs as a result of the periodic nature of sensing.

In a CSS scenario with imperfect reporting, CCC unreliability will naturally impose relatively superior local detection performance on SUs to compensate the reporting loss in order to reach required global detection and false alarm rates. It is worth mentioning that such a compensation is still necessary to mitigate the loss caused by the sub-optimality of the fusion rule exploited at the FC. If SUs have heterogeneous sensing and reporting channel conditions, obtaining an optimal setting requires a finer level of design attention. To illustrate, enforcing SUs with non-identical SNRs and reporting error probabilities to have identical local false alarm and misdetection probabilities may not always yield an optimal outcome in terms of energy expenditure and system throughput. In a cluster-based CSS, on the other hand, forming SU clusters in a fair manner falls into a multi-objective optimization problem since each cluster and its members would like to get enough throughput to get required QoS for every unit of energy they spent within the CSS.

In case of a primary network with a non-contiguous spectrum, scheduling the PCs with consideration of induced energy cost and gained utilization also adds an extra dimension to the aforementioned issues. That is, scheduling a wide and fragmented (i.e., non-contiguous) set of PCs should also consider the effects of time and energy consumption in radio reconfiguration. This is also known as the *channel switching energy* cost whose effect on energy and throughput efficiency needs to be considered especially when the initial operating frequency is spectrally distant from the scheduled PC's frequency. Another energy expenditure factor related to CSS scheduling is the *reporting energy cost* which is surely non-negligible if the CSS operates on an SDF or quantized SDF basis due to the amount of data required to be transmitted to the FC.

1.1.3 Energy Harvesting

Information and communications technologies have been contributing to 2%-3% of the global carbon footprint [16], which is very close to the airline industry, and it is expected to increase annually at a rate of 4% until 2020 [3]. As a revolutionary way of achieving green communication networks, harvesting energy from alternative natural resources (e.g., solar, vi-

brational, electromagnetic, thermoelectric, RF signals, etc.) and converting it to electrical energy to power communication devices has led the EE communications system design into a paradigm shift. Unlike the traditional grid-powered and non-rechargeable and/or battery-powered wireless devices, EH devices are energy self-sustained components which are key to enable energy self-sustained and self-maintained communication networks. While this approach yields a more environmentally friendly ICT by reducing the carbon footprint, it establishes the basis of untethered wireless networks by allowing the deployment of energy self-sufficient communication nodes within unreachable places (e.g., remote rural areas, the human body, structure components, etc.) [17].

In addition to the renewable energy resources which may not be always accessible, ambient RF signals offers another promising energy source with the ability of being available regardless of time and location. A CR equipped with an RF-to-DC converter circuit can especially benefit from ambient RF signals in case of a busy PC discovery, thus, it does not have to take the busy PCs out of consideration any more. If such an SU needs extra energy for its future purposes and do not have a back-loaded data to transmit, it can wisely prefer to stay in busy PCs and scavenge the ambient primary signals. However, the amount of harvested energy from ambient RF signal heavily depends on the wavelength and the received power strength [18]. Another paramount limitation on RF energy harvesting is the sensitivity of the RF-to-DC converter circuitry. Even though today's radios can make information reception with -60 dBm power sensitivity, RF energy harvesters can operate with signal powers as low as -10 dBm [19].

In this context, communication society recently has focused on EH communications in addition to the goal of achieving more spectrum for less energy consumption. For a given amount of energy, conventional EE-CRNs aims to minimize the total sensing energy consumption subject to the fundamental *collision constraint* as mentioned earlier. In EH systems, on the other hand, the energy needed for sensing and data transmission arrives intermittently and in random magnitudes as a result of the random nature of energy harvesting sources. Then, the ultimate goal of energy energy efficient and energy harvesting (EEH) CRNs would be not only to minimize the overall energy consumption but to also maintain sensing and transmitting tasks under random and intermittent energy arrivals. Such a goal dictates an extra fundamental limit

on the capacity of traditional CRNs: *energy-causality constraint* which states that the energy harvested by a time instant must be greater than or equal to the consumed energy until that time instant [17]. Consequently, these two constraints constitute the fundamental limitations on EEH-CRNs.

To store harvested energy, super-capacitors are mostly preferred due to their high power density, good recycling ability, and near perfect storing efficiency. Albeit their favorable features, super-capacitors are *half-duplex* EH constrained which prevents SUs from charging and discharging simultaneously [20]. Due to the time-slotted operation of CRNs, such a restriction directly introduces another trade-off factor since available time now must be apportioned among three time demanding factors: harvesting, sensing-switching-reporting, and secondary data transmission. Even without half-duplex constraint, this apportion still applies to solely RF-empowered SUs since a single antenna cannot be used for harvesting, sensing and transmitting simultaneously. In short, all previously argued trade-offs and technical challenges are required to be reconsidered to transform EE-CRNs into EEH-CRNs.

In EH-CSS schemes, energy states of SUs evolve over time such that energy state in the next timeslot depends on the energy state and the action taken in the current timeslot. At a given time instant, SUs are required to take necessary actions contingent upon the current stored energy level, the stochastic energy arrival process, and the amount of data to be transmitted. For instance, an SU may decide on being in a dormant and/or active states. While an SU prefers to be in harvesting mode and store energy for future purposes, it favors to be in the spectrum access mode to sense and transmit in the active state. A mixed strategy may be an alternative action, where SUs harvest, sense and transmit in a timeslot. From an EEH perspective, to minimize the energy consumption subject to the collision and energy causality constraints, optimal harvesting and sensing ratio along with the optimal detection threshold are required to be calculated for each SU according to their distinctive sensing and reporting channel conditions. With solely RF-empowered SUs, EEH-CSS scheduling task has especially a higher design complexity. Besides the set of PCs scheduled for sensing to obtain more spectrum, SUs may need a set of busy PCs for RF energy harvesting. Such a set of channels

would especially be beneficial to be exploited in harvesting mode and this set can be formed based on statistical properties of PC activity and received power strength.

All aforementioned technical challenges and tradeoffs are crucial to develop an EEH-CRN which is capable of self-sustaining its spectrum and energy demands in an opportunistic and non-intrusive manner such that it keeps its harm to the primary network and the environment at a negligible level while self-maintaining the untethered communication by maximizing its operation life via energy-efficient measures. Therefore, this thesis aims to achieve green communications by developing the EHE-CRNs with the consideration of aforementioned practical concerns and design challenges.

1.2 Main Contributions

All previously addressed fundamental trade-offs are inseparably interweaved and have inevitably significant impacts on the CSS performance. In the sequel, the main contributions of this dissertation to the insight and design of green cooperative spectrum sensing and scheduling are delineated.

1. In Chapter 3, we address EE-CSS policies for large scale CRNs which consist of multiple PCs and large number of SUs with heterogeneous reporting and sensing qualities on different PCs. After developing a general CH selection procedure tat is applicable for both HDF and SDF schemes, we approach multi-objective and fair clustering problem from micro and macro perspectives as follows:

    1.1. Similar to sensing channels, the CCC is also subject to the adherse propagation conditions which may result in an imperfect reporting environment. Instead of using a commonly studied single-hop reporting technique in which cluster members directly report to the CHs, employing multihop path diversity might result in a superior reporting performance in terms of robustness, delay and communication range. Results of [13] have clearly revealed the fact that the affordable *bit error probability* (BEP) of the CCC is blocked by a wall at which required SNR to obtain target detection performance goes to infinity. Thus, we propose a procedure to select

the CH which yields: 1) The best CH which gives the minimum total multihop error rate, and 2) the optimal reporting routing path from SUs to the CH using *Dijkstra's algorithm*. Obtained results have shown that the multihop diversity has a superior robust reporting and a potential to alleviate the BEP wall phenomenon.

1.2. For the micro perspective, we consider clusters as a group of SUs dedicated to sense a single PC. Although most of the works in the literature traditionally consider the cooperation of SUs with identical/homogeneous sensing quality metrics (e.g, SNR), this approach would not yield an optimal cooperation cost in a heterogeneous environment where SUs experience various SNRs on different PCs. By enforcing each SU to report with identical detection and false alarm probabilities at the CH side, traditional global summary statistic of CH follows *Binomial* distribution. Nevertheless, in a heterogeneous cluster, SUs with relatively low SNRs must sense longer to conform to the target reported detection performance. Consequently, avoiding the heterogeneity returns a higher energy expenditure and a lower throughput since the CH must wait for the slowest SU with the lowest SNR to feed the final decision back to the cluster members. In light of these issues, we propose a novel EE-CSS scheme which tolerates SUs to report with different probabilities, where the global summary statistic of CH follows *Poisson-Binomial* distribution. We further develop a convex framework which jointly optimizes detection threshold and sensing duration of each SU to minimize the total energy consumption of the cluster subject to global PU protection and spectrum utilization constraints. Numerical results has clearly demonstrated that the taking the heterogeneity into account yield a lower total energy consumption and higher time left for secondary transmission.

1.3. The negative impact of treating non-identical SUs equally, on the other hand, does also have significant disadvantages in the SDF based CSS where each SU quantize the local observations and report corresponding quantization level in a binary sequence. Conventionally determining a fixed sensing duration for each SU, which is a.k.a. fixed sample size test (FSST), may not always result in an EE cooperation. After deriving the distributions of the test statistic over an imperfect multihop reporting

path, we propose a weighted sample size test (WSST) to obtain a more EE regime by assigning sensing duration of SUs proportional to their SNRs. Results demonstrated the achieved performance enhancement by WSST is significant.

1.4. If the spectrum utilization and energy consumption are defined as currency and commodity, respectively, an ultimate design goal of the macro perspective would be clustering SUs in such a way that commodity per currency is maximized. Additionally, fairness is another design metric to be considered since an SU would naturally like to get a fair benefit while spending energy for others. Therefore, we formulate the multi-objective clustering optimization (MOCO) problem which fairly minimizes the clusters' energy consumption while fairly maximizing the achievable throughput. Then, we adopt and demonstrate how to use the Non-dominated Sorting Genetic Algorithm-II (NSGA-II) to solve MOCO.

2. In Chapter 4, CSSS of heterogeneous CRNs are considered such that there exists PCs with different characteristics and SUs with various sensing and reporting qualities for different PCs. Unlike the Chapter 3, only a subset of the PCs are scheduled and sensed by SUs which can join more than one cluster at a time.

2.1. The energy and spectrum efficiency are coupled as a single objective such that the energy spent per achieved data rate is minimized subject to global detection and false alarm constraints to protect PUs from SU interference and ensure a certain spectrum utilization, respectively. Accordingly, assuming SUs have different reporting error rates for different PCs, a mixed integer non-linear programming (MINLP) problem is formulated to determine: 1) the optimal subset of PCs to be scheduled for sensing, 2) the SU assignment set for each scheduled PC, and 3) sensing durations and detection thresholds of each SU on PCs it is assigned to sense. Moreover, we formulate the optimal sensing order to minimize the channel switching latency which is a linear function of the total frequency distance [21]-[22].

2.2. For specific instances of above combinatorial problem, an equivalent convex framework is developed for heterogeneous CRNs. For comparison, optimal detection and

sensing thresholds are also derived for homogeneity assumption as a suboptimal solution to the heterogeneous case.

2.3. Exploiting the convex framework in 2.2, we develop an prioritized ordering heuristic to order channels under spectrum, energy and spectrum-energy limited regimes. After that, a scheduling and assignment heuristic is proposed and shown to have a very close performance to exhaustive optimal solution. The behavior of the CRN is then numerically studied under these regimes with respect to different number of SUs, PCs and SNR distributions.

3. In Chapter 5, we focus on a single cluster where heterogeneous SUs sense a certain PC.

3.1. A *full-duplex hybrid* EH-CR module is first proposed to mitigate the half-duplex constraint by exploiting two different energy storage and harvest energy from both renewable sources, e.g. solar, and ambient RF signals.

3.2. After demonstrating the differences in the timeslotted operation of SUs due to their heterogeneous sensing and reporting channel characteristics, we develop the energy state evolution of both systems under stochastic energy arrivals. To find an optimal myopic EH policy, a convex optimization frame work is then developed to jointly obtain the optimal harvesting ratio, sensing duration and detection threshold of each SU which maximizes the sum of the achievable throughput of cooperating SUs during the current timeslot subject to *collision and energy-causality* constraints. Obtained results clearly demonstrated that the combination of the Poisson-Binomially distributed HDF, which assigns the SUs different local detection and false alarm probabilities based on their sensing and reporting channel qualities, and the proposed full-duplex EH system provide the best result in terms of sensing energy cost reduction, achievable throughput maximization and harvested energy accumulation.

1.3 Thesis Organization

The rest of the thesis is organized as follows: In Chapter 2, the fundamental elements of spectrum sensing is provided. The sensing regulations and its practical challenges are first

detailed in Section 2.1 and Section 2.2. Thereafter, common spectrum sensing techniques is followed by a comparative summary in Section 2.3. Based on these, proposed cooperation schemes are discussed in Section 2.4.

Right after a brief introduction to Chapter 3, Section 3.2 presents the related work in the literature. Section 3.3 describes the generalized best CH selection procedure for single-bit hard and quantized multi-bit soft decision fusion CSS schemes. Then, Sections 3.4.1.1, 3.4.1.2, and 3.4.1.3 give the details of ideal, HDF-based, and quantized SDF-based CSS schemes, respectively. Section 3.4.2.1 provides a background in multi-objective evolutionary algorithms and Section 3.4.2.2 formulates the MOCO problem and explains its solution using NSGA-II. In the following, simulation results and analysis are presented in Section 3.5. Finally, section 3.6 summarizes the chapter.

Following an overview of CSSS problem, Section-4.3 introduces the system model. Then, Section 4.4 provides the details of CSS under heterogeneity and homogeneity modes. Section 4.5 derives the coupled energy & spectrum efficiency and formulates the CSSS problem. Section 4.6 develops the proposed heuristic approached. Finally, simulation results and analysis are presented in Section-4.7 and Section-4.8 summarizes the chapter.

Chapter 5 begins with an detailed overview of energy harvesting CRNs. Thereupon, Section-5.3 models the proposed full-duplex system based on stochastic energy arrivals. Section-5.4 introduces the proposed CSS scheme. Thereafter, Section-5.5 characterizes the energy state evolution of each SU and formulates the convex myopic policy optimization. Numerical results are presented in Section-5.6 and the chapter is summarized in Section-5.7.

Chapter 6 eventually concludes the thesis and outline its main contributions to the green CRNs in Section 6.1. Some potential open problems and possible future work is then presented in Section 6.2.

CHAPTER 2. BACKGROUND ON SPECTRUM SENSING

Before going into the details and distinguishing features of the sensing techniques, it might be useful to state some regulations, fundamental limitations and technical challenges associated with the spectrum sensing for the sake of a clear comparison.

2.1 Sensing Regulations

Regulatory bodies require that signal to interference ratio (SIR) at any primary receiver does not fall below a certain level that is mostly related to primary receivers' robustness against interference, primary band, and service type. For this purpose, the FCC has introduced the *interference temperature* model by which an upper bound is defined to limit the aggregate level of interference caused by multiple transmissions. Accordingly, *interference range* of SUs can be defined as the maximum distance at which SU interference is harmful to PUs. Therefore, SUs within the interference range of PUs must have a *detection sensitivity* so that they are able to detect primary signals with certain detection and false alarm probabilities under a predetermined minimum SNR level [23].

In OSA, while utilizing a spectrum hole, SUs periodically monitor the occupied primary spectrum by sensing in order to detect the PU emergence. If periodic spectrum sensing is culminated with a decision in favor of the PU presence, SUs are required to evacuate the channel immediately in order not to interfere with the primary network communications. This is one of the most fundamental constraints enforced by OSA based CRNs and will be referred to as collision constraint throughout this dissertation.

On the other hand, the sensing period is a measure of time which restricts the permissible maximum interference duration to the primary network and is determined by regulatory bodies

based on the delay sensitivity of the primary channels. To put it another way, the sensing period is a metric of the QoS degradation since it determines the maximum delay of evacuating the primary channel. This periodic character of the OSA system naturally imposes a tradeoff between sensing and data transmission as it is not possible to momentarily sense and transmit using a single antenna. Therefore, sensing duration needs to be kept as low as possible in order to maximize the available time left for data transmission.

2.2 Sensing Challenges

2.2.0.1 Channel Uncertainty

Due to the radio propagation characteristics, transmitted primary signals experience channel impairments such as path loss, shadowing and multipath fading. A low received signal SNR may not necessarily imply the PU absence since primary signal can experience a deep fading or severe shadowing effects because of obstacles. Under these channel uncertainties, an SU may claim the absence of PUs in error, which is referred as *hidden terminal problem* [24] which is depicted in Figure 2.1.

2.2.0.2 Noise Uncertainty

To meet detection sensitivity regulations, noise power spectral density (PSD) must be carefully estimated to set the detection threshold accurately. However, the estimation accuracy is limited due to the thermal noise variations and calibration errors [25]. Moreover, if the detection solely depends on the received SNR, a weak primary signal may not be distinguished from noise under *noise uncertainty*. In this case, the detection threshold must be set according to the worst case scenario to guarantee that the false alarm rate is below a certain desired value. The SU is also obligated to satisfy the collision constraint in addition to the false alarm rate, however, the required number of samples to meet these target probability levels goes to infinity below an SNR threshold [26], which is also known as the *SNR wall*. In other words, even conducting infinite time of sensing would not yield desired detection probability if the received SNR is below the SNR wall.

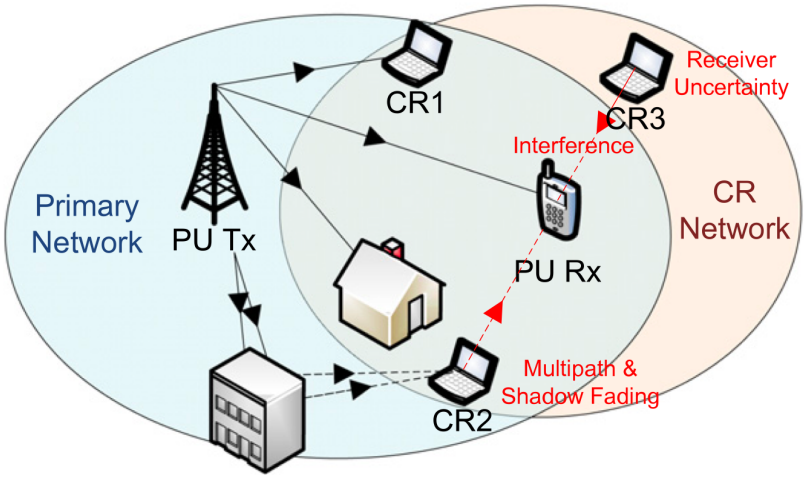

Figure 2.1: Demonstration of channel impairments: hidden terminal, multipath fading, shadowing, and receiver uncertainty [12].

In Figure 2.1, CR2 is affected by the hidden terminal phenomenon since it receives multiple replicas of the attenuated primary signal and experiences shadowing due to the building which obstructs the line-of-sight (LoS) of the primary base station. Even if CR3 has a LoS reception, the received signal strength is very low as a result of path loss effects over the long distance and it may require an infeasible sensing duration due to the receiver uncertainty and SNR wall phenomenon. As aforementioned, SUs are required to distinguish these weak primary signals with high detection sensitivity that is not always available in practice owing to the hardware limitations and costs. Alternatively, SUs may increase their sensing duration to obtain more reliable results, however, this might directly effect the system throughput.

2.3 Local Spectrum Sensing

In a conventional manner, spectrum sensing is considered to be a task of achieving the spectral awareness about the PC in the *sensing space* with the dimensions of *time*, *location* and *frequency*. Although a more involved hyperspace which takes *codes* and *angle of arrivals* as additional dimensions provides a better insight into the spectral opportunity, identifying the spectrum holes within such a huge hyperspace requires advanced research skills and enormous computational power. Besides the multi-dimensionality, for a given point within the sensing

space, characteristics of the present primary signals (such as energy, waveform, bandwidth, modulation type, carrier frequency, etc.) have also an impact on the final conclusion of a decision maker [24]. Based upon these characteristics, a number of sensing techniques is proposed within the literature. Following subsections reviews these techniques.

2.3.1 General Signal Model

For future references, a general signal model will be considered for primary and secondary networks comprising of M PCs with indices m and N SUs with indices n, respectively. Carrier frequency and bandwidth of PC m is denoted by f_m^c and W_m, respectively. Defining the idle and busy state of the primary channel m as hypotheses $\mathcal{H}_m^0$ and $\mathcal{H}_m^1$, respectively, the k^{th} sample of the received primary signal taken by SU n on PC m is given by

$$r_m^n(k) = \begin{cases} z_m^n(k) & , \ k \in [1, S_m^n], \ \mathcal{H}_m^0 \\ h_m^n(k)\, p_m(k) + z_m^n(k) & , \ k \in [1, S_m^n], \ \mathcal{H}_m^1 \end{cases} \tag{2.1}$$

where $h_m^n(k)$, $p_m(k)$, $z_m^n(k)$, and S_m^n denote the complex composite channel gain between the PU m and the SU n, the transmitted primary signal by PU m, the additive white Gaussian noise (AWGN) which is modeled as circularly symmetric complex Gaussian (CSCG) random variable with zero mean and variance σ_z^2, and the number of samples, respectively.

For the path loss between PUs and SUs, a generic analytic model is adopted to inherit necessary design parameters from an empirical model [27] in which the received signal power by the SU n on the PC m is given by

$$\mathbb{P}_{m,n}^r = \mathbb{P}_m^t k_m \phi_m^t \phi_n^r \left[\frac{d_0}{d_m^n}\right]^{\theta_m} \tag{2.2}$$

where $\mathbb{P}_m^t$ and $\mathbb{P}_{m,n}^r$ represent the transmitted signal power by PU m and the received signal power by SU n on the primary channel m, respectively; k_m is a unitless constant that depends on the primary signal wavelength and the reference distance d_0; θ_m is the path-loss exponent that represents the rate at which the path loss increases with the distance between the SU n and the PU m, d_m^n; and ϕ_m^t and ϕ_n^r are the transmitter and the receiver antenna gains, respectively. Accordingly, the complex composite channel gain,

$$h_m^n = \sqrt{P_{m,n}^r}\ g_m^n \ , \tag{2.3}$$

characterizes the propagation medium between the PU m and the SU n in terms of the received primary signal power, $P^r_{m,n}$, and the complex channel gain, g^n_m.

2.3.2 Energy Detector (ED)

Energy detection, also known as periodogram or radiometry, is the most common spectrum sensing method in CRNs due to its low computational and implementation complexity [24], [28], [29], [30]. Moreover, on the contrary of some sensing techniques presented below, energy detectors (EDs) do not require *a priori* information about primary signals. Consequently, EDs have been extensively exploited in the literature as the underlying sensing technique as it is a generic and favorable method thanks to its simplicity, compatibility and low cost.

To detect primary signals, ED measures the received signal energy for a time interval and compares it with a predetermined threshold to decide on the PU existence. Based on the signal model given in Equation (2.1), the local test statistic of the SU n on the PC m is given by

$$\mathcal{K}^n_m = \sum_{k=1}^{S^n_m} y^n_m(k) \underset{\mathcal{H}^0_m}{\overset{\mathcal{H}^1_m}{\gtrless}} \varepsilon^n_m \tag{2.4}$$

where the number of samples is the time-bandwidth product $S^n_m = W_m \tau^n_m$ where τ^n_m denotes the sensing duration. Throughout the thesis, number of samples will be preferred metric in analysis of sensing duration and energy consumption since S^n_m and τ^n_m are proportional. Following from the early work of Urkowitz [31], $\mathcal{K}^n_m$ can be described as

$$\mathcal{K}^n_m \sim \begin{cases} \chi^2_{2S^n_m} & , \ \mathcal{H}^0_m \\ \chi^2_{2S^n_m}(2\gamma^n_m) & , \ \mathcal{H}^1_m \end{cases} \tag{2.5}$$

where γ^n_m is the instantaneous SNR of SU n at channel m, $\chi^2_{2S^n_m}$ denotes the central chi-square distributions with $2S^n_m$ degrees of freedom and $\chi^2_{2S^n_m}(2\gamma^n_m)$ denotes the non-central chi-square distributions with $2S^n_m$ degrees of freedom with a non-centrality parameter, $2\gamma^n_m$.

In the case of deterministic $h_{m,n}$, i.e. g^n_m is constant in Equation (2.3), using the cumulative distribution functions of the aforestated distributions, probabilities of false alarm and detection

are given as [32]

$$P^{f}_{m,n}\left(S^{n}_{m},\varepsilon^{n}_{m}\right)=\mathcal{P}\left(\mathcal{K}^{n}_{m}>\varepsilon^{n}_{m}|\mathcal{H}_{0}\right)=\frac{\Gamma\left(S^{n}_{m},\varepsilon^{n}_{m}/2\right)}{\Gamma\left(S^{n}_{m}\right)} \tag{2.6}$$

$$P^{d}_{m,n}\left(S^{n}_{m},\varepsilon^{n}_{m},\gamma^{n}_{m}\right)=\mathcal{P}\left(\mathcal{K}^{n}_{m}>\varepsilon^{n}_{m}|\mathcal{H}_{1}\right)=\mathcal{Q}_{S^{n}_{m}}\left(\sqrt{2\gamma^{n}_{m}},\sqrt{\varepsilon^{n}_{m}}\right) \tag{2.7}$$

where $\Gamma\left(\cdot\right)$ is the gamma function, $\Gamma\left(x,a\right)=\int_{x}^{\infty}e^{-t}t^{a-1}dt$ is the incomplete gamma function, and $\mathcal{Q}_{c}\left(a,b\right)$ is the generalized Marcum-Q function which is defined as

$$\mathcal{Q}_{c}\left(a,b\right)=\frac{1}{a^{c-1}}\int_{b}^{\infty}x^{c}e^{-\frac{x^{2}+a^{2}}{2}}I_{c-1}\left(ax\right)dx$$

where I_{c-1} is the $\left(c-1\right)^{th}$ order modified Bessel function of the first kind.

On the contrary of deterministic channel gain assumption, if h^{n}_{m} follows a certain distribution, $P^{d}_{m,n}$ given in equation (2.7) is the conditional probability detection for a given instantaneous SNR, γ^{n}_{m}. Therefore, one needs to average this conditional probability over all possible instants as follows

$$P^{d}_{m,n}=\int_{\gamma}\mathcal{Q}_{S^{n}_{m}}\left(\sqrt{2x},\sqrt{\varepsilon^{n}_{m}}\right)f_{\gamma}\left(x\right)dx \tag{2.8}$$

where $f_{\gamma}\left(x\right)dx$ is the fading distribution. In the case of *Rayleigh* fading, γ^{n}_{m} is exponentially distributed and the closed form expression for equation (2.8) is derived as [33]

$$P^{d}_{m,n}\left(S^{n}_{m},\varepsilon^{n}_{m},\bar{\gamma}^{n}_{m}\right)=e^{-\frac{\varepsilon^{n}_{m}}{2}}\sum_{i=0}^{S^{n}_{m}-2}\frac{1}{i!}\left(\frac{\varepsilon^{n}_{m}}{2}\right)^{i}+\left(\frac{1+\bar{\gamma}^{n}_{m}}{\bar{\gamma}^{n}_{m}}\right)^{S^{n}_{m}-1}\left[e^{-\frac{\varepsilon^{n}_{m}}{2\left(1+\bar{\gamma}^{n}_{m}\right)}}-e^{-\frac{\varepsilon^{n}_{m}}{2}}\sum_{i=0}^{S^{n}_{m}-2}\frac{1}{i!}\frac{\varepsilon^{n}_{m}\bar{\gamma}^{n}_{m}}{2\left(1+\bar{\gamma}^{n}_{m}\right)}\right]$$

where $\bar{\gamma}^{n}_{m}$ is the average SNR [34].

For large S^{n}_{m} and normalized noise variance, another renowned and mostly exploited set of equations for false alarm and detection probabilities is given by [35]

$$P^{f}_{m,n}\left(S^{n}_{m},\varepsilon^{n}_{m}\right)=\mathcal{Q}\left[\left(\varepsilon^{n}_{m}-1\right)\sqrt{S^{n}_{m}}\right] \tag{2.9}$$

$$P^{d}_{m,n}\left(S^{n}_{m},\varepsilon^{n}_{m},\gamma^{n}_{m}\right)=\mathcal{Q}\left[\left(\varepsilon^{n}_{m}-\gamma^{n}_{m}-1\right)\sqrt{\frac{S^{n}_{m}}{2\gamma^{n}_{m}+1}}\right] \tag{2.10}$$

where $\mathcal{Q}\left(x\right)=\frac{1}{\sqrt{2\pi}}\int_{x}^{+\infty}e^{-y^{2}/2}dy$ denotes the right-tail probability of a normalized Gaussian distribution. It should be noted that the equation set of (2.9) and (2.10) are necessary to present for a fair comparison with other studies in the literature, however, it is less general than the equation set given in (2.6) and (2.7) since authors assume that the primary signal is complex-valued and phase shift keying (PSK) modulated signal.

2.3.3 Feature Detector (FD)

In contrast to its simplicity and compatibility, the ED is highly susceptible to noise uncertainty and SNR wall phenomenon as any other moment-based detector. From an information theoretic intuition, the reliability and the rigor of the sensing decision increases with the increase in acquisition of accurate knowledge regarding the primary signal characteristics. As a consequence, the ED could not meet required performance level under all circumstances since it does not take primary signal features into consideration.

However, practical signal structure of the contemporary communication systems has very distinctive features and the exploitation of which can provide a substantial performance enhancement compared to ED. Thus, one of the alternatives for the detection of PU transmissions is to take the advantage of known statistical properties of the primary signals. Assume that the primary signals are normally distributed and that enough number of samples are taken to invoke the central limit theorem (CLT). Considering the fact that Gaussian signals are fully determined by their first and second moments, the estimated first and second moments of the primary signals are sufficient to provide practical accuracy to deal with the noise uncertainty and SNR wall phenomenon [30].

As an illustration, orthogonal frequency-division multiplexing (OFDM), which is one of the most common techniques in modern communication systems, inserts a cyclic prefix (CP) to each data block. The CP is simply the same as the last portion of the data symbol and introduces distinctive correlation properties by which near-optimal spectrum sensing algorithms can be designed [36], [37]. Denoting the number of symbols in a cyclic prefix and in a data block as T_c and T_d, respectively, the autocorrelation coefficient of SU m on the primary channel m can be given as

$$\rho_m^n = \frac{T_c}{T_c + T_d} \frac{\gamma_m^n}{1 + \gamma_m^n} \tag{2.11}$$

As its local test statistic, a feature detector (FD) employs the log-likelihood ratio (LLR) test which is given by

$$\mathcal{K}_m^n = \Lambda_m^n \underset{\mathcal{H}_m^0}{\overset{\mathcal{H}_m^1}{\gtrless}} \varepsilon_m^n \tag{2.12}$$

where the LLR, Λ_m^n, is conditionally distributed as [36]

$$\Lambda_m^n|\mathcal{H}_m^0 \sim \mathcal{CN}\left(0, \frac{2S_m^n(\rho_m^n)^2}{[1-(\rho_m^n)^2]^2}\right) \tag{2.13}$$

$$\Lambda_m^n|\mathcal{H}_m^1 \sim \mathcal{CN}\left(\frac{2S_m^n(\rho_m^n)^2}{1-(\rho_m^n)^2}, 2S_m^n(\rho_m^n)^2\right) \tag{2.14}$$

where $\mathcal{CN}(\cdot)$ denotes complex Gaussian distribution. Based on (2.13) and (2.14), the probabilities of false alarm and detection of SU n within cluster m are given by [36]

$$P_{m,n}^f\left(S_m^n, \varepsilon_m^n\right) = \mathcal{P}\left(\Lambda_m^n > \varepsilon_m^n|\mathcal{H}_m^0\right) = \frac{1}{2}\operatorname{erfc}\left(\sqrt{S_m^n}\ \xi_m^n\right) \tag{2.15}$$

$$P_{m,n}^d\left(S_m^n, \varepsilon_m^n, \rho_m^n\right) = \mathcal{P}\left(\Lambda_m^n > \varepsilon_m^n|\mathcal{H}_m^1\right) = \frac{1}{2}\operatorname{erfc}\left(\sqrt{S_m^n}\ \frac{\xi_m^n - \rho_m^n}{1-(\rho_m^n)^2}\right) \tag{2.16}$$

where $\xi_m^n = \frac{1-(\rho_m^n)^2}{2S_m^n\rho_m^n}\left(\varepsilon_m^n + S_m^n \log\left(1-(\rho_m^n)^2\right)\right) + \rho_m^n$.

For the multipath reception case, consider a multipath order O with independent tap coefficients $g_m^n(i)$, for $i = 1, 2, \ldots, O$ and assume that $g_m^n(i)$s are also independent of the primary signal and the additive noise. Although the autocorrelation function is spread due to the time dispersion in a multipath fading channel, averaging the second-order statistics over multiple OFDM symbols can alleviate the impact of multipath fading to achieve a detection performance close to the that of AWGN channel [36]. Accordingly, the average SNR at the SU receiver is given as $\bar{\gamma}_m^n = \sum_{i=1}^O \bar{\gamma}_m^n(i) = \sum_{i=1}^O \mathbb{E}\left[|g_m^n(i)|^2\right]\gamma_m^n$ where $\bar{\gamma}_m^n(i)$ is the average SNR of the i^{th} path. Hence, the detection and false alarm probabilities under multipath fading can be calculated from (2.15) and (2.16) by substituting γ_m^n with $\bar{\gamma}_m^n$. In the sequel, without loss of generality, AWGN and multipath fading scenarios will be addressed together by assuming $\sum_{i=1}^O E\left[|g_m^n(i)|^2\right] = 1$.

2.3.4 Other Techniques

2.3.4.1 Matched Filtering

If the receiver has *a priori* knowledge about primary signal such as the modulation type, order, waveform, etc., *matched filter* is known to be the optimal method for detection [38]. It requires short sensing time to achieve a certain processing gain such that the number of samples required to be taken grows by $O\left(SNR^{-1}\right)$ [39]. However, matched filters have very poor

performance if the transmitted signal information is not accurate and the SU does not have time and frequency synchronization with the PUs. In addition, the SU needs filter circuitry for every type of primary signal, which is not practical in terms of hardware cost and implementation complexity [40].

2.3.4.2 Cyclostationary Feature Detector (CFD)

Auto-correlation function of the primary signals exploited in FDs is not only time-varying but also periodic, and that is effectively employed by cyclostationary feature detectors (CFDs) to obtain superior sensing performance [41], [42], [43], [44], [45]. Cyclostationary nature of PU signals arises from the spectrum redundancy caused by periodicity of modulated and/or coded signals, which leads to spectral correlation among widely separated frequency components [46], [47]. Based on the fact that the noise is a wide-sense stationary process without correlation, transmitted signals can be distinguished from WSS noise using their cyclostationarity features along with the spectral correlation [46]. Unlike the ED, which is heavily dependent upon the PSD, analyzing spectrum correlation function [47] and the cyclic autocorrelation function [48] of primary signals, CFD is able to work well under low SNR conditions. Additionally, recognizing the distinctive features of primary signals, cyclostationarity can be even employed to distinguish different PU transmissions [45].

2.3.4.3 Covariance-Based Sensing (CBS)

The idea of covariance based detectors has originated from the fact that the statistical covariance matrices or auto-correlations of primary signals and noise are different from each other. Thus, CBS is robust against noise estimation uncertainty. In the case of detecting correlated signals, it gives a superior performance because the test statistics are generated from covariance matrix of received primary signal samples such as the ratio of its maximum and minimum eigenvalues [49], the ratio of its diagonal and off-diagonal elements [50], and its maximum eigenvalue [51]. In [52], a cooperative spectrum sensing method is developed by exploiting a recent result on the limiting distribution of the smallest eigenvalue in complex Wishart matrices. However, if the exact structure of transmitted signals are unknown to the

detector, exploitation of *blind detectors* may give a better result without requiring any prior knowledge [49], [50].

2.3.4.4 Multiband and Compressive Sensing

To get higher chance of finding spectrum holes, a wide band of spectrum must be sensed, which intuitively requires higher sampling rates and energy consumption. A natural way of dealing with wideband sensing is dividing it into multiple subbands and jointly sense for spectrum opportunities, which is a.k.a. *multiband sensing* [53], [54]. The other possible approach argues that if the original observed signal is sparse in some manner, then it is possible to sample the received signal at sub-Nyquist rate, which is referred as *wideband compressive sensing* [55]. In [56] and [57], wideband compressive sensing is considered under the collaboration of SUs. For cooperative multihop CRNs, a distributed compressive sensing scheme is developed by forcing the consensus of local spectral estimates [58].

2.3.5 Summary

In spite of the diverse sensing techniques discussed in this chapter, none of them could be used as the best choice for any situation. Contingent upon the availability of *a priori* information and environment, there exist many criteria to factor in to decide on the most proper one such as required accuracy, sensing duration, implementation and computational complexity, and network requirements. For example, if the *a priori* knowledge of the signal to be detected is not available, energy detection is known to be robust to the unknown dispersed channel and fading. However, ED assumes perfect noise PSD estimation, thus the noise uncertainty results in SNR wall and high false alarm probability [25]. On the one hand, matched filtering requires perfect information about the primary signals and accurate synchronization, otherwise its performance reduces dramatically. On the other hand, FDs and CFDs need to know autocorrelation and cyclic properties of PUs which may not be available in practice, respectively. Furthermore, this method requires excessive analog to digital converter capabilities and signal processing abilities [49]. Even though CFD exhibits good performance under non-stationary noise, cyclic features may be entirely unavailable because of the adverse propagation environment [24].

2.4 Cooperative Spectrum Sensing (CSS)

As briefly mentioned in Chapter 1, local detection performance of individual SUs is susceptible to detrimental channel effects such as path loss, multipath fading, and shadowing, etc. Even if there exists an on going primary network activity, an SU can observe very weak signal strength due to shadowing which may be because of the obstacles between the primary transmitter and the SU. Alternatively, an SU might receive attenuated primary signal copies from surrounding reflectors in a multipath fading scenario. If an SU is very far away from the PU transmitter but close enough to the PU receiver, on the other side, it may suffer from the receiver uncertainty and treat this weak primary signal as background noise. In all of these cases, SUs will most probably decide in favor of the absence of the primary network activity due to weak signal reception and their utilization of the PCs will cause interference to primary network communication. However, an SU with high SNR can expeditiously and accurately sense the PC and let SUs with poor channel sensing conditions know about the presence of the primary activity. As a remedy, cooperation of SUs is proposed to improve sensing accuracy [59].

In the most primitive sense, cooperative sensing takes the advantage of spatial diversity of SUs to improve the overall sensing performance of the secondary network which can be referred to as *cooperative gain*. For example, receiver uncertainty and hardware cost of the individual SUs can be alleviated by cooperation such that receiver sensitivity can be adjusted to the level of path loss for a fixed cost. However, the cooperative gain is not free of the *cooperation overhead* which refers to any extra cost of sensing, energy, communication, complexity and delay.

2.4.1 Categorization of CSS

Based on the local decision sharing method among the SUs, CSS can be categorized into three models: centralized [60]-[61], distributed [62] and relay-assisted [63].

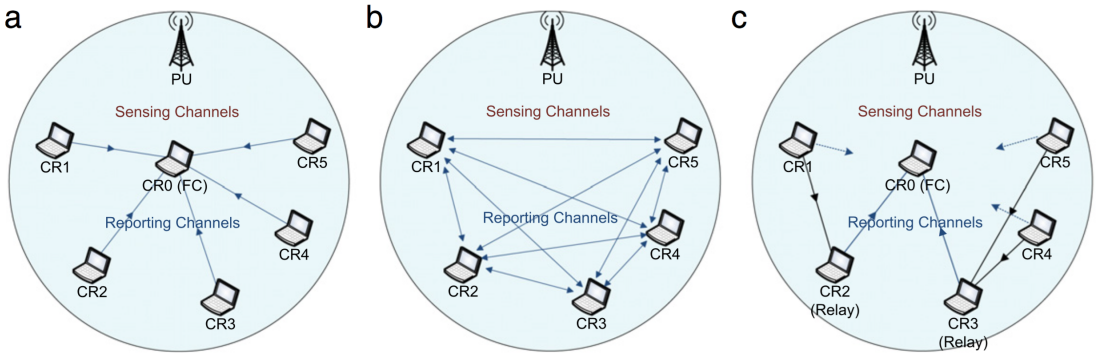

Figure 2.2: Categorization of CSS: (a) centralized, (b) distributed, and (c) relay-assisted [12].

2.4.1.1 Centralized CSS

In centralized CSS, SUs perform local sensing and share this information with a decision maker, which is also known as *fusion center* (FC), over a dedicated common control channel (CCC), which is also known as the *reporting channel* . After receiving and combining all local decisions, FC makes a final decision regarding the presence of the primary activity based on a predetermined global detection method. This global decision is then diffused back to the cooperating SUs. A centralized cooperation scheme is depicted in Figure 2.2-a where (CR0) serves as the FC.

2.4.1.2 Distributed CSS

On the contrary, distributed CSS does not require a FC to obtain a global decision regarding the primary network activity. SUs prefer to communicate among themselves to conclude in a unified global decision. As shown in Figure 2.2-b CR1-CR5 transmits their local results to each other using a distributed algorithm. Based on received messages, each SU makes a global decision employing a local criterion and report back its own decision. This procedure is repeated in an iterative manner until the distributed algorithm converges into a global decision. Compared to the centralized CSS, SUs serve as members and FCs at the same time.

2.4.1.3 Relay-Assisted CSS

In addition to the distributed and centralized CSS, relay-assisted cooperative sensing exploits the sensing and reporting channel quality diversity of SUs. As an illustration, an SU with weak sensing channel conditions and strong reporting channel performance can cooperate with another SU with strong sensing channel conditions and weak report performance as shown in Figure 2.2. Therefore, the relay-assisted model can be regarded as multi-hop cooperative sensing which will be addressed in Chapter 3.

2.4.2 Data Fusion Methods

Data fusion is a process of combining reported local sensing data to conclude in a global decision regarding the activity of primary networks. The type and size of the local sensing data may differ according to the CCC bandwidth and reliability. In the literature, there exists three well known data fusion methods: 1) *Hard decision fusion* (HDF) where SUs only report their local sensing results in hard binary form , 2) *Soft decision fusion* (SDF) where SUs send their entire local observations or their own test statistic, and 3) *Quantized soft decision fusion* where SUs can quantize their local test statistics and report in the form of a bit sequence. Intuitively, SDF can achieve the best performance among others in return for CCC overhead. The HDF is the simplest and modest method in terms of complexity and bandwidth requirement, respectively. However, quantized SDF can achieve very high detection performance in return for relatively higher complexity and CCC overhead.

2.4.2.1 Hard Decision Fusion

The most common fusion for the HDF is $K-out-f-N$ detector which sums reported hard bits from N SUs and compare it with a threshold to obtain the global decision. Voting rules are typically considered in three different cases: 1) *OR rule* where $K = 1$ and it requires at least one SU report the existence of primary activity, 2) *AND rule* where $K = N$ and it requires all SUs report the existence of primary activity, and 3) *Majority rule* where $K = \lceil N/2 \rceil$ and it requires the majority of SUs to report the existence of primary activity. Denoting the reported

local decision of SU n as u_n and received local decisions by the FC as $\tilde{u}_n$, the global test can be given as

$$\mathcal{K} = \sum_{n=1}^{N} \tilde{u}_n \underset{\mathcal{H}_0}{\overset{\mathcal{H}_1}{\gtrless}} K \tag{2.17}$$

where $\mathcal{H}_0$ and $\mathcal{H}_1$ denote the binary hypotheses for the absence and presence of PU, respectively. Based on the distribution of $\tilde{u}_n$, we define two different schemes

1. *Homogeneous Scheme*: $\tilde{u}_n$s are independent and identically distributed (i.i.d) Bernoulli random variables, thus, $\mathcal{K}$ is a Binomial random variable. The practical interpretation of homogeneous scheme could be put as follows: Denoting $\tilde{P}_n^f = \mathcal{P}\left[\tilde{u}_n = 1|\mathcal{H}_0\right]$ and $\tilde{P}_n^d = \mathcal{P}\left[\tilde{u}_n = 1|\mathcal{H}_1\right]$, each SU is enforced to adjust their local false alarm and detection probabilities to satisfy $\tilde{P}_n^f = \tilde{P}_{n'}^f,\ \tilde{P}_n^d = \tilde{P}_{n'}^d,\ \forall n,\ n'$. If the reporting channel is imperfect, SUs are also required to compensate the channel errors to satisfy the above requirement. We note that if SUs have identical sensing quality, which is a function of the SNR, homogeneous scheme gives the optimal results by treating all SUs equally.

2. *Heterogeneous Scheme*: $\tilde{u}_n$s are independent but unidentically distributed (i.u.d) Bernoulli random variables, hence, $\mathcal{K}$ follows a Poisson-Binomial distribution. This a generalization of the homogeneous scheme and the interpretation of it could be put as follows: Unlike the homogeneous scheme, each SU is relaxed to have unidentical reports, so that one can assign different local detection accuracy requirements based on sensing and reporting quality of SUs. As will be pointed out repeatedly throughout the thesis, such a flexibility yields a performance enhancement in heterogeneous CRNs, assuming homogeneity in heterogeneous environments may cause significant performance losses.

2.4.2.2 Soft and Quantized Soft Decision Fusion

Chair-Varshney rule is known to be the optimal fusion rule to combine local results and it is based on log-likelihood ratio (LLR) test [64]. Under Rayleigh fading sensing channels, the performance of equal gain combining (EGC), selection combining (SC) and switch-and-stay combining (SSC) is studied using EDs [33]. Results have revealed the fact that SC and SSC have an order of magnitude cooperative gain while the the EGC reaches approximately two orders

of magnitude cooperative gain. EGC and maximal ratio combining (MRC) is then studied in [65] to combine the weighted local measurements. The proposed method reduces to EGC and MRC under high and low SNR regimes, respectively. A quantized SDF is also proposed by partitioning the entire range of test statistic in to four subregions. A much more complete research is conducted in [13] where HDF and quantized SDF schemes are compared with ideal case under the imperfect reporting channels using maximum output entropy quantizers and auto-correlation based FDs in SUs. Alternatively, Lloyd max quantizers and EDs is also studied in [66].

2.4.3 Chapter Summary

In this chapter, we first gave a background on sensing challenges and practical design limitations, which is followed by a set of various sensing schemes with different implementation complexity and local detection performance. As pointed out in the summary, there is no a sensing technique fits well in all domains of design considerations. While some techniques are favorable with their low cost and simplicity, they might not be able to give sufficient accuracy in adverse radio environments. On the other hand, high performance techniques may require extra computation resources and/or a priori information regarding the primary signal characteristics. CSS is then introduced to mitigate the inadequacy of individual SUs by taking the geographical diversity since SUs may not experience the same channel impairments all places and times. Different categories of CSS are presented along with common data fusion techniques. Throughput this thesis, we focus on HDF and quantized SDF methods under the centralized and relay-assisted CSS schemes with heterogeneous sensing and reporting channel qualities.

CHAPTER 3. MULTI-OBJECTIVE CLUSTERING FOR MULTI-CHANNEL CSS

3.1 Overview

We consider a large scale cluster-based heterogeneous cognitive radio networks comprising of M PCs and N SUs each of which has different sensing quality in PCs and different reporting quality in the CCC. Such a network setting is depicted in Figure 3.1. Each cluster is responsible for sensing only one channel at a time. Time is divided into fixed-length slots, T, in each of which a PC is either in the busy or idle state for the whole slot. SUs can join at most one cluster during a time slot.

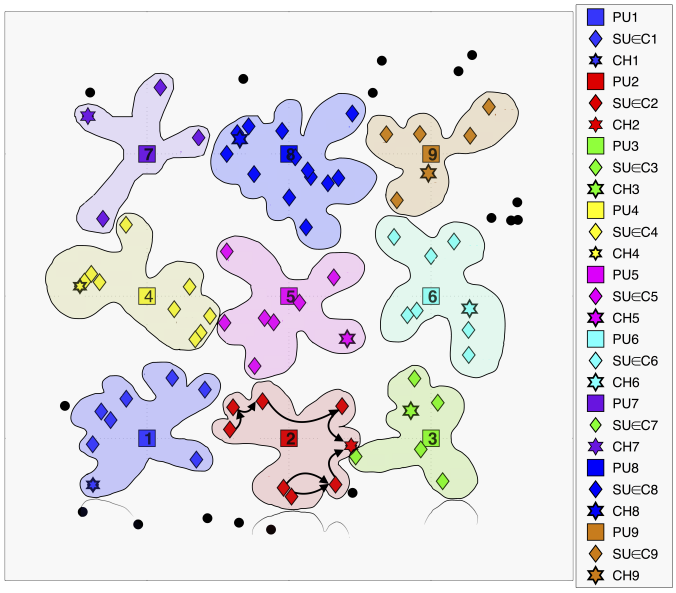

Figure 3.1: Demonstration of a large scale CRN with $M = 9$ PCs and $N = 90$ SUs. SUs assigned to a cluster have a diamond shape with the color of the PU which is sensed by the cluster. The cluster heads are shown in hexagonal shapes. An example of the multihop reporting is also illustrated for cluster 2.

The general problem of cluster-based cooperative spectrum sensing can be described as obtaining the optimal cluster formations and the optimal values of cooperation parameters of the formed clusters (e.g., sensing duration, detection threshold, quantization thresholds and levels, reporting path of each SU, and the head of each cluster, etc.) such that energy cost and throughput gain is fairly distributed among clusters subject to the collision and spectrum utilization constraints.

Accordingly, energy and throughput efficient fair clustering leads into a non-trivial multi-objective MINLP problem as it inherits the formidable characteristics of multi-objective, integer and non-linear problems. The hardship of dealing with such a problem may be well understood when it is compared to a single-objective MINLP which can take a very long running time to solve even for moderate size of networks.

3.1.1 Chapter Contributions and Novelty

In this chapter, the MINLP related challenges will be handled by approaching this extremely complex problem from a two tier solution strategy: *macro* and *micro* perspectives. While the macro perspective tackles the SU and cluster association problem considering the intra-cluster energy costs and throughput gains along with inter-cluster fairness, the micro perspective deals with the intra-cluster total energy cost and throughput gain. Pictorially, the macro perspective selects the candidate cluster instances as depicted in Figure 3.1 where each cluster is responsible for sensing only one PC and the micro perspective finds the optimal cooperation parameters of the cluster instances.

1. Micro perspective focuses on a given cluster where SUs report their local observations regarding activities of a PC over a CCC to a CH which fuses the local reports to come up with a global decision. Similar to sensing channels, the CCC is also subject to channel impairments which may result in an imperfect reporting environment. Instead of using the mostly studied singlehop reporting technique in which cluster members directly report to CHs, employing a multihop path with the minimum error rate among all possible paths might result in a better reporting performance in terms of robustness, delay, and communication range. Results in [13] have clearly revealed that the increase in BEP of

the CCC is blocked by a *BEP wall* where the required additional SNR to achieve the ideal CSS performance goes to infinity. To put it another way, for given SNRs, SUs with unreliable reporting links have to obtain a better local detector performance to compensate the reporting errors which results in more energy consumption. Thus, we propose a procedure to find: 1) The optimal reporting route to a specific SU from others, and 2) The best CH which gives the minimum total multihop error rate induced from the optimal routing path from cluster members to the CH.

2. Although one of the common and relatively more tractable approach is assuming that SUs have with identical/homogeneous sensing and reporting quality metrics (i.e., SUs have the same SNR, sensing duration, detection thresholds, BEP etc.), this assumption would not yield an optimal cooperation cost in a heterogeneous environment where SUs experience different sensing and reporting channel effects. In *hard decision fusion* (HDF) based CSS, for example, the CH collects and sums the binary values reported by SUs within the cluster. By enforcing all SUs to have identical detection and false alarm probabilities at the CH side, regardless of their sensing and reporting environment, traditional global summary statistic of the CH follows *Binomial* distribution. With this approach, SUs with relatively low SNR and/or high BEP must sense longer to ensure target detection performance in the heterogeneous case. Consequently, not taking the heterogeneity into account returns higher energy expenditure and lower throughput since the CH must wait for the slowest SU to feed the final decision back to the cluster. In light of this, a novel EE-CSS scheme is proposed to take the advantage of sensing and reporting channel diversities and to allow SUs to report with nonidentical detection and false alarm probabilities, where the global summary statistic of CH follows a *Poisson-Binomial* distribution. A convex framework is further developed to jointly find the optimal detection threshold and sensing duration of each SU to minimize the total energy consumption of the cluster subject to global PU protection and spectrum utilization constraints.

3. This chapter also considers the case of quantized *soft decision fusion* (SDF) based CSS. Based on the quantization of *log-likelihood ratio* (LLR) distribution, each SU determines

the observed LLR value and reports corresponding quantization levels in a multi-bit binary sequence to the CH which computes the final decision. Similar to the traditional HDF case, determining a fixed sensing duration for SUs with nonidentical sensing and reporting channel quality, which is a.k.a. fixed sample size test (FSST), may not always result in an EE cooperation. By assigning sensing duration to SUs proportional to their autocorrelation coefficient, weighted sample size test (WSST) is proposed to obtain a more EE regime.

4. If the spectrum utilization and energy consumption are defined as currency and commodity, respectively, the ultimate design goal of the macro perspective would be clustering SUs in such a way that commodity per currency is maximized. Therefore, a multi-objective clustering optimization (MOCO) is proposed to fairly minimize the clusters' energy consumption while fairly maximizing their achievable throughput subject to global detection and false alarm probability constraints. Since MOCO is a mixed integer problem with an optimal Pareto set, it is heuristically solved using the Non-dominated Sorting Genetic Algorithm-II (NSGA-II).

3.1.2 Chapter Organization

The rest of this chapter is organized as follows: Section 3.2 presents the related work in the literature. Section 3.3 describes the generalized best CH selection procedure for single-bit hard and quantized multi-bit soft decision fusion CSS schemes. Then, Sections 3.4.1.1, 3.4.1.2, and 3.4.1.3 give the details of ideal, HDF-based, and quantized SDF-based CSS schemes, respectively. Section 3.4.2.1 provides a background in multi-objective evolutionary algorithms and Section 3.4.2.2 formulates the MOCO problem and explains its solution with NSGA-II. In the following, simulation results and analysis are presented in Section 3.5. Finally, section 3.6 summarizes the chapter.

3.2 Related Work

Some of the recent research addressing the EE-CSS can be exemplified as follows: Using amplify-and-forward relaying, Huang et al. consider an EE-CSS scheme with the goal of minimizing the total energy consumption subject to detection performance constraints [67]. In [68], Deng et al. divide the sensing nodes into a number of non-disjoint feasible subsets which satisfy the detection requirements. Then, they extend the network lifetime by successively activating each subset while keeping others in a sleep mode. The work in [69] considers a single SU and multiple PCs and optimizes the average energy cost of spectrum sensing, channel switching, and data transmission subject to some sensing reliability, delay, and throughput constraints. In [70], the authors provide a theorem along with the closed-form expression to determine the optimal number of CRs in order to obtain an EE-CSS. Then, they propose a terminal assignment strategy. Authors of [71] first derive a closed form expression for SU priority and detection threshold, then, they propose a convex optimization framework to minimize the energy consumption in CSS. From a different perspective, [72] achieves EE-CSS by reducing the total number of reports exchanged between the SUs and the CH, which is an efficient approach where the reporting energy is dominant.

On the other hand, quantized SDF is considered to be a practical yet an efficient method in [13] and [66]since SDF reporting affects the bandwidth limitation of CCC. Employing feature detector, authors in [13] study the effect of channel errors in HDF and quantized SDF-based CSS and clearly show the existence of the error wall at which successful detection is not possible. On the other hand, [66] uses an energy detector with a Lloyd-Max (LM) quantizer and its results show that it gives a better performance than the Maximum-Output entropy quantizer in [13]. However, studies in [66] and [13] do not consider the energy efficiency, clustering and fusion center selection.

The study in [73] is first to address the energy efficiency in cluster based CSS. They first propose a voting scheme based on SUs' own confidence, then develop a cluster-collect-forward scheme to save energy spent on vote-collection and information exchange. Without targeting the energy efficiency [74], Guo et al. obtain the optimal number of clusters to minimize the

cooperation overhead without any performance loss of reliability. In [75], a clustering technique is adopted to save energy consumed in reporting results and exchanging information. In [76], to reduce reporting time and bandwidth requirement, a dynamic CH selection scheme is proposed based on the sensing qualities of SUs. Kozal et al. propose a multihop reporting scheme to reduce the reporting power consumption. [77].

As distinct from the existing work, we develop a comprehensive frame work which fairly divides the SUs into clusters to minimize clusters' energy cost and maximize their throughput. Moreover, within each cluster, we took the advantage of multihop reporting diversity to develop a novel CH selection algorithm which is applicable to both HDF and SDF based CSS schemes. More importantly, we leverage the sensing quality heterogeneity of the cooperating SUs to develop energy efficient HDF and SDF schemes. In particular, a novel HDF method which allows SUs to report in different local detection performance is developed along with the convex optimization framework which finds SUs' optimal local detection parameters to minimize the energy expenditure. The same spirit is also applied to the SDF case using WSST which is a weighted case of the well-known FSST.

3.3 Cluster Head Assignment and multihop Path Selection

Before going into the cooperative spectrum sensing and multi-objective clustering problem details, how to select the best CH first is needed to be explained because following discussions are based on the assumption that the best CH and optimal routing path from cluster members to the CH are given. SUs cooperate among themselves by reporting their local decisions over a noisy CCC to the CH and receive decision and control feedback from CHs. Even though many studies in the literature have only focused on a direct singlehop reporting link between SUs and CHs, this may not always result in a reliable and energy efficient cooperation between SUs and CHs, especially when SUs with limited maximum transmission power in a cluster are spread over a wide area. In this case, the limited communication range of CHs/SUs may cause some SUs/CHs to lie outside the communication range of each other, or the channel quality between some SUs and the CH may not be good. Hence, SUs/CHs will not be able to reliably receive

information from CHs/SUs, due to the channel impairments over relatively large distances, which will eventually impact the accuracy of the fusion result.

Alternatively, exploiting a multihop method for the reporting phase does not only alleviate the communication range limitation and poor reporting channel quality but also gives a chance to exploit an algorithm which finds the best multihop path with maximum success probability from cluster members to a specific CH. Based on this idea, the SU which gives the minimum total error rate can be selected as the CH among the cluster members. Taking all of these into consideration results in a superior reporting performance in terms of robustness, reporting delay and communication range.

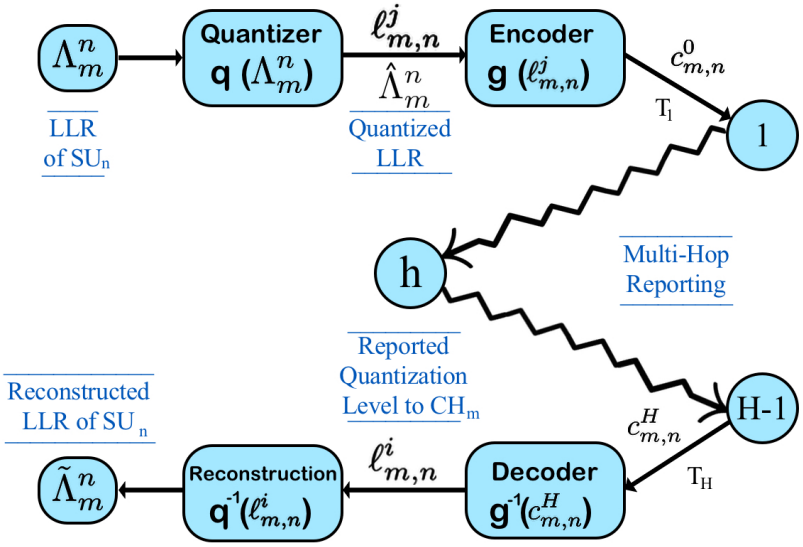

Figure 3.2: Multihop Reporting of SU n within cluster m

3.3.1 Cluster Topology and Path Characterization

The graph representing cluster m, $\mathcal{G}_m(\mathcal{C}_m, \mathcal{E}_m, \Omega_m)$, is defined in terms of the set of SU nodes $\mathcal{C}_m$, the set of edges $\mathcal{E}_m$, and the set of edge weights Ω_m. The neighboring set of $SU_n \in \mathcal{C}_m$ is denoted as $\Psi_m^n = \left\{ n' | \, \gamma_{n',n} \geq \bar{\gamma}, \, \forall n' \in \mathcal{C}_m \right\}$ where $\gamma_{n,n'}$ and $\bar{\gamma}$ are the received signal SNR by SU n' from SU n and the SNR threshold for communication range, respectively. Then, $\mathcal{E}_m = \left\{ e_{n,n'}^m \, | \, n, n' \in \mathcal{C}_m, \, n \neq n', \, n' \in \Psi_m^n \right\}$ represents the direct edge/hop from SU_n to $SU_{n'}$. Even if the path loss for the edges $e_{n,n'}^m$ and $e_{n',n}^m$ may be the same, it is highly probable to experience different fading effects due to the channel randomness. Therefore, we do not assume

link symmetry between SU pairs within the clusters. In [78], a procedure is proposed to find the best CH which gives the minimum total reporting error under the HDF-based CSS. In this and the following subsection, this procedure will be generalized to support multi-bit reporting (quantized SDF) methods.

The best CH selection procedure is as follows: Initially, SUs transmit pilot signals to determine which SUs are in their communication range by identifying the channel quality metrics among themselves. Following the pilot tone, SUs arbitrarily and temporarily select an SU among themselves to be the CH and share the channel metrics measured during the pilot tone. Then, the temporary CH runs an algorithm to find the best CH with minimum total reporting error along with the optimal multihop routes from all cluster members to the CH. Based on the results of this algorithm, the temporary CH announces the new CH to SUs and devolve its responsibilities.

Assuming every $SU_n \in \mathcal{C}_m$ employs an L_m-level quantizer with the quantization levels set $\mathcal{L}_m = \left\{\ell^j_{m,n} | 1 \leq j \leq L_m\right\}$, a generalized multihop-multibit reporting framework is illustrated in Figure 3.2 where SU_n first obtains the quantized LLR value from observed local LLR Λ^n_m such that $\hat{\Lambda}^n_m = q(\Lambda^n_m) = \ell^j_{m,n},\ 1 \leq j \leq L_m$ based on the quantization scheme which will be described in Section 3.4.1.3. Then, the encoder maps the observed quantization level $\ell^j_{m,n}$ into a $b_m = \log_2(L_m)$-bit binary codeword, $c^0_{m,n} = g(\ell^j_{m,n})$. SUs operate on these codewords using a decode and forward (DF) protocol in a bit-by-bit basis over the path from SU_n to any other cluster member $SU_{n'}$, which is denoted by $n \rightsquigarrow n'$ and consists of independent H^n_m-hops. Each hop is modeled as a binary symmetric channel (BSC) and is characterized by its $L_m \times L_m$ channel transition matrix, $\mathbf{T_h}, 1 \leq h \leq H^n_m$. The entry in the j^{th} row and i^{th} column of $\mathbf{T_h}$, $t^h_{i,j}$, is the probability of detecting $c^i_{m,n}$ given that $c^j_{m,n}$ is transmitted from the previous node, which is given by

$$t^h_{i,j} = \mathcal{P}_h(c^i_{m,n} | c^j_{m,n}) = (1-\epsilon_h)^{b_m - \delta(i,j)} \epsilon_h^{\delta(i,j)} \tag{3.1}$$

where ϵ_h is the crossover probability of the h^{th} hop and $\delta(i,j)$ is the Hamming Distance between $c^i_{m,n}$ and $c^j_{m,n},\ 1 \leq i,j \leq L_m$. Exploiting $\mathbf{T_h}$ matrices, the end-to-end multihop transition

matrix can be calculated as

$$\mathbf{T}_{n \rightsquigarrow n'} = \prod_{h=1}^{H_m^n} \mathbf{T}_{\mathbf{h}} \tag{3.2}$$

which follows from the independent hop assumption and Markov property resulting from the nature of DF protocol which means that the detected symbol from the previous hop is the transmitted symbol for the next hop. Consequently, the i, j entry of $\mathbf{T}_{n \rightsquigarrow n'}$ gives the probability of receiving the LLR quantization level $\ell_{m,n}^i$ given that the source transmitted the LLR quantization level $\ell_{m,n}^j$,

$$t_{i,j}^{n \rightsquigarrow n'} = \mathcal{P}(\tilde{\Lambda}_m^n = \ell_{m,n}^i | \hat{\Lambda}_m^n = \ell_{m,n}^j), \ 1 \leq i, j \leq L_m \tag{3.3}$$

where $\tilde{\Lambda}_m^n = g^{-1}\left(c_{m,n}^{H_m^n}\right) = \ell_{m,n}^i$ denotes the reconstructed (received) quantization level.

3.3.2 The Best Cluster Head Selection

Denoting the cardinality of $\mathcal{C}_m$ as $|\mathcal{C}_m| = C_m$, among C_m SUs, CH is the SU that gives the minimum total reporting error induced from the optimal routes from cluster members to the CH. We weight the hop/edge from any $SU_k \in \mathcal{C}_m$ to any $SU_l \in \mathcal{C}_m$ with the symbol success probability (SSP) $w_{k,l}^m$ which is nothing but any main diagonal element of the channel transition matrix of the hop. Depending upon this edge weighting[1], SSP of the multihop path from SU_n to an arbitrary CH $SU_{n'}$ is given by $\Omega(n \rightsquigarrow n') = \prod_{k,l \in n \rightsquigarrow n'} w_{k,l}^m$. In fact, the optimal path which maximizes the $\Omega(n \rightsquigarrow n')$ is the one which minimizes the negative sum of logarithms of $\Omega(n \rightsquigarrow n')$ as follows

$$n \rightarrow n' = \underset{n \rightsquigarrow n'}{\operatorname{argmin}} \left(- \sum_{k,l \in n \rightsquigarrow n'} \log(w_{k,l}^m) \right) \tag{3.4}$$

By transforming the computation from a multiplication operation into a summation operation, *Dijkstra's algorithm* can be employed to calculate the reporting route with the minimum path cost. Defining $\Omega_m^{n'}$ as the total reporting error probability induced from selecting $SU_{n'} \in \mathcal{C}_m$ to be the CH of cluster m, $\Omega_m^{n'} = -\sum_{\substack{n \in \mathcal{C}_n \\ n \neq n'}} \log\left(\Omega\left(n \rightarrow n'\right)\right)$, the SU gives the minimum total reporting error is chosen to be the best CH as follows

$$CH_m = \underset{n' \in \mathcal{C}_m}{\operatorname{argmin}} \ \Omega_m^{n'} \tag{3.5}$$

[1]We ignore the case in which a symbol may be corrupted in an even number of hops, hence resulting in correct reception of the symbol, since the probability of this occurrence is very small

3.4 Multi-Objective Clustering Optimization

3.4.1 Micro Perspective: Intra-Cluster Optimization

Albeit its simplicity and popularity, ED operates under the assumption of perfect noise variance knowledge, which results in a poor detection performance under estimation errors. Also, noting that ED is subject to an SNR wall under which accurate detection is impossible, exploiting known features of primary signals can provide SUs with an improved detection performance and robustness [30]. Accordingly, we prefer to use a FD which detects PUs using the second-order statistics of primary signals.

3.4.1.1 Benchmark: Ideal CSS

The ideal CSS scheme is first proposed as the performance evaluation and comparison of the hard and soft decision fusion schemes is built upon the energy loss between the proposed and ideal cases. In the ideal case, CH collects exact LLR values reported from SUs over a perfect CCC and obtains global summary test statistic as follows

$$\mathcal{K}_m^{ide} = \sum_{n=1}^{C_m} \Lambda_m^n \underset{\mathcal{H}_m^0}{\overset{\mathcal{H}_m^1}{\gtrless}} \kappa_m^{ide} \tag{3.6}$$

Based on the local LLR distributions given in (2.13) and (2.14), conditional distributions of the global test statistic are given as

$$\mathcal{K}_m^{ide}|\mathcal{H}_m^0 \sim \mathcal{CN}\left(0,\ 2\sum_{m=1}^{C_m} \frac{S_m^n(\rho_m^n)^2}{[1-(\rho_m^n)^2]^2}\right) \tag{3.7}$$

$$\mathcal{K}_m^{ide}|\mathcal{H}_m^1 \sim \mathcal{CN}\left(2\sum_{m=1}^{C_m} \frac{S_m^n(\rho_m^n)^2}{1-(\rho_m^n)^2},\ 2\sum_{m=1}^{C_m} S_m^n(\rho_m^n)^2\right) \tag{3.8}$$

which reduces to the fixed sample size test (FSST) in [36] if we set $S_m^n = S_m,\ \forall n$. Following from (3.7) and (3.8), global false alarm and detection probabilities, $Q_m^f = \mathcal{P}\left(\mathcal{K}_m^{ide} > \kappa_m^{ide} \mid \mathcal{H}_m^0\right)$ and $Q_m^d = \mathcal{P}\left(\mathcal{K}_m^{ide} > \kappa_m^{ide} \mid \mathcal{H}_m^1\right)$, can be derived similar to (2.15) and (2.16). Accordingly, the optimal energy expenditure of cluster m is referred to as

$$E_m^{ide} = \min_{\substack{S_m^n, \kappa_m^{ide} \\ n \in \mathcal{C}_m}} \left\{ \sum_n S_m^n \mid Q_{th}^d \le Q_m^d,\ Q_m^f \le Q_{th}^f \right\} \tag{3.9}$$

which can be equivalently written as a convex problem due to the linearity of the objective function and the log-concavity of the constraints using similar steps followed in Appendix A.1.

3.4.1.2 Hard-Decision Fusion Based CSS

For a given SU cluster formation $\mathcal{C}_m$ and the CH selection as described in the previous section, each $SU_n \in \mathcal{C}_m, \forall n$ reports their final binary decision $u_m^n \in \{0,1\}$ to the cluster head $CH_m = SU_c \in \mathcal{C}_m$ over the optimal multihop route between SU_n and CH_m, $n \rightarrow CH_m$, with the BER $p_{n\rightarrow CH_m}$ which is any main diagonal entry of the end-to-end transition matrix, $\mathbf{T}_{n\rightarrow CH_m}$. If we denote the received decision bit by the CH_m as $\tilde{u}_m^n \in \{0,1\}$, local false alarm and detection probabilities received by the CH_m are given by

$$\begin{aligned}\tilde{P}_{m,n}^d &= \mathcal{P}\left[\tilde{u}_m^n = 1 | u_m^n = 0\right] \mathcal{P}\left[u_m^n = 0 | \mathcal{H}_m^1\right] \\ &+ \mathcal{P}\left[\tilde{u}_m^n = 1 | u_m^n = 1\right] \mathcal{P}\left[u_m^n = 1 | \mathcal{H}_m^1\right] \\ &= t_{1,0}^{n\rightarrow CH_m}\left(1 - P_{m,n}^d\right) + t_{1,1}^{n\rightarrow CH_m} P_{m,n}^d \end{aligned} \tag{3.10}$$

$$\begin{aligned}\tilde{P}_{m,n}^f &= \mathcal{P}\left[\tilde{u}_m^n = 1 | u_m^n = 1\right] \mathcal{P}\left[u_m^n = 1 | \mathcal{H}_m^0\right] \\ &+ \mathcal{P}\left[\tilde{u}_m^n = 1 | u_m^n = 0\right] \mathcal{P}\left[u_m^n = 0 | \mathcal{H}_m^0\right] \\ &= t_{1,1}^{n\rightarrow CH_m} P_{m,n}^f + t_{1,0}^{n\rightarrow CH_m}\left(1 - P_{m,n}^f\right) \end{aligned} \tag{3.11}$$

We define the test statistic for the global decision employed in CH_m as

$$\mathcal{K}_m^{hd} = \sum_{n\in\mathcal{C}_m} \tilde{u}_m^n \underset{\mathcal{H}_m^0}{\overset{\mathcal{H}_m^1}{\gtrless}} \kappa_m^{hd} \tag{3.12}$$

which is known as the k-out-of-N rule where CH_m decides on $\mathcal{H}_m^1$ for PC m if at least κ_m^{hd} of SUs report 1, i.e. $\mathcal{K}_m^{hd} \geq \kappa_m^{hd}$. In the literature, $\mathcal{K}_m^{hd}$ has been considered to be a binomial random variable under the assumption of independent and identically distributed (i.i.d) local detection and false alarm probabilities, i.e. $\tilde{P}_{m,n}^d = \tilde{P}^d$, $\tilde{P}_{m,n}^f = \tilde{P}^f, \forall n$. This conventional approach assumes a cluster consisting of SUs with homogeneous sensing and reporting quality. However, a more general approach is necessary to achieve a more EE-CSS scheme by taking the heterogeneity of SUs into consideration. Hence, having non-identical local detection and false alarm probabilities and reporting path characteristics, $\mathcal{K}_m$ has a *Poisson-Binomial* distribution

by which global detection and false alarm probabilities are given as [79]

$$Q_m^d = \mathcal{P}\left(\mathcal{K}_m^{hd} \geq \kappa_m^{hd} | \mathcal{H}_m^1\right) = \sum_{\kappa_m^{hd}}^{C_m} \sum_{A \in F_{\kappa_m^{hd}}} \prod_{i \in A} \tilde{P}_{m,i}^d \prod_{j \in A^c} \left(1 - \tilde{P}_{m,j}^d\right) \tag{3.13}$$

$$Q_m^f = \mathcal{P}\left(\mathcal{K}_m^{hd} \geq \kappa_m^{hd} | \mathcal{H}_m^0\right) = \sum_{\kappa_m^{hd}}^{C_m} \sum_{A \in F_{\kappa_m^{hd}}} \prod_{i \in A} \tilde{P}_{m,i}^f \prod_{j \in A^c} \left(1 - \tilde{P}_{m,j}^f\right) \tag{3.14}$$

where $F_{\kappa_m^{hd}}$ is the set of all subsets of κ_m^{hd} integers that can be selected from $\{1, 2, 3, \ldots, C_m\}$ where C_m is cardinality of $\mathcal{C}_m$. Since F_{κ_m} has $\binom{C_m}{\kappa_m^{hd}}$ elements, using an efficient method to calculate (3.13) and (3.14) is very important for time complexity, especially when C_m is very large. For this purpose, probability mass function (pmf) and cumulative distribution function of *Poisson-Binomial* random variables can be expeditiously calculated in order of $\mathcal{O}(C_m \log_2 C_m)$ from polynomial coefficients of the probability generating function of $\mathcal{K}_m^{hd}$ [80]. Another important decision phase design parameter is the optimal voting rule selection for clusters. In Section 3.5, the impact of the voting rule on the sensing reliability and energy efficiency will be shown with respect to reporting error and energy consumption.

Regardless of the type of detector employed in SUs, detection performance is a function of the observation duration and sensing channel characteristics. Although obtaining more samples from the primary signal yields more accurate results, it is extravagant with the power consumed in analog to digital conversion and fast Fourier transformation, which are known to be the two major energy demanding components of the receiver [81]. In other words, the more the SUs collect samples the more the energy expended to perform conversion and transformation operations to calculate required test statistics. Depending upon the factors above, the energy spent for sensing and processing per sample is assumed to be identical for each SU, i.e., $E_{m,n}^s = E_s$, $\forall m, n$. It is also assumed that the SUs transmit with identical reporting energy per bit, $E_{m,n}^x = E_x$, $\forall m, n$. To reduce the notational complexity, the optimization variables and parameters related to cluster m is represented in a vectorized form, for example,

$\boldsymbol{s_m} = [S_m^1, \ldots, S_m^{C_m}]^T$. Then, the energy consumed in cluster m is given by

$$E_m^{hd} = E_s \mathbf{1}^T \boldsymbol{s_m} + E_x \mathbf{1}^T \boldsymbol{h_m} \tag{3.15}$$

where $\mathbf{1}$ and $\boldsymbol{h_m}$ denote vector of ones and the number of hops to the CH_m.

P 3.1 $(\boldsymbol{s_m}, \boldsymbol{\varepsilon_m})$:

1: $\min\limits_{\boldsymbol{s_m}, \boldsymbol{\varepsilon_m}} \quad E_m^{hd} = E_s \mathbf{1}^T \boldsymbol{s_m} + E_x \mathbf{1}^T \boldsymbol{h_m}$

2: s.t. $\quad Q_{th}^d \leq Q_m^d(\tilde{\boldsymbol{P}}_{\boldsymbol{d}})$

3: $\quad Q_m^f(\tilde{\boldsymbol{P}}_{\boldsymbol{f}}) \leq Q_{th}^f$

Accordingly, Hard Decision based General Problem (**P 3.1**) formulate the problem of minimizing the total energy consumption induced from sensing and reporting activities of SUs within cluster m for given voting rule κ_m^{hd} and the number of hops $\boldsymbol{h_m}$ calculated from Section 3.3. In **P 3.1**, the objective in Line 1 is a linear function of $\boldsymbol{s_m}$ which needs to be minimized with respect to $\boldsymbol{s_m}$ and $\boldsymbol{\varepsilon_m}$. Lines 2 and 3 are global constraints of cluster m to satisfy required protection of PUs from SU interference and sufficient spectrum utilization to SUs, respectively.

Even if **P 3.1** has a linear objective, it is not in a general convex optimization problem form due to the non-convex nature of the error function in (2.15) and (2.16) where $\text{erfc}(\cdot)$ is a convex and concave non-increasing function for $\text{erfc}(\cdot) \geq 0.5$ and $\text{erfc}(\cdot) \leq 0.5$, respectively. Based on the convex composition rules [34], to have $P_{m,n}^f$ and $P_{m,n}^d$ to be convex and concave functions in (S_m^n, ε_m^n), Hessian matrix of the inside expressions in (2.15) and (2.16) must be negative and positive semi-definite, respectively. However, both of them are neither positive nor negative semi-definite, thus, neither convex nor concave functions.

To alleviate this issue, **P 3.1** is transformed into a *bilevel optimization* with convex upper level problem (ULP) and lower level problem (LLP) based on the following parameterized nature of the **P 3.1**. For a fixed $\bar{\varepsilon}_m^n$ in the feasible set

$$\mathcal{F}_m = \left\{ \varepsilon_m^n, S_m^n \mid Q_{th}^d \leq Q_m^d(\tilde{\boldsymbol{P}}_{\boldsymbol{d}}),\ Q_m^f(\tilde{\boldsymbol{P}}_{\boldsymbol{f}}) \leq Q_{th}^f,\ \forall n \in \mathcal{C}_m \right\},$$

as S_m^n increases, E_m^{hd}, $P_{m,n}^d$, $\tilde{P}_{m,n}^d$, and $Q_m^d(\tilde{\boldsymbol{P}}_{\boldsymbol{d}})$ increase, $\forall n \in \mathcal{C}_m$. Hence, optimum E_m^{hd} is attained at the point $Q_m^d(\tilde{\boldsymbol{P}}_{\boldsymbol{d}}) = \bar{Q}_{m,n}^d$. For a fixed $\bar{S}_m^n$, on the other hand, $P_{m,n}^f$, $P_{m,n}^d$, $\tilde{P}_{m,n}^f$,

$\tilde{P}^d_{m,n}$, $Q^f_m(\tilde{\boldsymbol{P}}_{\boldsymbol{f}})$, and $Q^d_m(\tilde{\boldsymbol{P}}_{\boldsymbol{d}})$ increase as ε^n_m decreases. Noting that E^{hd}_m is not a function of ε^n_m, increase of $Q^f_m(\tilde{\boldsymbol{P}}_{\boldsymbol{f}})$ is bounded by Q^f_{th}, thus, the minimum feasible ε^n_m at $Q^f_m(\tilde{\boldsymbol{P}}_{\boldsymbol{f}}) = \bar{Q}^f_m$. In this fashion, the $\boldsymbol{\varepsilon_m}$is obtained by parameterizing $\boldsymbol{s_m}$ in the LLP and achieve the minimum E^{hd}_m by parameterizing $\boldsymbol{\varepsilon_m}$ in the ULP.

P 3.1-ULP ($\boldsymbol{s_m}$ — $\bar{\boldsymbol{\varepsilon}}_{\boldsymbol{m}}$) :

1: $\min_{\boldsymbol{s_m}}$ $\quad E_m = E_s \mathbf{1}^T \boldsymbol{s_m} + E_x \mathbf{1}^T \boldsymbol{h_m}$

2: s.t. $\quad -\log(Q^d_m(\tilde{\boldsymbol{P}}_{\boldsymbol{d}})) \leq -\log(Q^d_{th})$

3: $\quad -\boldsymbol{P_d}(\boldsymbol{s_m}, \bar{\boldsymbol{\epsilon}}_{\boldsymbol{m}}) \preceq -0.5$

4: $\quad {}^{\boldsymbol{3A\bar{\varepsilon}_m}}/_{\boldsymbol{B}} \preceq \boldsymbol{s_m} \preceq {}^{\boldsymbol{3A\bar{\varepsilon}_m}}/_{\boldsymbol{B-\rho_m}}$

5: $\quad \bar{\boldsymbol{\varepsilon}}_{\boldsymbol{m}} \in \mathcal{S}(\boldsymbol{s_m})$

P 3.1-LLP ($\boldsymbol{\varepsilon_m}$ — $\bar{\boldsymbol{s}}_{\boldsymbol{m}}$) :

1: $\min_{\boldsymbol{\varepsilon_m}}$ $\quad \left|\log(Q^f_{th}) - \log(Q^f_m(\tilde{\boldsymbol{P}}_{\boldsymbol{f}}))\right|$

2: s.t. $\quad \boldsymbol{P_f}(\bar{\boldsymbol{s}}_{\boldsymbol{m}}, \boldsymbol{\epsilon_m}) \preceq 0.5$

where $\preceq$ denotes element wise non-equality. In **P 3.1-ULP**, the total energy consumption of cluster m is minimized for a given $\bar{\boldsymbol{\varepsilon}}_{\boldsymbol{m}}$ which is obtained by exploiting the optimal solution set of **P 3.1-LLP** for a given $\bar{\boldsymbol{s}}_{\boldsymbol{m}}$, $\mathcal{S}(\boldsymbol{s_m}) = \{\bar{\boldsymbol{\varepsilon}}_{\boldsymbol{m}} \mid \boldsymbol{\varepsilon_m} \in \text{argmin}\{\mathcal{F}_m\}\}$. The constraint in Line 2 is the standard convex form of the first constraint in **P 3.1**. Constraints in Line 3 and 4 are introduced to preserve the convexity of the problem. In **P 3.1-LLP**, the minimum feasible $\boldsymbol{\varepsilon_m}$ is obtained for given $\boldsymbol{s_m}$ at the point of $Q^f_m(\tilde{\boldsymbol{P}}_{\boldsymbol{f}}) = Q^f_{th}$. Once more, the only constraint is introduced to preserve the convexity of the problem, and interested readers are referred to Appendix A.1 for a more detailed convexity analysis.

3.4.1.3 Quantized Soft Decision Fusion Based CSS

As a remedy for the communication overhead which stems from reporting the raw LLR values directly to the CH, quantization is an attractive tool to achieve more accurate sensing yet a reasonable CCC overhead. In this regard, while [13] employs a *Maximum Output Entropy* (MOE) Quantizer to maximize the output entropy, the authors of [66] implement a *Lloyd-Max*

(LM) quantizer to minimize the local quantization distortion and shows that LM provides a better performance than MOE.

Denoting the probability distribution function (pdf) of Λ_m^n as $f_{\Lambda_m^n}(x)$, an L_m-level quantizer divides x by L_m-1 thresholds, which is denoted by the set $\Delta_m^n = \left\{\Delta_{m,n}^j | 1 \leq j \leq L_m\right\}$, into L_m non-overlapping intervals, which is denoted by the set $\mathcal{I}_{m,n}^j \in \left(\Delta_{m,n}^{j-1}, \Delta_{m,n}^j\right]$, $j = 2, 3, \ldots, L_m - 1$. These intervals are represented by the quantization level set $\mathcal{L}_m^n = \left\{\ell_{m,n}^j | 1 \leq j \leq L_m\right\}$ which comprises of discrete outputs of the quantizer function $q(\cdot)$. By doing so, the pdf is converted into a probability mass function (pmf) such that the observed Λ_m^n fall into an interval with the probability calculated by the area of the interval under $f_{\Lambda_m^n}(x)$, i.e.,

$$p_{\hat{\Lambda}_m^n}(\ell_{m,n}^j) = \mathcal{P}\left(\Lambda_m^n \in \mathcal{I}_{m,n}^j\right) = \int_{\Delta_{m,n}^{j-1}}^{\Delta_{m,n}^j} f_{\lambda_m^n}(x)\, dx \tag{3.16}$$

However, pmf of the received quantization levels, $p_{\tilde{\Lambda}_m^n}(\ell_{m,n}^i)$, does not follow the the same distribution any more because of the imperfect reporting. That is, a quantization level received at the CH may result from any transmitted level at the source. Taking all possibilities into account, the $p_{\tilde{\Lambda}_m^n}(\ell_{m,n}^i)$ can be written in terms of the end-to-end transition matrix entries as follows

$$p_{\tilde{\Lambda}_m^n}(\ell_{m,n}^i) = \sum_{j=1}^{L} \mathcal{P}(\hat{\Lambda}_m^n = \ell_{m,n}^j)\mathcal{P}(\hat{\Lambda}_m^n = \ell_{m,n}^i | \hat{\Lambda}_m^n = \ell_{m,n}^j) = \sum_{j=1}^{L} \mathcal{P}(\hat{\Lambda}_m^n = \ell_{m,n}^j)\ t_{i,j}^{n \rightsquigarrow n'} \tag{3.17}$$

After collecting all reports, the CH sums $\tilde{\Lambda}_m^n$s and compare the global test statistic $\mathcal{K}_m^{sd}$ with a threshold to decide on the channel occupancy as follows

$$\mathcal{K}_m^{sd} = \sum_{n=1}^{C_m} \tilde{\Lambda}_m^n \underset{\mathcal{H}_m^0}{\overset{\mathcal{H}_m^1}{\gtrless}} \kappa_m^{sd} \tag{3.18}$$

It is worth noting that the global test statistic is the summation of C_m independent discrete random variable, thus, its pmf can be derived using convolution sum of marginal pmfs given in (3.17) [82]. Therefore, the support values of global pmf is the Cartesian product of reporting SUs' quantization levels, i.e. $\mathcal{L}_m = \mathcal{L}_m^1 \times \cdots \times \mathcal{L}_m^{C_m}$. Consequently, the global false alarm and detection probabilities are given as

$$Q_m^d = \mathcal{P}\left(\mathcal{K}_m^{sd} \geq \kappa_m^{sd} | \mathcal{H}_m^1\right) \tag{3.19}$$

$$Q_m^f = \mathcal{P}\left(\mathcal{K}_m^{sd} \geq \kappa_m^{sd} | \mathcal{H}_m^0\right) \tag{3.20}$$

Accordingly, the Soft Decision based General Problem (**P 3.2**) formulate the minimization problem of the total energy consumption induced from sensing and reporting activities of SUs within cluster m for a given quantization bit number b_m. By use of FSST, **P 3.2** can be written as

$$\underline{\textbf{P 3.2 } (S_m, \kappa_m^{sd} | b_m) \textbf{ :}}$$

$$\begin{aligned} 1: \quad & \min_{S_m, \kappa_m^{sd}} && E_m^{sd} = C_m E_s S_m + E_x b_m \mathbf{1}^T \boldsymbol{h_m} \\ 2: \quad & \text{s.t.} && Q_{th}^d \leq Q_m^d \\ 3: \quad & && Q_m^f \leq Q_{th}^f \end{aligned}$$

where Q_m^f and Q_m^d are monotonically decreasing with κ_m^{sd} while Q_m^d is monotonically increasing with S_m for a given κ_m^{sd}, $\bar{\kappa}_m^{sd}$. Then, by parameterizing the detection threshold as

$$\bar{\kappa}_m^{sd} = \min_{x \in \mathcal{L}_m} \left\{ \mathcal{P}(\mathcal{K}_m^{sd} > x \mid \mathcal{H}_m^0) \leq \bar{Q}_m^f \right\}, \tag{3.21}$$

the optimum value is attained at $Q_m^d = \bar{Q}_m^d$. Due to the linearity of the objective and monotonic nature of the cumulative distribution functions, **P 3.2** can simply be solved by *Golden Section Method*. Even though setting a fixed sample size for each SU and minimizing the energy expenditure is optimal in a homogeneous cluster, this may not always yield an optimal result in a heterogeneous cluster. Under the venue of heterogeneous cluster, we propose a weighted sample size test (WSST) approach where total sample number under FSST is weighted based on SUs' autocorrelation coefficients as follows

$$S_m^n = C_m S_m \frac{\rho_m^n}{\sum_{n \in \mathcal{C}_m} \rho_m^n} \tag{3.22}$$

In other words, instead of sharing the total $C_m S_m$ number of samples equally as in FSST, SUs share it proportional to their sensing quality, ie. ρ_m^n. Even if it may not be the optimal solution, numerical results shows a significant performance enhancement.

3.4.2 Macro Perspective: Inter-Cluster Optimization

3.4.2.1 Background on Multi-Objective Evolutionary Algorithms

Multi-objective optimization (MO), a.k.a multi-criteria or vector optimization, is a process of optimizing a collection of objective functions systematically and simultaneously . Unlike the

single-objective optimization, there is no single global solution to a multi-objective problem and it is important to determine a set of solutions which fit a criteria to be the optimum. Such a point is predominantly known as *Pareto optimal* [83], definition of which is given as follows:

Definition 3.1: *Pareto optimal: If we denote the decision vector as* $\boldsymbol{x}$ *, the feasible decision space as* $\boldsymbol{X}$*, and the objective function vector as* $\boldsymbol{F}(\boldsymbol{x})$*, a point* $\boldsymbol{x}^{\star} \in \boldsymbol{X}$ *is Pareto Optimal iff there does not exists any other feasible point* $\boldsymbol{x} \in \boldsymbol{X}$ *such that* $\boldsymbol{F}(\boldsymbol{x}) \leq \boldsymbol{F}(\boldsymbol{x}^{\star})$ *and* $F_j(\boldsymbol{x}) \leq F_j(\boldsymbol{x}^{\star})$ *for at least one function.*

For a given problem, Pareto optimal set might be consisting of multiple Pareto optimal points. In this case, the designer should distinguish the differences between the optimal points and make a further decision based on the priority of the objective functions which is generally problem specific. We note that Pareto optimal points are also referred to as *non-dominated* points due to the intuition of condition given at the end of the Definition 3.1.

Evolutionary algorithms (EA), which are generic population based meta-heuristic approaches inspired by biological evolution, were shown to be performing well for many MO problems if it is adapted and applied carefully. In particular, genetic algorithm is one of the most popular EAs the specific mechanics of which adopts the terminology of microbiology and genetic operations. For example, *population* represents a set of solutions and a *generation* represents an iteration. While a *chromosome* is comparable to a single candidate solution, a *gene* is simply a single entry of a chromosome [84].

Since they do not need the gradient information, EA can be effective regardless of the objective functions and constraints. EAs combine the use of random numbers and information from previous generations to evaluate and improve population of solutions. Encoding is the first step of the implementation, which can be described as determination of the form of a chromosome. Following the proper design of the encoding scheme, an initial population of chromosomes is randomly generated, which is the first generation, and three essential genetic operations are iteratively applied to this initial population: *mutation*, *crossover*, and *selection*.

As being analogous to the terminology in biology, crossover is a way of introducing variations into the population of designs by mixing two different populations. While mixed populations are

called *parent*, resulting new members of the population right after the crossover operation are called *children*. Deciding on the properties of the crossover operation is a heuristic design issue and there exist many ways to do it including tournament selection, rank selection, truncation selection, and so on. Mutation operation, on the other hand, is introduced for maintaining the genetic diversity from one generation to the next. It is also analogous to its biological counterpart and randomly alters one or more gene values in a chromosome from its initial state. For example, in case of a binary valued chromosome, it switches some of the genes from zero to one or vice versa. Selection involves choosing the chromosomes from current generation to be employed in the next generation based on the fitness value which is simply the value of the objective function for a given design vector, (i.e., chromosome).

When it comes to applying genetic algorithms into multi-objective problems, it is required to determine how to consolidate the notion of Pareto optimality, validate the constraints and decide which potential members should be passed on to the next generation. Hereupon, we consider and employ NSGA-II which is a fast and elitist multi-objective genetic algorithm (MOGA) [85] where a random parent population P_0 is first created for the initial generation and the usual genetic operators are used to create an offspring population Q_0 of size O. Since elitism compares a current population with the previously found Pareto set, the t^{th} generation is described different from the initial one as shown in Figure 3.3:

First, a combined population $R_t = P_t \cup Q_t$ of size $2O$ is formed by merging P_t and Q_t and the population R_t is sorted according to non-domination. Then, the best O members of the members are selected to be the parents of the next generation, P_{t+1}, using the crowded-distance operator. After that, selection, crossover and mutation operators are executed on P_{t+1} to create the offspring population of the $(t+1)^{th}$ generation, Q_{t+1}. Omitting the further details of NSGA-II, interested readers are referred to [85] for broader and in-depth explanations.

3.4.2.2 Multi-Objective Clustering Problem Formulation

Even though the clustered CSS paradigm is highly exploited in the literature for sensing a single channel, the multi-channel case, which requires clustering potential SUs to sense multiple PCs with the consideration of energy-throughput efficiency objectives along with the sensing

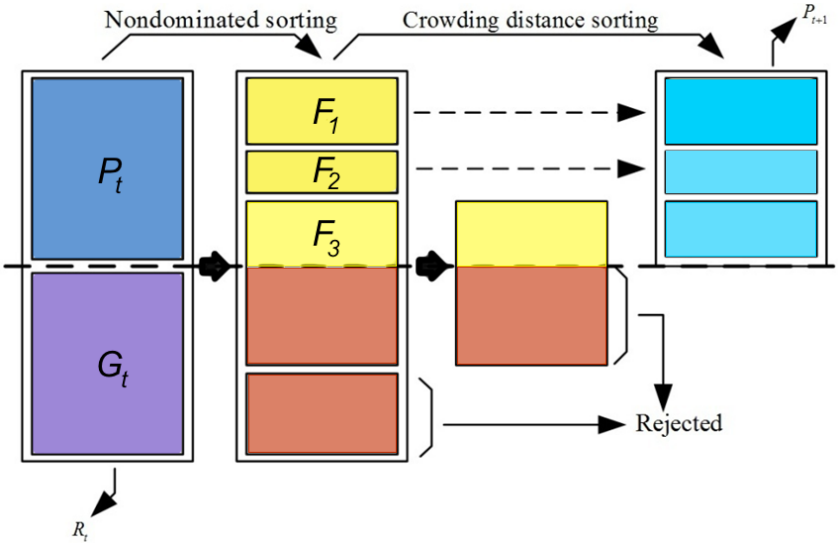

Figure 3.3: Non-dominated Sorting Genetic Algorithm-II procedure

reliability constraints, has not been studied in depth yet. For a given sensing period, if there exists N SUs available to help with sensing and there exists M potential PCs to sense, a clustering of the SUs is required to minimize/maximize the intra-cluster and balancing the inter-cluster energy expenditure/throughput subject to the cooperation reliability constraints. The indicator function $\mathbb{I}_m(n)$ is defined to represent the membership of SU n in cluster m. For each cluster, three types of objective vectors are defined to be minimized: $\mathbf{F} \in \mathbb{R}^M$, $\mathbf{G} \in \mathbb{R}^M$, and $\mathbf{H} \in \mathbb{R}^2$ with elements

$$F_m = E_m, \ 1 \leq m \leq M \tag{3.23}$$

$$G_m = \max_{n \in \mathcal{C}_m} S_m^n, \ 1 \leq m \leq M \tag{3.24}$$

$$H_1 = \max_m F_m - \min_m F_m, \ 1 \leq m \leq M \tag{3.25}$$

$$H_2 = \max_m G_m - \min_m G_m, \ 1 \leq m \leq M \tag{3.26}$$

where F_m denotes the intra-cluster total energy consumption minimization within cluster m, G_m denotes the intra-cluster maximum sensing time minimization within cluster m, such that the time available after sensing phase is maximized for maximizing the achievable throughput. H_1 and H_2 handle the inter-cluster total energy consumption and throughput balance, respec-

tively. Based on these objectives, the multi-objective clustering Algorithm 3.1 which clusters the network is formulated as follows:

Algorithm 3.1 : MOCO

1: Min $\mathbf{F}$, $\mathbf{G}$, $\mathbf{H}$
2: s.t. $\sum_{m=1}^{M} \mathbb{I}_m(n) \leq 1, \forall n$
3: $\sum_{n=1}^{N} \mathbb{I}_m(n) \geq 1, \forall m$
4: $Q_{th}^d \leq Q_m^d, \forall n$
5: $Q_m^f \leq Q_{th}^f, \forall n$
6: $\rho_{m,n} \leq \rho, \forall m, n$

Line 2 enforces that an SU can sense at most one channel during a sensing period. Line 3 makes sure that each PC is sensed by at least one SU. Lines 4 and 5 are global decision probability constraints need to be satisfied for reporting and decision phase reliability. The constraint in Line 6 on the sensing time is especially beneficial to take SUs with unnecessarily low sensing quality out of consideration to reduce the amount of time in evaluating the fitness functions.

As mentioned earlier, Algorithm 3.1 is a multi-objective non-linear combinatorial optimization problem which is well known to be NP (Non-deterministic Polynomial-time)-hard. Since it has conflicting objectives, there may exists a set of *non-dominated solutions* by which none of the objective functions can be improved without degrading some of the other objective values. Finding non-dominated solutions of such a combinatorial problem requires an infeasible computation time, especially for large numbers of SUs and PCs. Therefore, employing meta-heuristic methods to obtain a sufficient solution within a reasonable time frame is preferable in practice. In this respect, chromosome encoding scheme shown in Table 3.1 is exploited. Each chromosome vector represents a macro perspective solution, $\mathbf{s} \in (0 \cup \mathbb{Z})^{+N}$. whose indices (genes) represent SUs and corresponding values of the vector represent the cluster to which SUs are assigned. That is, $\boldsymbol{s}$ is a clustering instance of the network as shown in Figure **??** and we need to evaluate the micro perspective to obtain its corresponding fitness value. Note that if a gene has a value of 0, then the corresponding SU is selected to sense no PC.

Table 3.1: A random chromosome representation for solution **s**

PUs	$M-5$	M	4	$\cdots$	m	$\cdots$	2	$M-1$
SUs	1	2	3	$\cdots$	n	$\cdots$	$N-1$	N

Therefore, the constraint in Line 2 which requires an SU to be assigned at most one PU is already satisfied. For the constraint in Line 3, chromosomes are checked at the end of every genetic operation and genes violating these constraints are replaced with a proper value randomly. Constraints in Line 4 and 5 are handled directly by the method proposed in NSGA-II. At each generation, the indices of solution **s** which have common values is grouped into the same cluster, and evaluate fitness functions and constraint values following the steps detailed in Section 3.4. Finally, solutions are ranked and sorted based on their fitness value to create the next generation. This iterative procedure is repeated until a target generation size, $\mathbb{G}$, is satisfied.

3.5 Results and Analysis

The primary network is assumed to be using OFDM technology as it is a key technique with a broad range of employment in today's wireless systems. Due to the practical and theoratical considerations, a symbol and the cyclic prefix length of 32 and 8 is exploited, respectively. Thereupon, a single OFDM block is enough to invoke the central limit theorem to keep results consistent with the theory. All simulation results were obtained and plotted using Matlab.

Table 3.2: Default parameters used for obtaining results

Par.	**Value**	**Par.**	**Value**	**Par.**	**Value**
E_s	$1\mu J/sample$	W_m	$1MHz$	σ_z^2	1
E_x	$0.07mJ/bit$	T_c	8	T_d	32
N	40	M	4	$\mathbb{P}$	50
Q_{th}^d	0.99	Q_{th}^f	0.01	$\mathbb{G}$	20
T	2	$\phi_{m,n}^r, \phi_{m,n}^t$	1	θ_m	3

3.5.1 Cluster Head Selection

To demonstrate the performance of proposed multihop reporting and the CH selection procedure, the total reporting error is depicted in Figure 3.4 for the network scenario given in Figure 3.1. In Figure 3.4, the green dashed line with star markers shows the total reporting error caused by multihop technique for each cluster based on the clustering topology in Figure 3.1. On the other hand, the solid red line with square markers and the dashed red lines with diamond markers show the worst and the best case of singlehop technique, respectively. Comparing to the best case singlehop reporting, a superior performance is obtained through the proposed method.

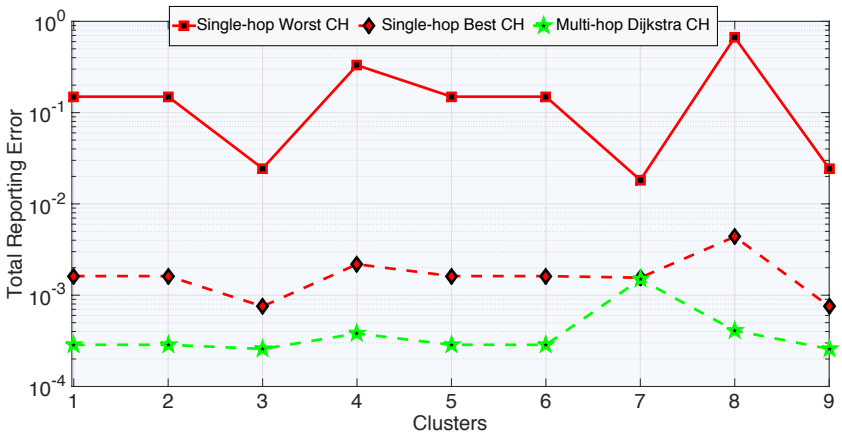

Figure 3.4: Comparison between singlehop and multihop approaches

However, Figure 3.4 only considers a single network topology realizations and it is necessary to evaluate the performance over a large number of randomly generated network topologies. Therefore, a cluster of 10 SUs is randomly distributed over a 200 $m \times 200$ m area. Direct reporting links among SUs are modeled as Rayleigh flat fading channels with random channel gains along with the simplified path loss model with random path loss exponents, and a constant reference distance, $d_0 = 20m$. Using 5000 random cluster realizations, we have calculated the total reporting error induced from the proposed multihop CH selection and the singlehop CH selection method where an SU with the minimum singlehop total reporting error is selected to be the CH. Results show that the total/average BEP of proposed CH selection and multihop

reporting method outperform the total/average BEP of single hop case by about an order of magnitude which can be observed from the Figures 3.8 and 3.10 in the following subsections.

3.5.2 CSS with Hard Decision Fusion

To analyze the inherited features of the proposed HDF-based CSS, a heterogeneous cluster is first considered such that it consists of 5 SUs with SNRs $[0, -5, -15, -20, -25]$ dB. Since a comparison of the traditional and proposed approaches is necessary, the reporting error is omitted in this example for clarity. Using traditional and proposed HDF with majority voting rule ($\kappa_{hd} = 3$) and global detection and false alarm probability targets of $Q_{th}^{d} = 0.99$ and $Q_{th}^{f} = 0.01$, respectively, obtained results are demonstrated in Figure 3.5.

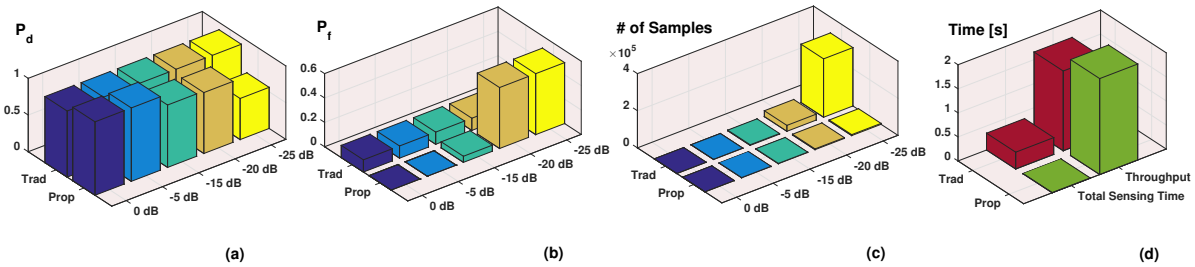

Figure 3.5: A simple heterogeneous cluster instance to compare traditional and proposed HDF-based CSS.

In subfigures (a) and (b), while traditional approach enforces SUs to report with local detection and false alarm probabilities of 0.9 and 0.1, respectively, proposed method enforces SUs with relatively high SNRs to have perfect detection and false alarm probabilities. For the values in (a) and (b), subfigure (c) demonstrates the sensing duration in terms of the number of samples where it clearly reveals the fact that enforcing low SNR SUs to have identical local detector performance requires large numbers of samples. Thus, this dominantly effects the total energy consumption and the achievable throughput for the cluster. Based on subfigures (a)-(c), subfigure (d) shows the superior performance of the proposed method in terms of the total sensing duration of SUs and available time left for secondary data transmission.

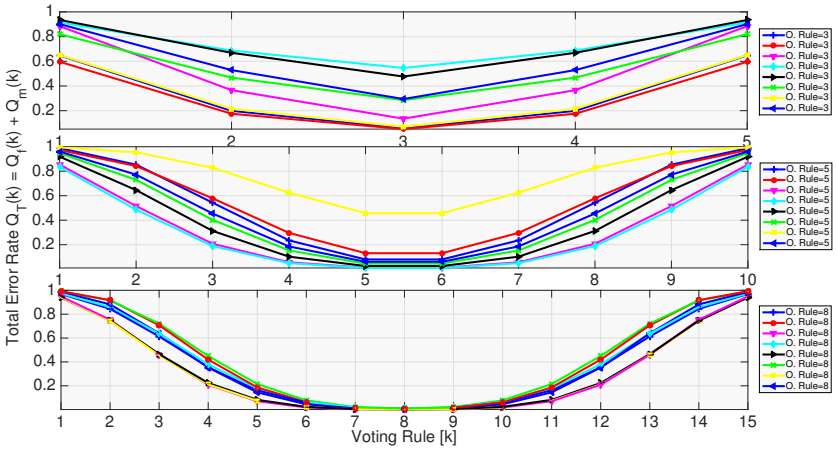

Figure 3.6: Total error rate vs different voting rules and cluster sizes

To show the effect of the voting rule on the reliability of the global decisions, the total sensing error rate is defined as the summation of the global false alarm and misdetection probabilities. The total sensing error rate is plotted in Figure 3.6 for three different cluster sizes (5, 10, 15), with eight different path error sets, where each of the error set is randomly selected between 10^{-4} to 0.3. The optimal voting rule is shown in the legend for each line and cluster size. As it can be seen in Figure 3.6, majority voting rule is the optimal case which is also shown to be the most energy efficient voting rule in upcoming results. Its energy efficiency is intuitive since in a non-optimal voting rule selection SUs have to have more accurate local results to compensate the non-optimality of the voting rule to achieve target global detection and false alarm rates. Thus, this directly increases the number of samples and expended energy for the sensing.

Next, the effect of the voting rule and the imperfect reporting is analyzed in terms of the required additional energy cost to the ideal case. For a cluster size of $N = 5$, Figure 3.7 depicts the energy loss induced from the non-ideality of the HDF-based CSS for different voting rules $K = 1, \ldots, 5$ with respect to average BEP of the single hop reporting case. It is important to remind that SUs experience different channel sensing quality of the target PC, so that, SNRs and autocorrelation coefficients of SUs are not identical. In this respect, there are two sets of voting rule results in Figure 3.7, one for traditional K-out of-N rule using the

Binomial distribution, and another for the proposed K-out of-N using the *Poisson-Binomial* distribution. It can clearly be seen that the proposed method which takes the sensing quality heterogeneity of the SUs into account outperforms the traditional one in terms of the energy loss. The results also show that the majority voting is the most energy efficient voting scheme under the two cases.

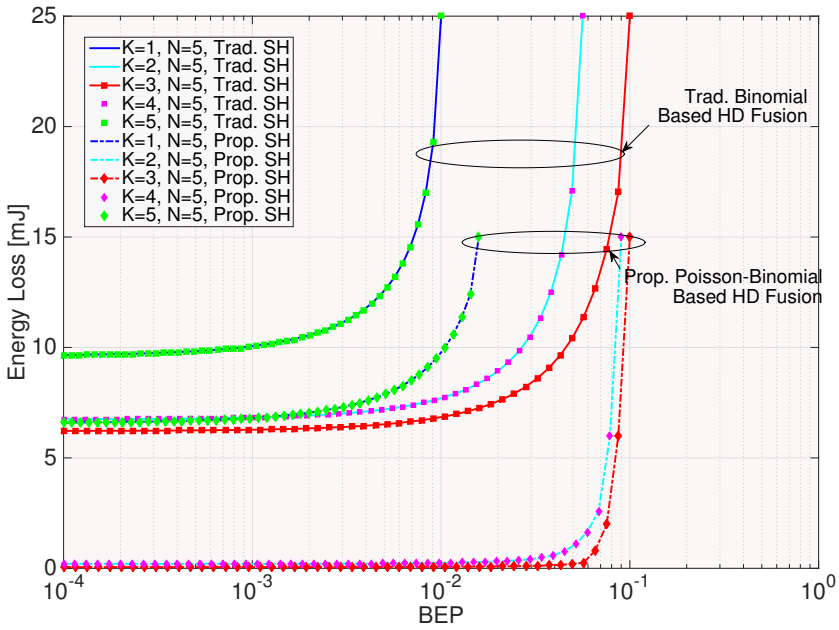

Figure 3.7: Comparison of energy loss caused from traditional and proposed HDF-based schemes using singlehop reporting.

The effect of the reporting error on the energy loss for both cases can also be observed from Figure 3.7. For $K = 3$, for example, energy loss of traditional approach is not affected by BEP until 10^{-3}, then, it starts to increase as the BEP increases. After a point, around 0.1, energy loss goes to infinity, which is known as the *BEP wall* and its existence has been shown first in [86] for SNR loss under the traditional K-out of-N fusion rule. The majority voting rule also gives the best performance in terms of the robustness against the BEP wall compared to the other voting rules. In addition to energy efficiency, the proposed *Poisson-Binomial* based approach exhibits a more stable performance against the BEP wall since it is not affected by the BEP increase up to 0.05.

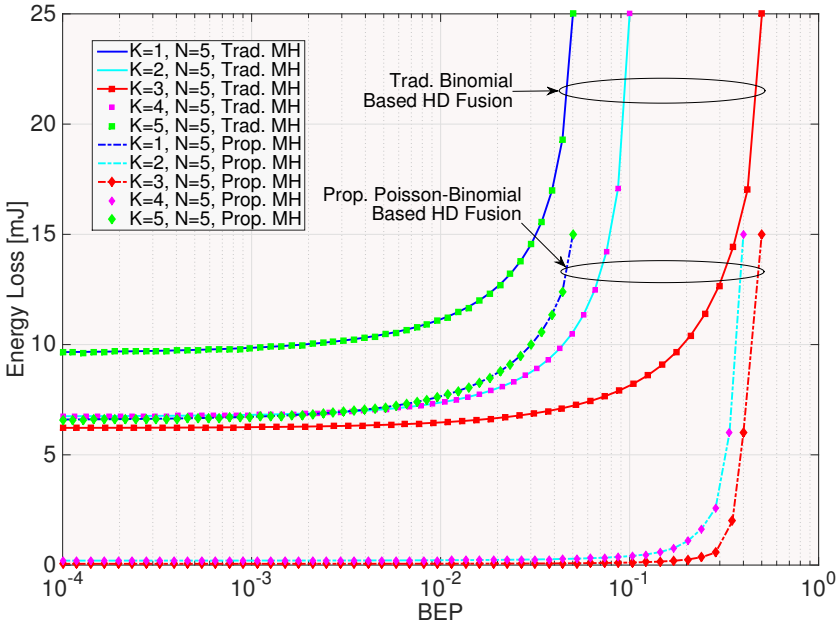

Figure 3.8: Comparison of energy loss caused from traditional and proposed HDF-based schemes using proposed multihop reporting and CH selection method.

Likewise, Figure 3.8 shows the performance of the traditional and proposed methods using multihop reporting and the best CH selection algorithm given in Section 3.3. It is obvious that the proposed method increases the robustness of the energy loss against the BEP wall effect by about an order of magnitude, where the BEP wall is located at 0.5.

3.5.3 CSS with Soft Decision Fusion

For a cluster size of 5, Figure 3.9 depicts the energy loss induced from the non-ideality of the quantized SDF with respect to the average BEP of the single hop reporting case. To put an evident comparison between hard and soft decision fusion, the best case of the HDF is also plotted. For the quantized SDF, there are two different sets of results: one for the FSST approach, and another for the WSST where sensing duration of SUs are weighted based on their sensing quality metrics. The single bit LM quantizer's FSST energy loss performance is shown to be superior to the best case HDF. On the other hand, single bit WSST gives a better energy efficiency than the $4-bit$ FSST scheme. Similar to Figure 3.8, the benefit of the

proposed multihop reporting based CH is apparent in terms of the BEP wall in Figure 3.10 where the BEP wall is located at 0.5.

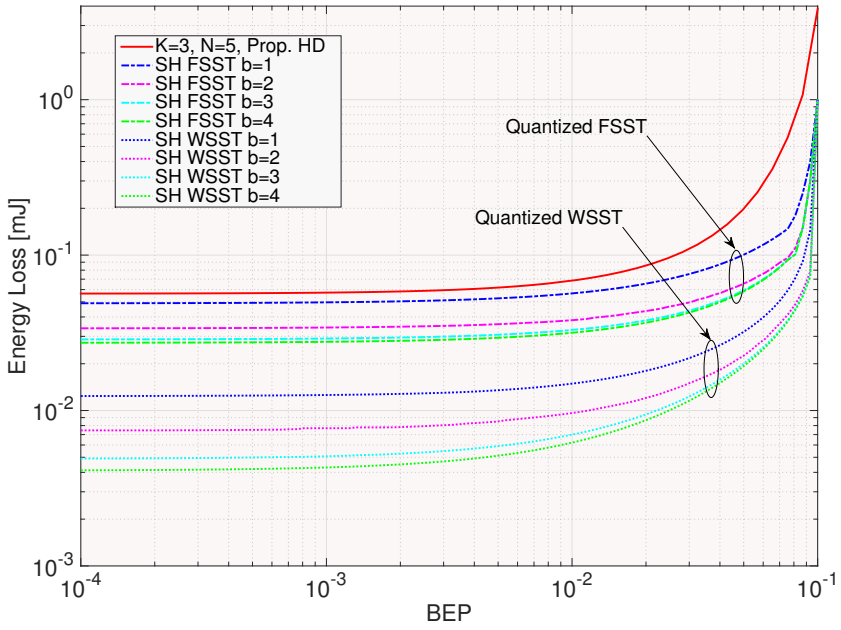

Figure 3.9: Comparison of energy loss caused from traditional and proposed quantized SDF-based schemes using singlehop reporting.

3.5.4 Multi-Objective Clustering Optimization

3.5.4.1 MOCO with a Coarse Micro Perspective

To begin with, MOCO is first addressed using a coarse micro perspective where each SU is enforced to have a local detection and false alarm probabilities 0.9 and 0.1, respectively. As shown in Figure 3.5, coarse approach simply neglects the heterogeneity of SUs sensing quality by enforcing each of them to have identical local detector performance. However, it still takes care of the proposed multihop reporting and the best CH selection presented in Section 3.3 and employs the Poisson-Binomial distributions to handle the non-identical reports of SUs due to different reporting errors. Indeed, this was the first attempt to solve MOCO problem [78] and the micro perspective has been kept simple to examine the macro perspective and multihop reporting more in depth.

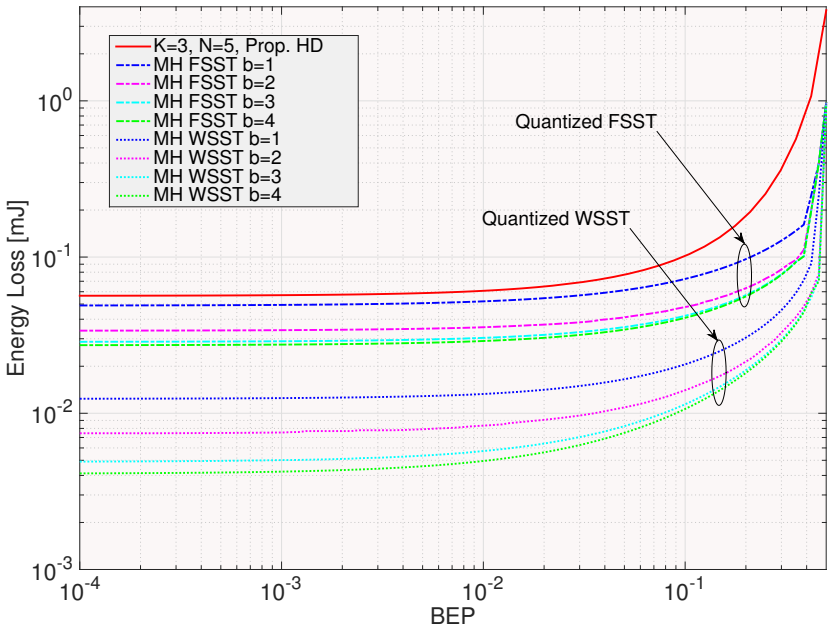

Figure 3.10: Comparison of energy loss caused from traditional and proposed quantized SDF-based schemes using proposed multihop reporting and CH selection method.

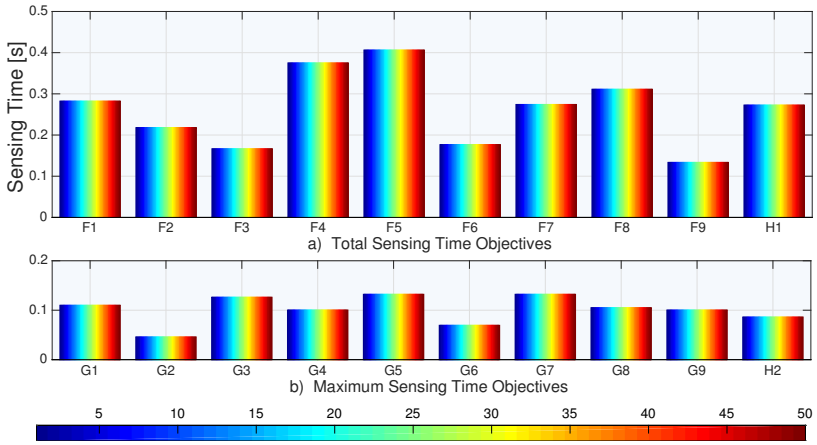

Figure 3.11: MOCO Results for coarse micro perspective.

For simulation results, the CRN shown in Figure **??** is considered where SUs are randomly distributed over an area of 2 $km \times 2$ km. Without loss of generality, PUs are located in certain positions for simulation and demonstration easiness as in Figure 3.12. For the local detectors, the energy detector is adopted for simplicity using the equations (2.6) and (2.9) for false alarm and detection probabilities, respectively. Throughout the simulation, the values in Table 3.2 in [78] are employed, unless it is explicitly stated otherwise. Since the coarse micro perspective focuses on hard decision fusion, reporting energy cost is neglected in the fitness functions. Accordingly, the results for MOCO objective values and clustering topology of the network using NSGA-II are shown in Figure 3.11 and Figure 3.12, respectively. Colorbar of Figure 3.11 ranges from 1 to 50 represents the populations of the final generation.

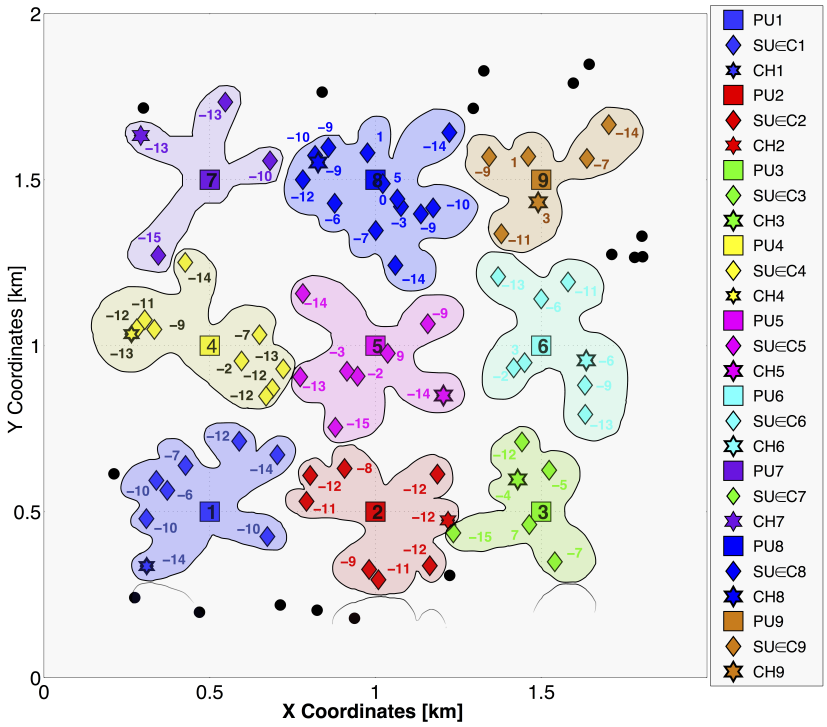

Figure 3.12: Clustered network topology based on results in Figure 3.11. Numbers next to the SUs show the SNR values of SUs for the PU 1. SUs selected to a cluster have a diamond shape with the color of the PU which is sensed by the cluster. The cluster heads of clusters are shown in hexagonal shapes.

In Figure 3.12, the amoeba-like shapes with opaque colors represent the clusters where square shape represents the PU with the number inside, diamond shapes represent cluster

members along with SNR values in dB units, and hexagon shapes represent CHs selected by the technique proposed in this paper. There is no need to compare the coarse and the proposed micro perspectives since it is obvious that the proposed one handle the heterogeneity in a more sophisticated and efficient way as it can be seen from Figure 3.5.

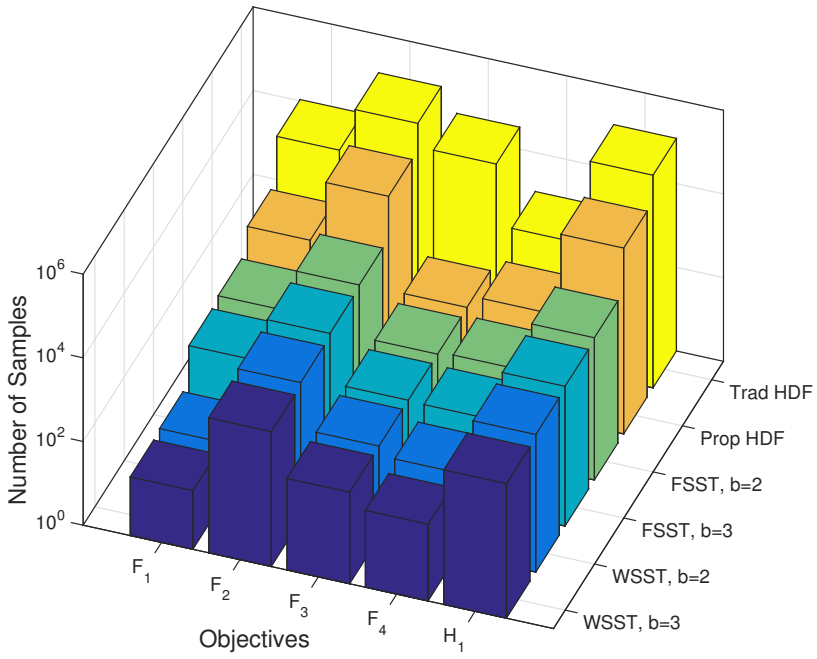

Figure 3.13: MOCO results for $\mathbf{F}$ and H_1 for different CSS schemes.

3.5.4.2 MOCO with Proposed Micro Perspective

For the population and generation sizes given in Table 3.2, the results for MOCO objective values of the network using NSGA-II are shown in Figure 3.13 and 3.14. Figure 3.13 presents the intra-cluster total energy consumption (F_1-F_4) and the inter-cluster objective H_1 with respect to different types of HDF and SDF based CSS schemes. The pattern in previous comparison among CSS schemes is also observed Figure in 3.13 where the $z-axis$ is logarithmically scaled. Figure 3.14 shows the intra-cluster achievable throughput (G_1-G_4) and the inter-cluster objective H_2 with respect to different types of HDF and SDF based CSS schemes. Again, $z-axis$ is logarithmically scaled and observed relations are parallel to the pattern in Figure 3.13.

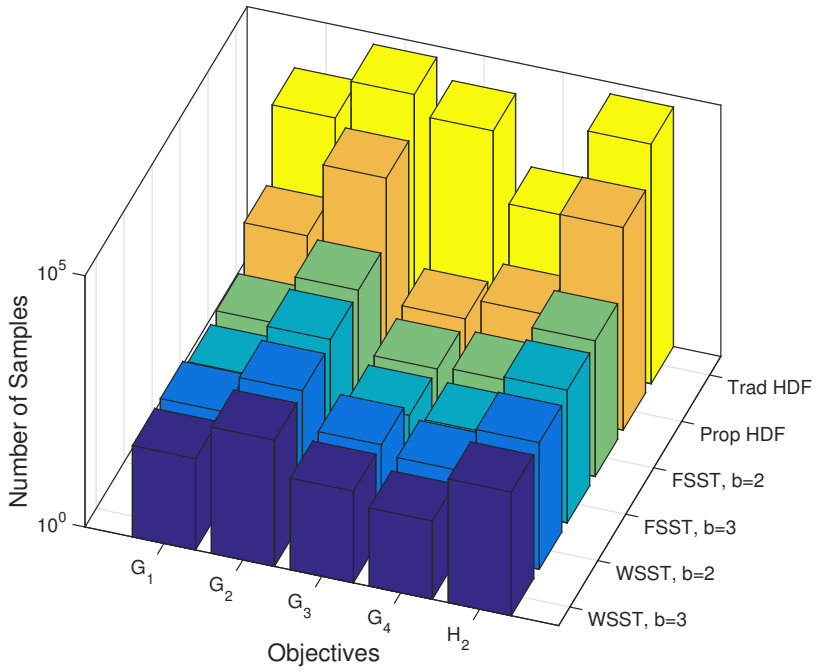

Figure 3.14: MOCO results for $\mathbf{G}$ and H_2 for different CSS schemes.

3.6 Chapter Summary

In this chapter, energy and throughput efficient clustering is studied from the micro and macro perspectives. Using the multihop diversity, a procedure is developed to find the best CH and optimal routing paths from SUs to CH, which is shown to be better in terms of the robustness to the reporting channel imperfection and energy cost. Results showed that the proposed multihop reporting and CH selection procedure mitigate the BEP wall phenomenon. From the micro perspective, it has been revealed that consideration of the sensing and reporting heterogeneity under both HDF and SDF based CSS has a significant impact on the intra-cluster energy consumption and achievable throughput. The proposed novel HDF scheme tended to enforce SUs with relatively high SNRs to have a perfect local detection performance while the low SNR SUs' local detection is released. On the other hand, the proposed WSST method, which decides on SUs' sample sizes proportional to their SNRs, was shown to have a much more energy efficient performance than the well known FSST for SDF schemes. For the macro

perspective, on the other hand, the MOCO problem is formulted and solved using NSGA-II to obtain network wide fair energy and throughput efficient partitioning of SUs.

CHAPTER 4. ENERGY & SPECTRUM EFFICIENT CSS SCHEDULING

4.1 Overview

Although clusters are formed for each PC without any exemption in Chapter 3, such an approach may not be both spectrum and energy efficient since some PCs may require extensively large amounts of sensing energy even if they provide poor quality of service due to their low apriori probability of being idle. In such a case, an optimal energy and spectrum efficient system may rather not sense that PC. Furthermore, MOCO obligates SU to have the association with only one cluster or PC at a time. However, if SUs have desirable sensing qualities on several PCs, assigning them to sense more than one channel might be more spectrum efficient since the secondary network naturally seek to discover as much as possible free bands. At this stage, channel switching delay and energy overhead should be considered in energy and throughput efficiency calculations since an SU need to reconfigure its radio parameters to execute sensing in a particular PC. Consequently, an energy and spectrum efficient cooperative spectrum sensing and scheduling scheme which minimizes the total energy consumption induced from sensing, reporting and switching operations per obtained data rate leads to a combinatorial problem due to the inextricably intertwined binary variables for channel scheduling and SU association. Moreover, enforcing the clusters to meet certain collision and spectrum utilization constraints will put a non-linear domain since one needs to find the optimal sensing duration and local detection threshold of each sensing SU on its assigned PCs.

4.1.1 Chapter Contributions and Novelty

To address the above problems, the energy and spectrum efficiency is coupled as a single objective such that the energy spent per achieved data rate is minimized subject to global detection and false alarm constraints to protect PUs from SU interference and ensure a certain spectrum utilization, respectively. Accordingly, assuming SUs have different reporting error rates for different PCs, CSS scheduling (CSSS) is formulated as an MINLP problem to determine: 1) the optimal subset of PCs to be scheduled for sensing, 2) the SU assignment set for each scheduled PC, and 3) sensing durations and detection thresholds of each SU on PCs it is assigned to sense. Moreover, we formulate the optimal sensing order to minimize the channel switching latency which is modeled as a linear function of the total frequency distance [21]-[22].

For specific instances of above combinatorial problem, ie. for a given set of scheduled PCs and set of SU assignment for ach scheduled PC, CSSS is first shown to be a non-convex problem. Accordingly, an equivalent convex framework is developed for heterogeneous CRNs using the monotonicity of the objective and log-concavity of the global collision and spectrum utilization constraints. For comparison, optimal detection and sensing thresholds are also derived assuming SUs have identical sensing qualities as a suboptimal solution to the heterogeneous case. Exploiting the established convex framework, we develop a prioritized ordering heuristic (POH) to order channels under spectrum, energy and spectrum-energy limited regimes. After that, a scheduling and assignment heuristic (SAH) is proposed and shown to have a very close performance to exhaustive optimal solution. The behavior of the CRN is then studied under these regimes with respect to various numbers of SUs, PCs and SNR distributions.

4.1.2 Chapter Organization

The rest of this chapter is organized as follows: First, Section-4.3 introduces the system model. Then, Section 4.4 provides the details of CSS under heterogeneity and homogeneity modes. After that, Section 4.5 derives the coupled energy & spectrum efficiency and formulates the CSSS problem. Section 4.6 develops the POH and SAH solution approaches. Finally,

simulation results and analysis are presented in Section-4.7 and Section-4.8 summarizes the chapter.

4.2 Related Work

Zhang and Tsang proves the energy efficiency optimality of the myopic policy using the framework of partially observable markov decision process (POMDP) in [87]. By successively activating a subset of sensors to sense and putting others into a sleep mode, an energy efficient CSS with an optimal scheduling method is considered for sensor aided CRNs [68]. Sun et al. considers a heterogeneous CRN scenario and develop a CSSS framework using discrete-convex in three steps. They simply use OR voting rule in their analysis to maximize a utility function as a weighted sum of capacity and energy expenditure [88]. Eryigit and others try to minimize total sensing and reporting energy consumption using OR voting rule in a error-free cooperation environment. They provide efficient heuristic methods after solving the combinatorial problem via outer linearization methods [89]. Even though all these previous studies have important contributions, they lack for generality of exploitation different voting rules and energy efficiency by assuming AND/OR voting rule for the sake of tractability since the majority voting rule is already pointed out to be the most energy efficient voting rule in the context of additional SNR requirement [13]. This is recently re-validated by [90] where authors use discrete-convexity tools to maximize the achievable throughput in both homogeneous and heterogeneous scenarios. Another shortcoming of the works in [87]-[90] is assumption of the perfect reporting environment. However, Chaudhari et al. clearly demonstrated the existence of a reporting error wall after which no reliable cooperation is possible regardless of how much energy spent [13], [91].

Another practical concern in multi-channel CSSS is channel switching delay and energy which is also disregarded in the previous works. In [21] and [22] channel switching factor is taken into account in the realm of resource allocation scheduling. In [92], authors propose a scheduling method which minimizes the energy cost caused by sensing, reporting and channel switching actions under the assumption that number of SUs is much more than the number of PUs employing the OR fusion rule under perfect reporting channel. Authors of [93] propose

a framework to minimize the ratio of summary of sensing-reporting-switching cost and the discovered spectrum under erroneous reporting and generalized voting rules.

4.3 System Model

We consider a large scale CRN scenario where the sensing scheduling of PCs and the assignment of SUs to sense scheduled PCs are determined by a central cognitive base station (CBS). The number of PCs and SUs are denoted by M and N, respectively. Similarly, the set of scheduled PCs and the set of assigned SUs are denoted as $\mathcal{M}$ and $\mathcal{N}$, respectively. The subset of $\mathcal{N}$ assigned to sense the same PC is referred to as a *cluster* and SUs can join more than one cluster at a time. We assume that the CBS has the information about the sensing and reporting quality of SUs and chooses a CH, which undertakes the role of fusion center, for each scheduled PC among the SUs assigned to sense that channel. After the determination of CHs and routing paths, report and control signaling between the SUs and CBS are exchanged over a CCC via the CHs. Timeslotted operation of the secondary network is depicted in Figure 4.1 where each timeslot of duration T is split into two stages: 1) *channel search* to discover spectrum holes and 2) *channel utilization* for secondary data transmission. We assume that sensing and reporting channel conditions does not change during a timeslot duration.

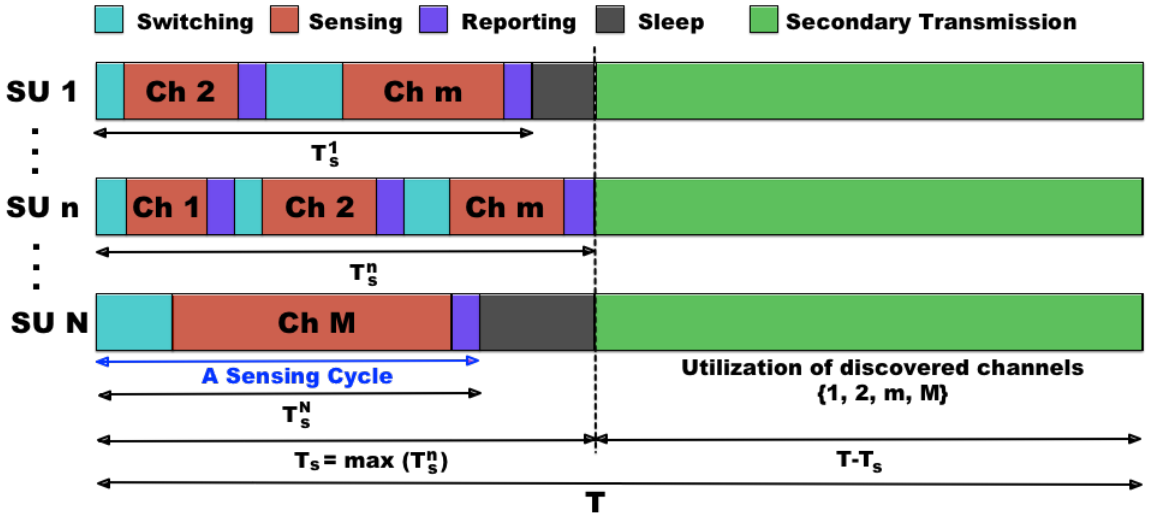

Figure 4.1: Demonstration of a scheduling timeslot consisting of switching-sensing-reporting cycles and secondary data transmission.

In the channel search stage, channel searching proceeds in switching-sensing-reporting *cycles* where an SU n first performs *channel switching* to adjust its operating frequency to the assigned PC m, then executes *sensing* for a required duration and finally reports its local decision to the CH over a multihop reporting path to receive a global decision feedback regarding the PC state. Accordingly, the channel search time of SU n, T_s^n, is determined by the summation of sensing cycles of all assigned PCs. We note that the duration of the channel search stage, thus the residual time for the channel utilization, is determined by the slowest SU since the CBS needs to wait for the arrival of all decisions to feedback the global decisions and resource allocation policy which is beyond the scope of this chapter. Therefore, channel search duration is given by

$$T_s = \max_{n \in \mathcal{N}} (T_s^n) \tag{4.1}$$

In the channel utilization stage, based on the global decision feedback received from the FCs, discovered available channels are utilized by SUs in the remaining available time, $T - T_s$, according to a certain resource sharing strategy. If an SU completes all necessary cycles before T_s, it puts itself into a sleep mode to save energy until it is allowed to utilize the discovered channels. For the remainder of the chapter, we define the following matrices and vectors to formulate the scheduling problem in a more compact way:

- $\boldsymbol{y} \in \{0,1\}^M$ is a vector of binary variables y_m which indicates that the PC m is scheduled to be sensed or not.
- $\boldsymbol{X} \in \{0,1\}^{M \times N}$ is a binary PU↔SU assignment matrix with entries $x_m^n \in \{0,1\}$ which indicates that the SU n is committed to sense the PC m if it is non-zero.
- $\boldsymbol{S} \in \mathbb{N}^{+^{M \times N}}$ is a positive real matrix with entries S_m^n which defines the number of samples of the SU n on the PC m.
- $\boldsymbol{\mathcal{E}} \in \mathbb{R}^{M \times N}$ is a real matrix with entries ε_m^n which defines the detection threshold of the SU n on PC m.
- $\boldsymbol{\Gamma} \in \mathbb{R}^{+^{M \times N}}$ is a positive real matrix with entries γ_m^n which represents the SNR of the SU n on the PC m.

- $\boldsymbol{P} \in \mathbb{R}^{M \times N}$ is the reporting bit error probability matrix with entries $p_m^n \in [0,1]$ which represents the reporting error between SU n and CH m.
- $\boldsymbol{f} \in \mathbb{R}^{+^M}$ is a vector with entries f_m^c which represents the carrier frequency of the PC m.

4.4 CSS model

4.4.1 Heterogeneous Mode

Since the focus of this chapter is the scheduling aspects of the CSS, a generic sensing method like *energy detection* is adequate for this purpose. EDs have been extensively exploited as the ubiquitous sensing technique in the literature due to its simplicity, compatibility with any signal type, and low computational and implementation complexity [24]. To detect primary signals, ED of SU $n \in \mathcal{N}$ measures the received signal energy of PC $m \in \mathcal{M}$ for a number of samples S_m^n and compares it with a detection threshold ε_m^n to make a local decision on binary hypotheses $\mathcal{H}_m^0$ and $\mathcal{H}_m^1$ which represents the absence and presence of PUs, respectively. For a large enough number of samples ($S_m^n \geq 30$) and normalized noise variance, probability of false alarm, $P_{m,n}^f = \mathcal{P}[\mathcal{H}_1|\mathcal{H}_0]$, and probability of detection, $P_{m,n}^d = \mathcal{P}[\mathcal{H}_1|\mathcal{H}_1]$, are given by (2.9) and (2.10), respectively.

After the local sensing process, SU n sends its hard result u_m^n to the CH over a binary symmetric CCC. Defining the error probability as $p_m^n = \mathcal{P}\left[\tilde{u}_m^n = 1|u_m^n = 0\right] = \mathcal{P}\left[\tilde{u}_m^n = 0|u_m^n = 1\right]$ where $\tilde{u}_m^n$ is the hard decision received by the CH, the local false alarm and detection probabilities received at the CH side are given by

$$\begin{aligned}
\tilde{P}_{m,n}^f\left(P_{m,n}^f\right) &= \mathcal{P}\left[\tilde{u}_m^n = 1|u_m^n = 0\right]\mathcal{P}\left[u_m^n = 0|\mathcal{H}_m^0\right] \\
&\quad + \mathcal{P}\left[\tilde{u}_m^n = 1|u_m^n = 1\right]\mathcal{P}\left[u_m^n = 1|\mathcal{H}_m^0\right] \\
&= p_m^n\left(1 - P_{m,n}^f\right) + \left(1 - p_m^n\right)P_{m,n}^f \qquad (4.2) \\
\tilde{P}_{m,n}^d\left(P_{m,n}^d\right) &= \mathcal{P}\left[\tilde{u}_m^n = 1|u_m^n = 0\right]\mathcal{P}\left[u_m^n = 0|\mathcal{H}_m^1\right] \\
&\quad + \mathcal{P}\left[\tilde{u}_m^n = 1|u_m^n = 1\right]\mathcal{P}\left[u_m^n = 1|\mathcal{H}_m^1\right] \\
&= p_m^n\left(1 - P_{m,n}^d\right) + \left(1 - p_m^n\right)P_{m,n}^d \qquad (4.3)
\end{aligned}$$

Denoting the set of cooperating SUs to sense the PC m as $\mathcal{C}_m$ with the cardinality $C_m = \sum_{n\in\mathcal{N}} x_m^n$, the CH collects $\tilde{u}_m^n$'s and makes the global decision using the following test

$$\mathcal{K}_m = \sum_{n\in\mathcal{C}_m} \tilde{u}_m^n x_m^n \underset{\mathcal{H}_m^0}{\overset{\mathcal{H}_m^1}{\gtrless}} \kappa_m \tag{4.4}$$

which follows the *Poisson-Binomial* distribution. Using equations (4.2) and (4.3) in Poisson-Binomial distribution, the CH obtains the global false alarm and detection probabilities by fusing the local reports as follows

$$\begin{aligned} Q_m^f\left(\tilde{P}_{m,n}^f\right) &= \mathcal{P}\left[\mathcal{K}_m \geq \kappa_m \mid \mathcal{H}_m^0\right] \\ &= \sum_{\kappa_m}^{C_m} \sum_{A\in F_\kappa} \prod_{n\in A} \tilde{P}_{m,n}^f \prod_{n\in A^c} \left(1-\tilde{P}_{m,n}^f\right) \end{aligned} \tag{4.5}$$

$$\begin{aligned} Q_m^d\left(\tilde{P}_{m,n}^d\right) &= \mathcal{P}\left[\mathcal{K}_m \geq \kappa_m \mid \mathcal{H}_m^1\right] \\ &= \sum_{\kappa_m}^{C_m} \sum_{A\in F_{\kappa_m}} \prod_{n\in A} \tilde{P}_{m,n}^d \prod_{n\in A^c} \left(1-\tilde{P}_{m,n}^d\right) \end{aligned} \tag{4.6}$$

where F_{κ_m} is the set of all subsets of κ_m integers that can be selected from $\mathcal{C}_m$. Since F_{κ_m} has $\binom{C_m}{\kappa_m}$ elements, using an efficient method to calculate Eq. (4.5) and (4.6) is very important, especially when C_m is very large. For this purpose, probability mass function (pmf) and cumulative distribution function of *Poisson-Binomial* random variables can be expeditiously calculated from polynomial coefficients of the probability generating function of $\mathcal{K}_m$ [80].

4.4.2 Homogeneous Mode

In the heterogeneous mode, SUs with different sensing qualities are treated distinctly and allowed to contribute to Q_m^f and Q_m^d with different $\tilde{P}_{m,n}^f$ and $\tilde{P}_{m,n}^d$, respectively. As a special and traditional case, homogeneous mode imposes SUs to satisfy $\tilde{P}_{m,n}^f = \tilde{P}_m^f,\ \tilde{P}_{m,n}^d = \tilde{P}_m^d,\ \forall n$ regardless of their non-identical SNRs. Accordingly, $\mathcal{K}_m$ is Binomially distributed since $\tilde{u}_m^n$ is a Bernoulli random variable in this mode.

4.5 CSS Scheduling Optimization

The ultimate design goal of an energy and spectrum efficient CSS scheduling scheme would be minimizing the energy expenditure per transmitted bit, i.e, [Joules/bit]. On the one hand,

such a purpose requires minimization of the opportunity cost via joint optimization of SU assignment along with the determination of sensing durations and detection thresholds with the consideration of distinctive sensing and reporting qualities of SUs subject to collision constraint regulations. On the other hand, it necessitates the optimal selection of PCs to maximize the achievable total throughput by maximizing the achievable data rate by scheduling PCs with higher possibility of being idle and maximizing the available time left for secondary transmission, $T - T_s$.

4.5.1 Energy and Spectrum Efficiency

Energy and spectrum efficiency of the CSS scheduling problem can be coupled into a single objective by minimizing the energy cost per obtained opportunity which can be formulated as the number of bits transmitted on discovered free PCs. Denoting the *apriori* probability of idle and busy states of the PC m as $\pi_m^0 = \mathcal{P}\left[\mathcal{H}_m^0\right]$ and $\pi_m^1 = \mathcal{P}\left[\mathcal{H}_m^1\right]$, respectively, the achievable data rate for a normalized noise power is given by

$$R = \frac{T - T_s}{T} \sum_{m \in \mathcal{M}} \pi_m^0 \left(1 - Q_m^f\right) W_m y_m \log_2\left(1 + \mathbb{P}_t\right) \tag{4.7}$$

where W_m and $\mathbb{P}_t$ denote the bandwidth of the m^{th} PC and the transmission power of the SUs, respectively. The opportunity cost is primarily induced from three factors: *channel switching cost*, *sensing cost*, and *reporting cost*.

4.5.1.1 Channel Switching Energy

To execute sensing assignments, SUs have to switch its operating frequency to desired channel's parameters in the beginning of corresponding cycles. We assume that the switching time satisfies the triangularity and linearity properties, i.e., $\tau_{sw} = \beta |f_{m-1}^c - f_m^c|$ where β is a switching factor that depends on parameters such as power consumption and used technology [21]-[22]. Based on the initial channel state, ordering the assigned PCs and starting to sense from the closest channel is the optimal policy as it is the shortest path. For instance, if we denote the initial channel state as f_0^c, the lowest/highest central frequency of assigned channels

as f^c_{low}/f^c_{high}, the absolute amount of switched frequency can be minimized by first tuning to the closest PC f^c_{low} (f^c_{high}) and then starting to sense channels in ascending (descending) order.

To calculate the total switching time of the SU n, we define the following vectors: the initial channel state of SU n, $\boldsymbol{x_n^0} \in \{0,1\}^M$ with zero entries except at the intitial frequency, the n^{th} column vector of $\boldsymbol{X}$, $\boldsymbol{x_n}$, $\boldsymbol{f_n} = \boldsymbol{x_n} \circ \boldsymbol{f}$, and $\boldsymbol{f_n^0} = \boldsymbol{x_n^0} \circ \boldsymbol{f}$ where ($\circ$) denotes the Schur product. Accordingly, the total channel switching time of SU n overall cycles can be given by (4.8)

$$T^n_{sw} = \beta \times \left[\max\left(\boldsymbol{f_n}\right) - \min\left(\boldsymbol{f_n}\right) + \min\left\{\left|\max\left(\boldsymbol{f_n}\right) - \max\left(\boldsymbol{f_n^0}\right)\right|, \left|\min\left(\boldsymbol{f_n}\right) - \max\left(\boldsymbol{f_n^0}\right)\right|\right\}\right] \tag{4.8}$$

Therefore, the total switching energy expenditure is given by

$$E_{SW} = P_{sw} T_{sw} = P_{sw} \sum_{n \in \mathcal{N}} T^n_{sw} \tag{4.9}$$

where P_{sw} and T_{sw} denote the channel switching power and total channel switching time, respectively.

4.5.1.2 Sensing Energy

Denoting the time spent per sample as τ_s, the total energy expenditure for the sensing is given by

$$E_S = P_s T_{sns} = P_s \tau_s \boldsymbol{e}^T \left(\boldsymbol{S} \circ \boldsymbol{X}\right) \tilde{\boldsymbol{e}} \tag{4.10}$$

where P_s is the sensing power and T_{sns} is the total sensing duration of SUs. In (4.10), $\boldsymbol{e}$ and $\tilde{\boldsymbol{e}}$ are unit vectors with sizes M and N, respectively.

4.5.1.3 Reporting/Controlling Energy

Similarly, denoting the time spent for reporting as τ_r, the total energy expenditure for the reporting is given by

$$E_R = P_r T_r = P_r \tau_r \ \boldsymbol{e}^T \boldsymbol{X} \tilde{\boldsymbol{e}} \tag{4.11}$$

where P_r is the reporting power and T_r is the total reporting/controlling duration of SUs. Hence, the accumulated energy consumption within the channel search stage due to these three factors is given as

$$E = E_{SW} + E_S + E_R \tag{4.12}$$

Coupling the obtained opportunity and its cost, the objective of the entire scheduling frame work can be given as

$$\eta\left(\boldsymbol{y},\boldsymbol{X},\boldsymbol{S}\right)=\frac{E}{R}\qquad[Joules/bit/s] \tag{4.13}$$

4.5.2 Problem Formulation

We formulate the optimal CSS scheduling problem which will be exploited as a benchmark for the performance of the proposed heuristic methods as follows

P 4.1 : CSSS

$$\min_{\boldsymbol{y},\boldsymbol{X},\boldsymbol{S},\boldsymbol{\varepsilon}}\ \eta=E/R$$

1: s.t. $\bar{Q}_{th}^{d}\leq Q_{m}^{d}\left(\tilde{P}_{m,n}^{d}\right),\ \forall m\in\{m|\ 1\leq y_m\}$

2: $Q_{m}^{f}\left(\tilde{P}_{m,n}^{f}\right)\leq\bar{Q}_{th}^{f},\ \forall m\in\{m|\ 1\leq y_m\}$

3: $x_{m}^{n}\leq y_m,\ \forall m;\forall n$

4: $\delta y_m\leq\sum_{n}x_{m}^{n},\ \forall m$

5: $30\leq S_{m}^{n}\leq\bar{S},\ \forall(m,n)\in\{m,n|\ 1\leq y_m,\ 1\leq x_{m}^{n}\}$

6: $0\leq T-T_s$

7: $x_{m}^{n},\ y_m\in\{0,1\},\ S_{m}^{n}\in\mathbb{N}^{+},\ \varepsilon_{m}^{n}\in\mathbb{R},\ \forall m;\forall n$

which is an MINLP problem whose mixed-integer nature is due to the variables $\boldsymbol{y}$, $\boldsymbol{X}$ and $\boldsymbol{S}$. Lines 1 and 2 of the CSSS are the collision and spectrum utilization constraints, respectively. Line 3 simply states that if the PC m is not scheduled to be sensed then any SU cannot be assigned to sense the PC m. Line 4, on the other hand, requires the cooperation of at least δ SUs if the PC m is scheduled to be sensed. If an SU is assigned to sense any channel, line 5 sets the lower bound of 30 on required number of samples to invoke the CLT to ensure the assumptions hold for (2.9) and (2.10) and sets the upper bound $\bar{S}=T/\tau_s$ which is the maximum number samples possible within a timeslot duration, T. Line 6 simply limits the searching stage duration T_s to the timeslot duration T. Finally, line 7 defines the domain of the optimization variables.

It is a practical approach to relax the problem by unintegerizing $\boldsymbol{S}$. After obtaining the optimal real valued solution, one can obtain the closest upper integer value, which does not negatively effect the system performance since $S_m^n >> 1$ and $\tau_s << 1$ in general. However, CSSS is still an MINLP problem due to $\boldsymbol{y}$ and $\boldsymbol{X}$ and it requires impractical time complexity even for moderate size of problems. Thus, developing fast and high-performance heuristics are necessary to achieve satisfactory sub-optimal results for practical purposes. In this regard, we will focus on CSSS for a given pair of $\boldsymbol{y}$ and $\boldsymbol{X}$, $(\bar{\boldsymbol{y}}, \bar{\boldsymbol{X}})$, and refer this subproblem to as CSSS$(\bar{\boldsymbol{y}}, \bar{\boldsymbol{X}})$ in the remaining part of the chapter. In other words, CSSS$(\bar{\boldsymbol{y}}, \bar{\boldsymbol{X}})$ is a single instant of all possible combinations and it is shown to be a non-convex problem in Lemma 4.1. Exploiting the convex composition rules given in Remark 4.1, the log-concavity of the Poisson-Binomial distributions and monotonicity of η, the CSSS$(\bar{\boldsymbol{y}}, \bar{\boldsymbol{X}})$ can be converted into an equivalent convex feasibility problem to develop heuristic solutions in the next section. In what follows, Lemmas 4.2 and 4.3 are first introduced to show the monotonicity and decoupled convexity of the reported local false alarm and detection probabilities under the assumption of $P_{m,n}^f \leq 0.5$ and $P_{m,n}^d \geq 0.5$. Using the log-concavity of Poisson-Binomial distribution in Appendix A.1.2, $\log(Q_m^f)$ and $\log(Q_m^d)$ can be shown as concave functions. Moreover, taking the monotonicity of η in Lemma 4.4 into consideration, Corollary 4.1 states that the optimal value of η will be attained at $Q_m^f = Q_{th}^f$ and $Q_d^f = Q_{th}^d$.

Lemma 4.1: *$P_{m,n}^f$ $\left(P_{m,n}^d\right)$ is neither convex nor concave function of (S_m^n, ε_m^n), and neither is Q_m^f $\left(Q_m^d\right)$. Hence, CSSS$(\bar{\boldsymbol{y}}, \bar{\boldsymbol{X}})$ is not a convex problem.*

Proof. Please see Appendix B.1. □

Remark 4.1: *For functions $b : \boldsymbol{R}^L \to \boldsymbol{R}$, $c : \boldsymbol{R}^K \to \boldsymbol{R}^L$, $a = b \circ c : \boldsymbol{R}^K \to \boldsymbol{R}$ is defined by $a(\boldsymbol{z}) = b(c(\boldsymbol{z})) = b(c_1(\boldsymbol{z}), \ldots, c_k(\boldsymbol{z}), \ldots, c_K(\boldsymbol{z}))$ for $\boldsymbol{z} \in \boldsymbol{R}^K$ [34].*

1. *a is convex if b is convex and non-increasing in each argument, and c_i is concave in $\boldsymbol{z}$, $\forall k$.*

2. *a is concave if b is concave and non-increasing in each argument, and c_i is convex in $\boldsymbol{z}$, $\forall k$.*

Lemma 4.2: *Assuming that* $P^f_{m,n}\left(g(S^n_m, \varepsilon^n_m)\right) \leq 0.5$, $P^d_{m,n}\left(h(S^n_m, \varepsilon^n_m, \gamma^n_m)\right) \geq 0.5$, $\forall m, n$,

1. *For a feasible* S^n_m, $\bar{S}^n_m$, g *and* h *are both increasing and linear functions of* ε^n_m. *Thus,* $P^f_{m,n}(g)$ $\left(P^d_{m,n}(h)\right)$ *is a decreasing convex (concave) function of* ε^n_m.

2. *For a feasible* ε^n_m, $\bar{\varepsilon}^n_m$, g (h) *is an increasing (decreasing) concave (convex) function of* S^n_m. *Thus,* $P^f_{m,n}(g)$ $\left(P^d_{m,n}(h)\right)$ *is a decreasing (increasing) convex (concave) function of* S^n_m.

Proof. Please see Appendix B.1. □

Lemma 4.3: *Monotonicity and parameterized convexity (concavity) of* $P^f_{m,n}$ $(P^d_{m,n})$ *also holds for the reported false alarm and detection probabilities* $\tilde{P}^f_{m,n}$ $(\tilde{P}^d_{m,n})$.

Proof. Please see Appendix B.1. □

Lemma 4.4: η *is a monotonically increasing function of the number of samples,* S^n_m, $\forall m, n$. *It is also a quasi-convex function of* (S^n_m), $\forall m, n$.

Proof. Please see Appendix B.2. □

Corollary 4.1: *For a feasible detection threshold* $\bar{\varepsilon}^n_m$ *and increasing* S^n_m, *while* $P^f_{m,n}$ *and* Q^f_m *decrease,* $P^d_{m,n}$, Q^d_m, *and* η *increase. In this case, the minimum* η *that satisfies the constraint* $Q^d_m \geq Q^d_m$ *is attained at* S^n_m *which satisfies* $Q^d_m = Q^d_m$. *For a given* $\bar{S}^n_m$ *and decreasing* ε^n_m, *on the other hand,* $P^d_{m,n}$, Q^d_m, $P^f_{m,n}$, *and* Q^f_m *increase, which is upper-bounded by* $Q^f_m \leq Q^f_m$. *Thus, the optimal value of* ε^n_m *is attained at* $Q^f_m = Q^f_m$.

Since each cluster m is separately required to satisfy global detection and false alarm requirements to achieve the optimal objective, $\eta^\star(\bar{\boldsymbol{y}}, \bar{\boldsymbol{X}}, \boldsymbol{S})$, Corollary 4.1 decouples (S^n_m, ε^n_m) from $(S^n_{m'}, \varepsilon^n_{m'})$, $\forall m' \neq m$, $\forall n$. Consequently, exploiting the parameterized convexity of the problem and the log-concavity of the Poisson-Binomial distribution (also the Binomial distribution as a

special case), CSSS($\bar{\boldsymbol{y}}, \bar{\boldsymbol{X}}$) can equivalently be written as a convex problem as follows:

$$\begin{aligned}
\textbf{P 4.2:} \quad & \min_{\boldsymbol{S}_m, \boldsymbol{\mathcal{E}_m}} \quad \left|\log\left(Q_{th}^f\right) - \log\left(Q_m^f\left(P_{m,n}^f\right)\right)\right| \\
1: \quad & \text{s.t.} \quad \log\left(Q_{th}^d\right) \leq \log\left(Q_m^d\left(P_{m,n}^d\right)\right) \\
2: \quad & \quad 1 \leq \varepsilon_m^n \leq \gamma_m^n + 1, \ \forall n \\
3: \quad & \quad 30 \leq S_m^n \leq \bar{S}, \ \forall n \\
4: \quad & \quad 0 \leq T - T_s \\
5: \quad & \quad S_m^n \in \mathbb{R}^+, \ \varepsilon_m^n \in \mathbb{R}, \ \forall n
\end{aligned}$$

where $\boldsymbol{S}_m$ and $\boldsymbol{\mathcal{E}}_m$ are the m^{th} row vectors of $\boldsymbol{S}$ and $\boldsymbol{\mathcal{E}}$, respectively. Line 2 ensures that $P_{m,n}^f \leq 0.5$, $P_{m,n}^d \geq 0.5$, $\forall m, n$. Quasi-convexity of the objective follows from Corollary 1 and P2 can be solved using primal decomposition methods [94].

Under the homogeneous CSS mode, SUs are enforced to provide identical local false alarm and detection probability reports, i.e. $\tilde{P}_{m,n}^f = \tilde{P}_f$ and $\tilde{P}_{m,n}^d = \tilde{P}_d$. In such a case, there is no need to solve P2 numerically since distinguishing sensing durations and detection thresholds of each SU is unnecessary. Therefore, Q_m^f (Q_m^d) directly becomes a function of $\tilde{P}_f$ ($\tilde{P}_d$) whose optimal value, $\tilde{P}_f^\star = \{\tilde{P}_f \mid Q_m^f = Q_{th}^f\}$ $\left(\tilde{P}_d^\star = \{\tilde{P}_d \mid Q_m^d = Q_{th}^d\}\right)$ could simply be computed using the bisection method. We note that there is also a close relationship between the cluster size and $\tilde{P}_f^\star$ ($\tilde{P}_d^\star$) such that as the cluster size increases $\tilde{P}_f^\star$ ($\tilde{P}_d^\star$) increases (decreases), which is quite intuitive since as the number of cooperating SUs increases local detector accuracy burden on SUs decreases. Accordingly, one can calculate $\tilde{P}_f^\star$ ($\tilde{P}_d^\star$) for different sizes of clusters offline and determine the exact local detection requirements depending upon the given cluster formation by ($\bar{\boldsymbol{y}}, \bar{\boldsymbol{X}}$) and the reporting channel quality as follows

$$P_{m,n}^{f^\star} = \frac{P_f^\star - p_m^n}{1 - 2p_m^n} \tag{4.14}$$

$$P_{m,n}^{d^\star} = \frac{P_d^\star - p_m^n}{1 - 2p_m^n} \tag{4.15}$$

which follows from (4.2) and (4.3) with the assumption of $p_m^n < 0.5$, $\forall m, n$. Indeed, $p_m^n \simeq 0.5$ has already been shown to be the imperfect reporting error wall beyond of which the reliable CSS is not possible no matter how much energy is spent [91]. Moreover, substituting (4.14) and

(4.15) into (2.9) and (2.10), respectively, optimal number of samples and detection thresholds are derived as

$$S_{m,n}^{\star} = \left[\frac{\mathcal{Q}^{-1}\left(P_{m,n}^{d\star}\right)\sqrt{2\gamma_m^n + 1} - \mathcal{Q}^{-1}\left(P_{m,n}^{f\star}\right)}{\gamma_m^n} \right]^2 \tag{4.16}$$

$$\varepsilon_{m,n}^{\star} = 1 + \frac{\mathcal{Q}^{-1}\left(P_{m,n}^{f\star}\right)}{\sqrt{S_{m,n}^{\star}}} \tag{4.17}$$

4.6 Energy & Spectrum Efficient Heuristics

In this section, we will develop fast, yet high performance heuristic solutions to alleviate the combinatorial nature of the CSSS problem by employing the proposed CSSS($\bar{\boldsymbol{y}}, \bar{\boldsymbol{X}}$) approaches. Although a coupled energy and spectrum efficiency metric is focused in the previous section, we will explore different scenarios to develop effective heuristics with regard to various network conditions. For instance, in a network scenario with heavy traffic conditions, SUs may demand for as much as possible throughput gain, which will be referred to as *spectrum limited regime*. On the contrary, SUs may not have enough energy resources and prefer to minimize their energy consumption to save remaining battery life for future bursty traffic conditions, which will be referred to as *energy limited regime*. Therefore, we will investigate three different regimes:

1. *Spectrum limited regime (SLR):* Maximization of the achievable total data rate by scheduling PCs regardless of the opportunity cost.

2. *Energy limited regime (ELR):* Minimization of the total energy consumption by assigning SUs regardless of the achievable data rate.

3. *Energy & spectrum limited regime (ESLR) :* Minimization of the coupled energy and spectrum efficiency as formulated in (4.13).

Fortunately, the convexity analysis in the Section 4.5 still applies to minimize E since it is a linear and increasing function of S_m^n. Similarly, maximizing R is equivalent to minimizing T_s which has already been shown to be a monotonically increasing convex function of S_m^n in Appendix B.2.

4.6.1 Prioritized Ordering Heuristic

We first begin with a channel ordering heuristic (POH) which prioritize channels according to the regime types as shown in Algorithm 4.1. POH provides us with an optimistic channel prioritization such that how solely scheduling a single primarily channel can perform if we greedily assign the best δ SUs to it. For every channel m, Algorithm 4.1 first orders SUs with respect to their SNR values on PC m and record this sorting as $\bar{\boldsymbol{\gamma}}_{\boldsymbol{m}}$ for future purposes. Thereafter, it forms $\bar{\boldsymbol{y}}$ with zero entries except at the m^{th} position and $\bar{\boldsymbol{X}}$ with zero entries except the first δ SUs of $\bar{\boldsymbol{\gamma}}_{\boldsymbol{m}}$. Based on the heterogeneity or homogeneity mode preference, performance metrics of channel m, $\langle \eta_m, E_m, R_m \rangle$, is calculated using P2 and (4.16), respectively. Finally, channels are sorted with respect to R, E and η under the SLR, ELR and ESLR, respectively.

Algorithm 4.1 POH

Input: $\boldsymbol{P}$, $\boldsymbol{\Gamma}$, δ
Output: Prioritized channel vectors and descending sorted $\boldsymbol{\Gamma}$

for $m = 1$ to M **do**
  $\bar{\boldsymbol{\gamma}}_{\boldsymbol{m}} \leftarrow$ Sort SUs in descending order wrt. γ_m^n
  $\bar{\boldsymbol{y}} \leftarrow$ Schedule only channel m to be sensed
  $\bar{\boldsymbol{X}} \leftarrow$ Assign the best δ SUs to channel m from $\bar{\boldsymbol{\gamma}}_{\boldsymbol{m}}$.
  if Mode = Heterogeneous **then**
    Compute $\langle \eta_m, E_m, R_m \rangle$ using P2($\bar{\boldsymbol{y}}$,$\bar{\boldsymbol{X}}$)
  else
    Compute $\langle \eta_m, E_m, R_m \rangle$ using (4.16) for given ($\bar{\boldsymbol{y}}$,$\bar{\boldsymbol{X}}$)
  end if
end for
$\bar{\boldsymbol{\Gamma}} \leftarrow$ Form ordered $\boldsymbol{\Gamma}$ from $\bar{\boldsymbol{\gamma}}_{\boldsymbol{m}}$s.
$\boldsymbol{c_R} \leftarrow$ Sort channels in descending order wrt. R_m.
$\boldsymbol{c_E} \leftarrow$ Sort channels in ascending order wrt. E_m.
$\boldsymbol{c_\eta} \leftarrow$ Sort channels in ascending order wrt. η_m.
return $\boldsymbol{c_\eta}$, $\boldsymbol{c_E}$, $\boldsymbol{c_R}$, $\bar{\boldsymbol{\Gamma}}$.

One of the key features of the proposed heuristic is the assignment of exactly δ SUs which is the minimum requirement for the cluster size. The underlying reason is that the total number of samples to meet the global detection and false alarm probabilities increases as the cluster size increases even if the required individual number of samples decreases because of the increase (decrease) in $\tilde{P}_f^\star$ ($\tilde{P}_d^\star$) by adding one more SU. Although it is not trivial to show this behavior analytically due to the lack of closed form $\mathcal{Q}$-function expression, variations in total number

of samples, $\tilde{P}_f^\star$, and $\tilde{P}_d^\star$ are numerically evaluated in Section 3.5. Likewise, reporting and switching energy consumption also increase with the cluster size since the number of reports and possible channel switching may occur with additional SUs.

While the outer loop takes $\mathcal{O}(M)$ steps, sorting operations in Line2 and Lines 12-14 are $\mathcal{O}(N \log N)$ and $\mathcal{O}(M \log M)$, respectively. The computation of performance metrics between lines 5-9 takes $\mathcal{O}(MN)$ steps at the worst case. Therefore, overall complexity of POH is $\mathcal{O}(MN \log N)$.

4.6.2 Scheduling and Assignment Heuristic

Algorithm 4.2 SAH

Input: $\boldsymbol{P}$, $\bar{\boldsymbol{\Gamma}}$, δ, $\boldsymbol{c_\eta}/\boldsymbol{c_E}/\boldsymbol{c_R}$
Output: The best solution with the corresponding $\bar{\boldsymbol{y}}$ and $\bar{\boldsymbol{X}}$.

1: $\Delta \leftarrow 0$
2: $i \leftarrow 1$
3: $\eta_0 \leftarrow \infty$ / $E_0 \leftarrow \infty$ / $R_0 \leftarrow -\infty$
4: $\mathcal{S}^\star \leftarrow \langle \eta_0, E_0, R_0 \rangle$
5: **while** $\Delta \leq 0$ && $i \leq M$ **do**
6: $\quad \bar{\boldsymbol{y}} \leftarrow$ Schedule the best i channels in $\boldsymbol{c_\eta}$ / $\boldsymbol{c_E}$ / $\boldsymbol{c_R}$
7: $\quad \bar{\boldsymbol{X}} \leftarrow$ Assign the best δ SUs to channels from $\bar{\boldsymbol{\Gamma}}$.
8: $\quad$ **if** Mode = Heterogeneous **then**
9: $\quad\quad \mathcal{S} \leftarrow$ Compute $\langle \eta_i, E_i, R_i \rangle$ by P2
10: $\quad\quad \Delta \leftarrow (\eta_i - \eta_{i-1})$ / $(E_i - E_{i-1})$ / $(R_{i-1} - R_i)$
11: $\quad\quad$ **if** $\Delta \leq 0$ **then**
12: $\quad\quad\quad \mathcal{S}^\star \leftarrow \langle \eta_i, E_i, R_i \rangle$
13: $\quad\quad$ **end if**
14: $\quad$ **else**
15: $\quad\quad \mathcal{S} \leftarrow$ Compute $\langle \eta_i, E_i, R_i \rangle$ by (4.16)
16: $\quad\quad \Delta \leftarrow (\eta_i - \eta_{i-1})$ / $(E_i - E_{i-1})$ / $(R_{i-1} - R_i)$
17: $\quad\quad$ **if** $\Delta \leq 0$ **then**
18: $\quad\quad\quad \mathcal{S}^\star \leftarrow \langle \eta_i, E_i, R_i \rangle$
19: $\quad\quad$ **end if**
20: $\quad$ **end if**
21: $\quad i \leftarrow i + 1$
22: **end while**
23: **return** $\mathcal{S}^\star$, $\bar{\boldsymbol{y}}$, $\bar{\boldsymbol{X}}$

Exploiting the POH outputs and following the initialization process, scheduling and assignment heuristic (SAH) schedules the first i channels from $\boldsymbol{c_R}$ / $\boldsymbol{c_\eta}$ / $\boldsymbol{c_E}$ under the SLR / ELR /

ESLR, and greedily assigns the best δ SUs from $\bar{\mathbf{\Gamma}}$. Afterwards, based on the heterogeneity or homogeneity mode preference, $\langle \eta_m,\ E_m,\ R_m \rangle$ is calculated using P2 and (4.16), respectively. Employing the shift between the consecutive iterations, Δ, the algorithm determines if there is a decrease (increase) in η and E (R) by scheduling i^{th} PC from the prioritized channel vector and updates the best solution space. The termination condition of the while loop is satisfied either there is no performance enhancement by the addition of the i^{th} PC or there is no PC left to schedule. In the SLR, SAH will run at most M iterations since it seeks for as much as possible data rate without concerning about the opportunity cost. In the ELR, on the other hand, SAH will schedule the most energy efficient channel and terminate since scheduling more channels will increase the opportunity cost. Finally, SAH will schedule as many PCs as possible as long as the energy efficiency does not increase. That is, it will also operate for M iterations in the worst case. Thus, while the time complexity under the ELR is constant, that under other regimes is $\mathcal{O}(M)$.

4.7 Results and Analysis

All simulation results were obtained and plotted using Matlab. Throughout the simulation, the values in Table 4.1 are employed, unless it is explicitly stated otherwise.

Table 4.1: Default parameters used for obtaining results

Par.	Value	Par.	Value	Par.	Value
P_s	1 W [89], [92]	τ_s	1 μs	Q_{th}^f	0.01
P_x	1 W [89], [21], [92]	τ_r	1 s [89], [92]	$_{th}^{d}$	0.99
P_{sw}	1 W[89], [21], [92]	β	0.1 ms/MHz[89], [21], [92]	T	2 s

4.7.1 Relationship among Cluster Size, Energy, $P_f^\star$, and $P_d^\star$

In Figure 4.2, total number of samples of SUs versus the cluster size ranging from 1 to 100 is depicted along with the corresponding $P_f^\star$ and $P_d^\star$ values which ensure Q_{th}^f and Q_{th}^d, respectively. Curves with diamond, square and circle shaped markers show homogeneous clusters which consist of SUs with identical SNRs of -5, -10 and -15 dB, respectively. The curve with the star shaped markers, on the other hand, considers a heterogeneous cluster which consists of

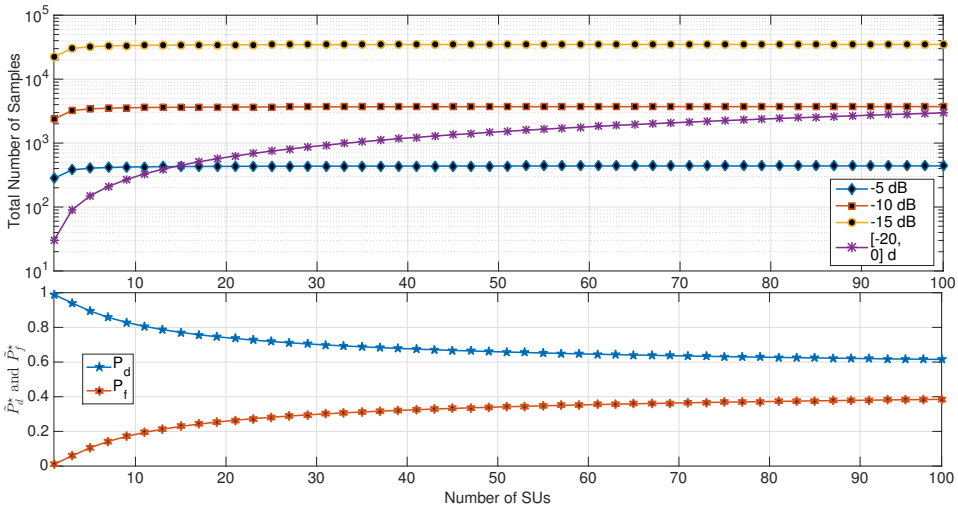

Figure 4.2: Total number of samples, $\tilde{P}_f^\star$, and $\tilde{P}_d^\star$ vs. cluster size.

non-identical SUs such that the cluster size C on the x-axis composed of the best C SUs among 100 SUs with SNRs range from -20 and 0 dB. In both cases, the total number of samples, thus the total sensing energy, increases with the cluster size. This is much more significant in the heterogeneous case that asymptotically approaches its mean value and homogeneous case with -10 dB. As can be seen from below subplot, enforcing SUs to have $P_{m,n}^f \leq 0.5$ and $P_{m,n}^d \geq 0.5$ does not contradict with practicality since $P_f^\star$ and $P_d^\star$ are still far beyond those limits even for impractically large cluster sizes.

4.7.2 Comparison Between Optimal and Heuristic Solutions

Figure 4.3 shows the comparison between the optimal exhaustive benchmark and heuristic solutions for an average of 30 CRN scenarios each of which comprises of 4 PCs and 8 SUs with SNRs randomly selected between 0 and -30 dB. The solid blue and red curves draw the optimal homogeneous (Binomial) and heterogeneous (Poisson-Binomial) modes, respectively. Similarly, the dashed curves with diamond and square shapes show the heuristic performance, which minimizes η using SAH with the given prioritized channel order $\boldsymbol{c}_\eta$ returned from POH, for homogeneous and heterogeneous modes, respectively. While the subplot (a) depicts the objective itself, subplot (b) and (c) demonstrate the corresponding opportunity cost and the

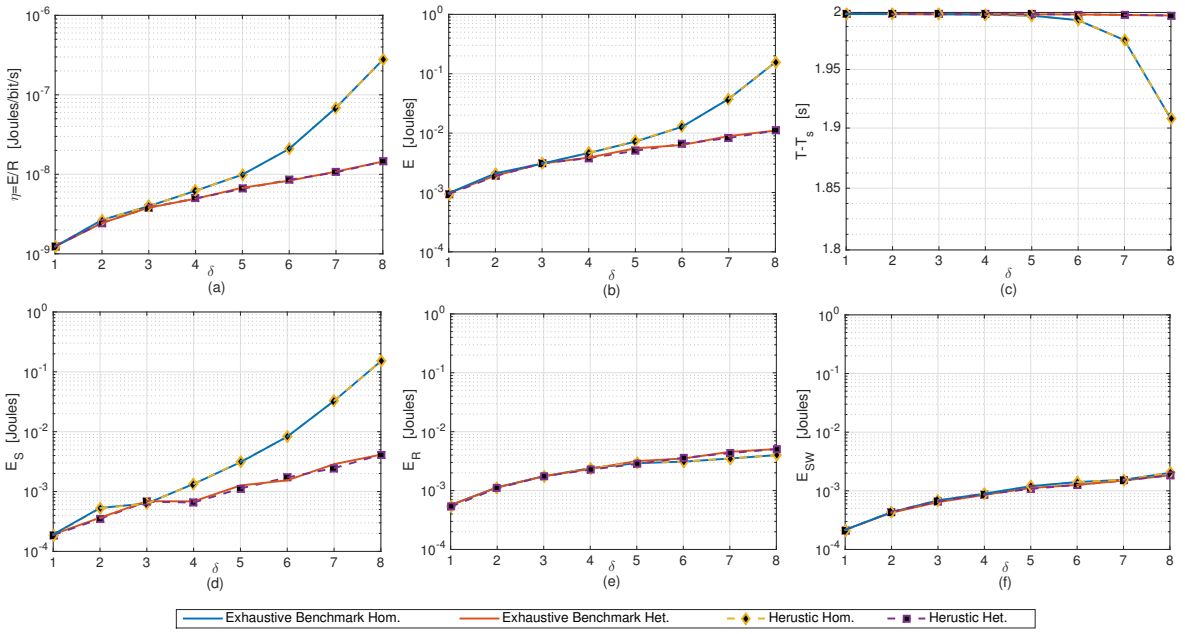

Figure 4.3: Comparison between the optimal and heuristic solutions for an average of 30 CRN scenarios with 4 PCs and 8 SUs with SNRs randomly selected between 0 and −30 dB.

remaining time for the secondary data transmission, respectively. It is clear from the figure that the proposed heuristic approach provides a very close performance to the benchmark in both modes. Taking the heterogeneity into account, on the other hand, especially gives a superior performance with respect the homogeneity assumption for 3 and more minimum number of SU requirement. This is because of considering SUs with relatively low SNRs and enforcing them to obtain exact local detection performance of SUs with relatively high SNRs. In other words, if cluster members have a broad range of SNRs heterogeneous mode shows superior performance than the homogeneous mode. On the contrary, if SUs have identical SNRs (i.e. cluster is homogeneous in reality) considering heterogeneity will not make any difference. Furthermore, the reasoning behind the assignment of exactly δ SUs is now more obvious due to the increasing trend of the η with regard to δ. Another significance of considering the heterogeneity is revealed in subplot (c) where available time left for the secondary transmission is dramatically reduced in homogeneous case as the slowest SU is enforced to have identical performance with others, which directly reduces the achievable throughput. Subplots (d), (e) and (f) detail the cost factors of the opportunity cost. As can be seen, reporting and switching energy consumption is very close

to the sensing for the heterogeneous mode for all δ values. However, sensing energy becomes more significant in homogeneous mode for higher δ valueAAAs since we enforce low SNR SUs to sense with identical detection performance. Moreover, reporting and switching energy consumption increase with δ because the number of channel switches and reports increase with the number of assigned SUs.

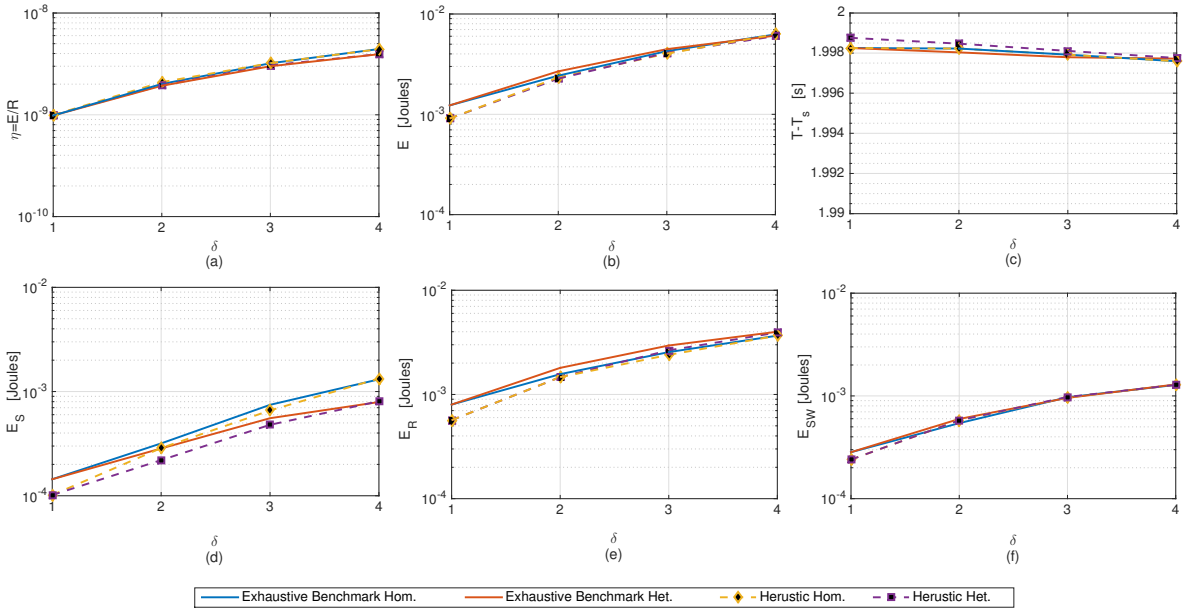

Figure 4.4: Comparison of optimal and heuristic solutions for an average of 30 CRN scenarios with 8 PCs and 4 SUs with SNRs randomly selected between 0 and -10 dB.

Likewise, Figure 4.4 shows the comparison between the optimal exhaustive benchmark and heuristic solutions for an average of 30 CRN scenarios each of which comprises of 8 PCs and 4 SUs with SNRs randomly selected between 0 and -10 dB. Even though we will not go over the underlying reasons of the curves, we will point out the followings: The proposed heuristic still gives very close performance to the optimal values and follows the same trend. Since the average SNR values is $-5dB$ and the SNR range is tight, the difference between the heterogeneous and homogeneous modes are not as significant as in Figure 4.3. However, we note that opportunity cost factors shows very close values due to the relatively high SNR values with respect to the Figure 4.3.

4.7.3 Numerical Results for SAH

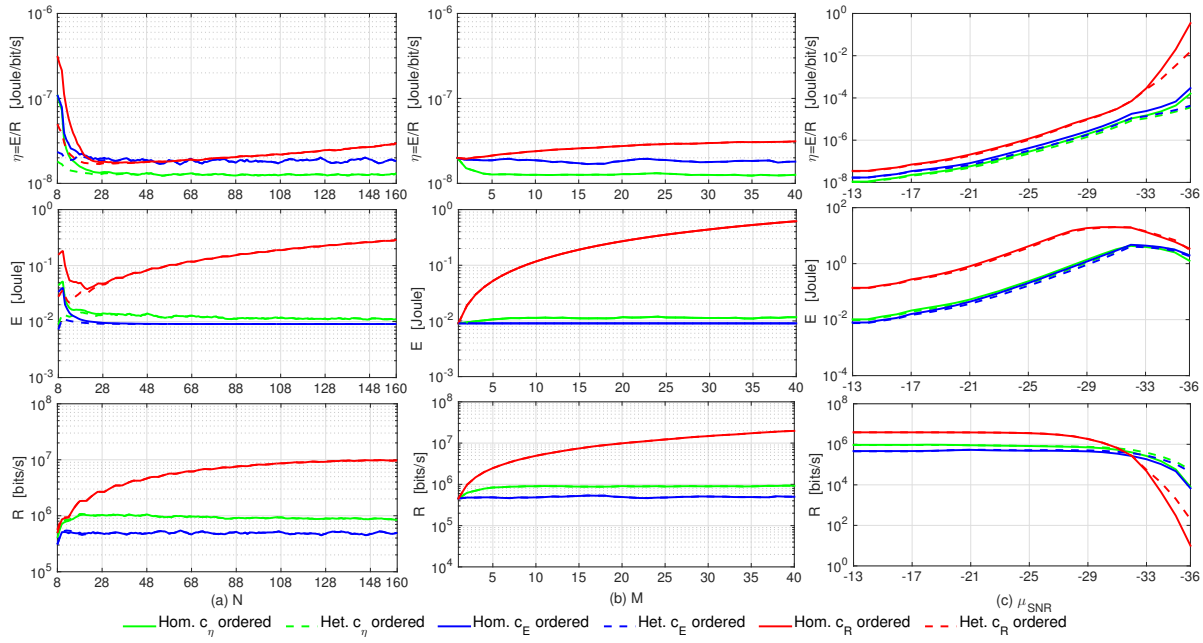

Figure 4.5: SAH results over 100 CRN scenarios with $M = 20$, $N = 100$, SNRs range from -30 to 0 dB and $\delta = 8$. Behaviors of η, E and R under different regimes with respect to (a) number of SUs, (b) number of PUs and (c) mean SNRs.

Figure 4.5 demonstrates the behavior of η, E and R under different regimes with respect to different number of SUs, number of PUs and SNR distributions in subplots (a), (b) and (c), respectively. While the solid green, blue and red lines draw the homogeneous mode under the ESLR, ELR, and ESR, respectively, the dashed lines with the corresponding colors are used for heterogeneous mode. We first note that the best η performance is always obtained under the ESLR regime using $\boldsymbol{c_\eta}$. Similarly, the best E and R performance is always observed under the ELR and ESR regimes using $\boldsymbol{c_E}$ and $\boldsymbol{c_R}$, respectively. On the other hand, the worst case of E (R) occurs under the SLR (ELR) since it does not care about energy (spectrum) during the channel ordering and SU assignment phases. However, η gives a mediocre E and R performance all the time since it couples both of them.

Figure 4.5-(a) shows the changes with respect to the number of SUs ranging from 8 to 160 for $M = 20$ and random SNRs between -30 dB and 0 dB. As the number of SUs increases, R under the SLR increases in every 8 steps since having a new set of δ SUs allows SAH to schedule

one more PC. E under the SLR first decreases until $N = 20$ and then start increases. This is primarily because of that small increments in number of SUs have more significant SU diversity if the number of channels is relatively high in comparison to number of channels. However, heterogeneity modes have a slight impact for $N \geq 20$ because network has more SU diversity and SNR range of the best δ SUs is tight due to the ordering. The increase of E under the SLR after $N = 20$ is directly related to the greedy demand for scheduling more channels. Therefore, η under the SLR is a result of the behavior of E and R and it gives the worst performance among others. E under the ELR is the best case and have a decreasing nature with respect to N, which is because of increasing SU assignment diversity and high chance of finding high SNR SUs to sense the most energy efficient channel. On the contrary, R under the ELR follows a mean value of 0.5 MHz since it only schedules the most energy efficient channel and PCs have an average apriori probability of 0.5, which is the worst case among others. As stated earlier, E and R under the ESLR regime provide a mediocre performance since it is not greedy either for E or R. As expected, it gives the best η performance since ordering and SU assignment is made based on η.

Figure 4.5-(b) shows the changes with respect to number of PCs ranging from 1 to 40 for $N = 100$ and random SNRs between -30 dB and 0 dB. Under the SLR, R monotonically increases with the number of PCs which is because of the increasing chance of finding PCs with higher apriori probabilities. Accordingly, E under the SLR increases with the R since more SUs are involved to sense more PCs, so does η. However, R, E, thus η remains almost constant under the ELR since the number of SUs is fixed and ELR only selects the most energy efficient channel which yields an average of 0.5 MHz data rate. Although E and R slightly increases with the number of PCs under the ESLR, η slightly decreases since R has a higher increasing peace than the E.

For $M = 20$ for $N = 100$, Figure 4.5-(c) shows the changes with respect to SNR scenarios where SNR distribution follows a normal distribution with variance 10 dB and mean values on x-axes. Although R does not experience a significant change until $28 - 30$ dB, E significantly increases with mean SNR of SUs. Even if the mean SNR and thus the total number of samples increases, SAH is able to find some PCs with low opportunity cost. After $28 - 30$ dB, however,

most of the PCs become infeasible to schedule due to the poor sensing quality of the entire SUs. Accordingly, SAH tends to schedule very few number of PCs due to their unaffordable, that is why R and E start to decrease. Behavior of η is simply a natural outcome of the underlying reasons we gave for E and R.

4.8 Chapter Summary

In this chapter, we considered a multi-channel CSS scheduling framework to minimize the induced sensing, reporting and channel switching energy per obtained opportunity subject to the global detection and spectrum utilization constraints. Apart from previous works, we factor the reporting error in and provide a general scheme which can be applied to any voting rule. After formulating an optimal MINLP problem, we develop an equivalent convex framework for specific instances of combinatorial solution space. In this way, we were able to develop very efficient yet fast heuristics for different regimes regarding the energy limitations and data rate demands the performance of which is compared to the exhaustive benchmark solution. We have also revealed the impact of heterogeneity and homogeneity assumption under different network scenarios.

CHAPTER 5. FULL-DUPLEX HYBRID ENERGY HARVESTING CSS

5.1 Overview

In addition to the goal of achieving more spectrum for less energy consumption in previous chapters, communication society is now targeting EH communications which provide significant advantages over traditional grid-powered and non-rechargeable and/or battery-powered wireless devices [95]. By harvesting required energy from alternative natural resources such as solar, vibrational, electromagnetic, thermoelectric, ambient wireless power etc., EH can achieve self-sustaining green communication. For a given amount of energy, conventional EE-CRNs aims to minimize the total sensing energy consumption subject to the fundamental *collision constraint* to prevent SUs from interfering with the PUs. In EH systems, on the other hand, energy needed for sensing and data transmission arrives intermittently and in random magnitudes of energy because of the random nature of energy harvesting sources. Then, the ultimate goal of EEH-CRNs would be, not only to minimize the over-all energy consumption, but to also maintain sensing and transmitting tasks under random and intermittent energy arrivals. Such a goal dictates an extra fundamental limit on the capacity of traditional CRNs: *energy-causality constraint* which states that the energy harvested by a time instant must be greater than or equal to the consumed energy until that time instant [17].

The generic energy harvesting system model can be classified into two types based on the battery availability to store the harvested energy: 1) *the harvest–use* systems mandate that the energy consumption rate should always be less than the instantaneous energy harvesting rate [96]; 2) *the harvest–store–use* systems contains a battery to store the harvested energy for the future purposes. In particular, RF harvesting is a suitable energy resource for green CRNs since CRs can utilize idle spectrum while harvesting energy from the busy channels.

Another appealing feature of the RF energy harvesting is the simultaneous information and power transfer capability [19]. However, as a single antenna cannot be used for sensing and transmitting at the same time, it can be shared by energy harvester and transceiver modules via either *time-switching* or *power-splitting* methods. In the sequel, time-switching methods in a harvest-store-use system is considered only since the previous chapters and most of the traditional cognitive radio network studies focus on a time-slotted operation of SUs.

As we mentioned earlier, the energy efficient cooperative spectrum sensing strategies are not applicable to energy harvesting systems any more and a radical paradigm shift is necessary to achieve an optimal energy harvesting cooperative spectrum sensing scheme. As an example, it is very crucial to have an action strategy which decides on being in the following modes:

- *Harvest Mode* is the case where SU exploits timeslot duration only for energy harvesting. This mode may be the optimal action to take when SUs neither have stored energy nor data packets to transmit. In a different scenario with a desirable energy arrival rate, SUs might have a light load of latency insensitive packets to transmit, however, harvesting and storing energy to be ready for potential upcoming packets might be a wise decision if the packet arrivals are bursty.

- *Harvest-Sense-Transmit Mode* could be more suitable if the packet and energy arrivals follows a continuous pattern where harvest and sense ratio is required to be optimized. Aside from the traditional sensing-throughput tradeoff, harvesting is introduced as an additional tradeoff domain. Therefore, subject to the collision and energy causality constraints, harvesting and sensing durations must be jointly optimized to harvest necessary energy while minimizing the sensing duration and maximizing the available time left for the secondary transmission. Moreover, based on the power allocation strategy and stored energy level, SUs may be required to harvest more to transmit with high powers to obtain more data rates.

- *Sense-Transmit Mode* might be the mode to operate as a traditional CR where the stored energy is plentiful and allocation of time for energy harvesting is not beneficial due to the insufficient energy arrival rates.

Nonetheless, deciding on such a strategy for each SU can be made in individual basis SUs based on their energy characteristics or in a community basis by a central unit. A more complicated issue arises when sensing scheduling of multiple primary channel is targeted due to different energy storage levels and energy arrival rates of SUs. Scheduling involves more complexity if SUs are solely empowered by RF energy harvesting, in such a case, while some SUs seek for idle channel discovery for spectrum utilization and some others look for busy channels for harnessing primary signals. In this case, traditional cooperative spectrum sensing scheduling methods are required to be redesigned to support the second kind of SUs above.

5.1.1 Chapter Contributions and Novelty

In this chapter, only the *harvest-sense-transmit* mode is considered since other two modes are a special case of the second one. The energy-arrival rate from renewable sources significantly affects the non-interrupted operation of a system which are purely empowered by renewable sources. Therefore, hybrid powered systems equipped with back-up non-renewable energy source may be more attractive to deal with the low energy-arrival rates in practice [97]. In this respect, a *full-duplex hybrid* EH-CR module is first proposed to mitigate the half-duplex constraint by exploiting two different energy storage and harvests energy from both renewable sources, i.e., solar, and ambient RF signals. After demonstrating the differences in the timeslotted operation of SUs as a result of their heterogeneous sensing and reporting channel characteristics, we develop the energy state evolution of both systems. Based on SUs' energy states, a convex myopic policy optimization frame work is developed to find the optimal energy harvesting policy to jointly obtain the optimal harvesting ratio, sensing duration, and detection threshold of each SU which maximizes the sum of the achievable throughput of SUs of the current timeslot subject to *collision and energy-causality* constraints.

Exploitation of two different storage devices/batteries is first considered in [20] where authors enforce the secondary battery (SB) to transfer its all available energy to the primary battery (PB). However, transferring the stored energy may not be necessary under a possible energy loss during the energy transfer. Therefore, a more general EH module is proposed to power the SUs directly from both PB and SB. Assuming SUs have homogeneous sensing and

reporting channels (i.e., identical SNRs as in [98], channel gains, reporting errors etc.), optimal sensing durations of all SUs will be the same. Based on this homogeneity assumption, *Binomially* distributed K-out-of-N rule is extensively employed to conclude a global decision by enforcing SUs to have identical detection and false alarm reports at the CH. In a practical scenario where SUs have heterogeneous sensing and reporting channel qualities, however, enforcing SUs to have identical local reports at the CH causes SUs with relatively low SNRs to sense for very long times. In addition to being energy inefficient, conventional K-out-of-N is also throughput inefficient since SUs with relatively high SNRs must wait for the slowest SU and the CH will not diffuse back the final decision until it collects all reports. Therefore, to capitalize from the sensing and reporting quality diversity of SUs, a *Poisson-Binomial* K-out-of-N rule is employed where SUs with different sensing and reporting qualities are allowed to have different reported detection performances. Obtained results clearly demonstrate that the combination of the proposed Poisson-Binomial based EEH-CSS and full-duplex systems provide the best result in terms of sensing energy cost reduction, achievable throughput maximization and harvested energy accumulation.

5.1.2 Chapter Organization

The rest of this chapter is organized as follows: Section-5.3 models the proposed full-duplex system based on stochastic energy arrivals. Section-5.4, introduces the proposed CSS scheme. After that, Section-5.5 characterizes the energy state evolution of each SU and formulates the convex myopic policy optimization. Numerical results are presented in Section-5.6. Finally, Section-5.7 summarizes the chapter.

5.2 Related Work

An influential work is presented in [99], which proposes a novel framework, enabling SUs to opportunistically harvest ambient RF energy as well as reuse the spectrum of PUs. Also, the transmission probability of SUs and the resulting system throughput of the CRN were derived under a stochastic-geometry model. In his early work, Sultan considers a non-cooperative spectrum sensing where a single SU tries to maximize the throughput while making decision

on being either dormant or active to sense the primary channel based on a Markov decision process [100]. Inspired by [101], Yin et al. studies the fundamental tradeoffs among harvesting, sensing, and transmission duration in CSS where SUs sense one-by-one and report via a perfect CCC [98].

Park et.al. focus on maximizing the expected total throughput of a single SU-PU system subject to energy causality and collision constraints. They divide the system operation into a spectrum-limited regime and an energy-limited regime depending on where the detection threshold lies. Their analytical and numerical findings show that the system is energy-limited if the energy arrival rate is lower than the expected energy consumption for a single spectrum access [102]. Based on a time-homogeneous discrete Markovian primary traffic model, they also develop a constrained POMDP, and then convert it to a computationally tractable unconstrained POMDP to obtain a spectrum access policy in which an SU decides on being active to sense and transmit or being idle to conserve energy [103]. Again considering the same primary traffic model, they also derive the upper bound on the achievable throughput as a function of the energy arrival rate, the temporal correlation of the primary traffic, and the detection threshold [104].

Authors of [105] consider a single-user multi-channel CRN setting and maximize the throughput of SU under energy causality constraint and fading channel conditions. Based on the probabilistic energy availability, primary network's belief state, and channel conditions a channel selection criterion is proposed to choose the best subset of channels for sensing. They construct a channel-aware optimal and myopic sensing strategies in a POMDP framework depending upon the proposed channel selection criterion. Usman and Koo consider a hybrid underlay-overlay energy harvesting CRN where SUs can harvest energy from the primary user's signal as well as from the other ambient sources [106]. Similar to previous works, they employ a POMDP to maximize long-term throughput of the system along with a energy threshold to determine the transmission mode (overlay or underlay). Numerical results have shown that the proposed system provides 60% improved throughput than overlay-only cognitive radio in certain cases and 43% enhanced throughput than a hybrid CRN harvesting energy only from the ambient sources.

Authors of [107] identify the optimal pairing of the sensing duration and the detection threshold in order to maximize the average throughput of the secondary network. Simulation results show that the optimal sensing duration is determined based on which constraint needs to have priority. Yin et. al. consider an energy harvesting CR system with a single SU-PU pair where SU operates on save-then-transmit protocol. They investigate the SU's optimal cooperation strategy and optimal action in non-cooperation/cooperation modes to maximize the SU's achievable throughout and derive the optimal closed-form solutions. Based on the optimal analytical results, they propose an optimal cooperation protocol to make the optimal decision. Numerical results has shown that it outperforms the non-cooperation protocol, the stochastic cooperation protocol, the optimal underlay transmission mode [108]. Authors of [109] propose a system model where the SUs are able to cooperate to maximize the overall network throughput through sensing. Different from other, they formulate the cooperative decentralized optimization problem as a decentralized POMDP and apply a decentralized learning algorithm based on the policy gradient and the Lagrange multiplier method to obtain optimal channel access policies. In [110], authors develop a CSS scheduling policy so that the time average utility generated by the sensors is maximized. Assuming infinite battery capacity, they first consider an offline setting and show that the optimal scheduling structure has a "majorization" property, and then propose a procedure to construct a collaborative sensing policy with the identified structure explicitly. For the online setting, on the other hand, they assume that the energy harvesting processes at individual sensors are independent but not necessarily identical Bernoulli processes and show that the expected long-term time average sensing utility has an upper bound under any feasible scheduling policy satisfying the energy causality constraints. After that, they propose a randomized myopic policy, which aims to select a number of sensors with the highest energy levels to perform the sensing task in each slot.

5.3 System Model

Consider a CRN comprised of a single PC and N time synchronous and self-powered EH-SUs. The PU works in a time slotted fashion such that the primary channel is either in a busy or idle state for a given timeslot. The sensing and reporting channels conditions assumed to be

constant during a timeslot. Similarly, SUs also cooperatively operate in timeslots of T seconds to harvest, sense and utilize the primary channel. To facilitate the analysis in this chapter, we assume that the SU always has data to transmit and demands for as higher achievable throughput if available. The stochastic energy arrival rate is modeled as a random variable Λ_n in $[Joule/s]$ which follows a general distribution function with mean λ_n and variance $\sigma^2_{\lambda_n}$. For example, Λ_n can be interpreted as the received amount of energy per time unit with respect to received luminous intensity of a solar panel in a particular direction per unit solid angle. The energy arrival rate within a timeslot t, λ_n^t, $\forall t$, is assumed to be time invariant. Accordingly, to store the harvested energy, super-capacitors are preferred storage devices due to their high power density, good recycling ability and near perfect storing efficiency (around 0.99). Albeit this favorable features, they are half-duplex EH constrained. This leads to a performance degradation in harvested energy amount and available time left for data transmission because SUs have to split the timeslot for harvesting and sensing-transmitting. Therefore, exploiting two different energy storage, a full-duplex energy harvesting model can be obtained to mitigate the half-duplex EH constraint limitations as shown in Figure 5.1 where the PB has a storing efficiency of $\zeta_n^1 \in [0,1]$ and storage capacity of B_n^1. The SB, on the other hand, can be either identical of the PB or a conventional lithium-ion battery with a lower storing efficiency $\zeta_n^2 < \zeta_n^1$ and relatively large storage, $B_n^2 >> B_n^1$. At the beginning of the each timeslot t, SU is aware of available energy levels in the PB ($B_n^1(t)$) and SB ($B_n^2(t)$).

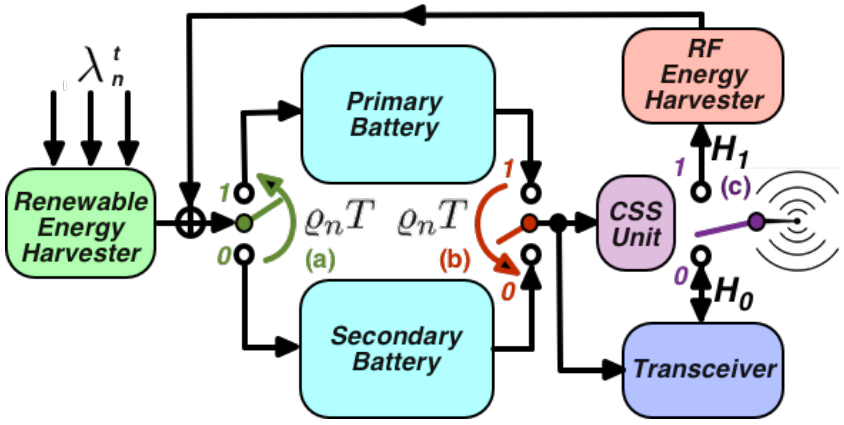

Figure 5.1: Full-Duplex Hybrid Energy Harvesting Model

In Figure 5.1, the switch (a) splits the renewable energy arrivals in time without interrupting the sensing-reporting-transmitting of the CR; $\varrho_n T$ and $(1-\varrho_n)T$ durations are allocated for storing the harvested energy on the PB and the SB, respectively. The switch (b) works in opposite direction of the switch (a) to power the SU, i.e., while the PB/SB collects energy arrivals the SB/PB powers the SU. In doing so, assuming negligible switching time, the SU is able to harvest energy for the whole timeslot while powering the SU uninterruptedly. Hence, the SU has $\left(B_n^{1,t}+B_n^{2,t}\right)$ energy for the remaining timeslot for sensing, reporting and transmission tasks. Right after execution of the local sensing, reporting and receiving the global decision, CSS unit toggles the switch (c) to position 0 in the case of PU absence to transmit secondary data with the remaining energy, otherwise it toggles the purple switch to position 1 to harvest RF energy from the primary channel with the harvesting rate which is given by

$$\lambda_n^{rf,t} = P(d_n^t)^{-\theta}\zeta_n^{rf}\ \mathbb{I}\left[P(d_n^t)^{-\theta} > \bar{P}\right]\ [Watt] \tag{5.1}$$

where P denotes the transmission power of the RF source, $(d_n^t)^{-\theta}$ is the path loss over the distance d_n^t with the corresponding path loss exponent θ, ζ_n^{rf} denotes the efficiency of RF-to-DC converter circuit, and $\mathbb{I}\left[P(d_n^t)^{-\theta} > \bar{P}\right]$ is the indicator function to impose RF-to-DC circuitry sensitivity on the received RF power such that there is no gain if the received power is less than the sensitivity threshold, $\bar{P}$.

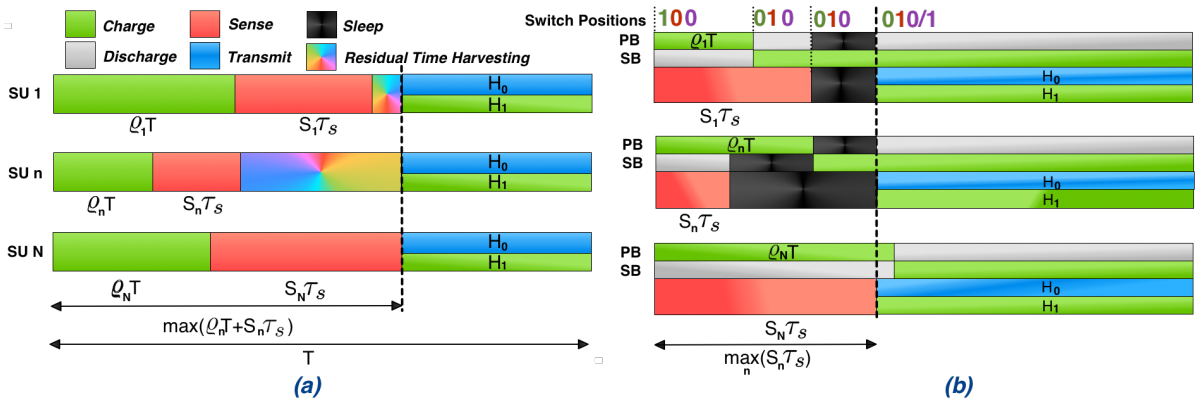

Figure 5.2: Time-slot Representation of (a) Half and (b) Full Duplex Energy Harvesting CRs

5.3.1 Time-slotted Operation for Half-Duplex System

Half-duplex system (HDS) can be obtained as a specific case of the proposed full-duplex model in Figure 5.1 by eliminating the SB and keeping the switch (b) in position 1 all the time. In the HDS, as shown on the left in Figure 5.2.a, SU n harvests renewable energy for $\varrho_n T$ seconds, and uses the stored available energy from the previous timeslot along with the harvested energy in the current timeslot to complete CSS tasks. Right after the sensing duration, SUs keep harvesting energy until they receive a global decision feedback from the CH, which is shown as a multicolor portion of the timeslot in Figure 5.2.a. Based on the decision, the residual time is used for the secondary data transmission by toggling the switch (c) to position 0 in case of $\mathcal{H}_0$, otherwise it is toggled to position 1 for RF energy harvesting until the beginning of the next timeslot.

5.3.2 Time-slotted Operation for Full-Duplex Systems

The timeslotted operation of the full-duplex system (FDS) is demonstrated in Figure 5.2.b where the positions of switches have also been shown in zeros and ones for the first SU to provide readers with more insight into the proposed model. By using the SB, the SUs are now able to harvest energy for the entire timeslot while also using the entire timeslot for sensing and transmitting/RF harvesting. As mentioned earlier, the different sensing duration of SUs problem still applies and SUs put themselves into *sleep mode* to save energy until they receive a decision from the CH. The benefit of employing a FDS is intuitive since the SUs are able to harvest for the whole timeslot instead of harvesting for just $\varrho_n T$ as in HDS. We also note that both HDS and FDS models may further be simplified for SUs which are solely empowered by RF energy harvesting by eliminating the renewable energy harvester and replacing it with the RF energy harvester.

5.4 CSS Model

Since the focus of this paper is the EH aspects of CRNs, a generic sensing method like *energy detection* is adequate for this purpose. Energy detectors (EDs) have been extensively

exploited as the ubiquitous sensing technique in the literature due to its simplicity, compatibility with any signal type, and low computational and implementation complexity [30]. We denote the *apriori* probability of idle and busy state of the primary channel as $\pi_0 = \mathcal{P}[\mathcal{H}_0]$ and $\pi_1 = \mathcal{P}[\mathcal{H}_1]$, respectively. To detect primary signals, ED of SU m measure the received signal energy for a number of samples S_n and compares it with a threshold ε_n to decide on the PU activity status. For a large enough number of samples ($S_n \geq 30$), probability of false alarm, $P_n^f = \mathcal{P}\left[\mathcal{H}_n^1|\mathcal{H}_n^0\right]$, and probability of detection, $P_n^d = \mathcal{P}\left[\mathcal{H}_n^1|\mathcal{H}_n^1\right]$, are given by (2.9) and (2.10), respectively.

After the local sensing process, SUs send their hard results u_n to the CH over a binary symmetric CCC. Denoting the reporting error probability as $p_n = \mathcal{P}[\tilde{u}_n = 1|u_n = 0] = \mathcal{P}[\tilde{u}_n = 0|u_n = 1]$ where $\tilde{u}_n$ is the hard decision received by the CH. The local false alarm and detection probabilities received at the CH side are given by

$$\begin{aligned}\tilde{P}_n^f &= \mathcal{P}[\tilde{u}_n = 1|u_n = 0]\,\mathcal{P}[u_n = 0|\mathcal{H}_0] \\ &\quad + \mathcal{P}[\tilde{u}_n = 1|u_n = 1]\,\mathcal{P}[u_n = 1|\mathcal{H}_0] \\ &= p_n\left(1 - P_n^f\right) + (1 - p_n)\,P_n^f \qquad (5.2)\\ \tilde{P}_n^d &= \mathcal{P}[\tilde{u}_n = 1|u_n = 0]\,\mathcal{P}[u_n = 0|\mathcal{H}_1] \\ &\quad + \mathcal{P}[\tilde{u}_n = 1|u_n = 1]\,\mathcal{P}[u_n = 1|\mathcal{H}_1] \\ &= p_n\left(1 - P_n^d\right) + (1 - p_n)\,P_n^d \qquad (5.3)\end{aligned}$$

The CH collects $\tilde{u}_n$'s and make the global decision using the following test

$$\mathcal{K} = \sum_n^M \tilde{u}_n \underset{\mathcal{H}_0}{\overset{\mathcal{H}_1}{\gtrless}} \kappa \qquad (5.4)$$

which follows the *Poisson-Binomial* distribution ($\mathcal{K}$ follows *Binomial* distributions as a special case $\tilde{P}_n^f = \tilde{P}^f$, $\tilde{P}_n^d = \tilde{P}^d$, $\forall n$). Using equations (5.2) and (5.3) in Poisson-Binomial distribution, the CH obtains the global false alarm and detection probabilities by fusing the local

reports as follows

$$Q_f = \mathcal{P}\left[\mathcal{K} \geq \kappa \mid \mathcal{H}_0\right] = \sum_{\kappa}^{N} \sum_{A \in F_\kappa} \prod_{m \in A} \tilde{P}_n^f \prod_{m \in A^c} \left(1 - \tilde{P}_n^f\right) \tag{5.5}$$

$$Q_d = \mathcal{P}\left[\mathcal{K} \geq \kappa \mid \mathcal{H}_1\right] = \sum_{\kappa}^{N} \sum_{A \in F_\kappa} \prod_{m \in A} \tilde{P}_n^d \prod_{m \in A^c} \left(1 - \tilde{P}_n^d\right) \tag{5.6}$$

where F_κ is the set of all subsets of κ integers that can be selected from $\{1, 2, 3, \ldots, N\}$. Since F_κ has $\binom{N}{\kappa}$ elements, using an efficient method to calculate Eq. (5.5) and (5.6) is very important, especially when N is very large. For this purpose, probability mass function (pmf) and cumulative distribution function of *Poisson-Binomial* random variables can be expeditiously calculated in order of $\mathcal{O}(N \log_2 N)$ from polynomial coefficients of the probability generating function of $\mathcal{K}$ [80].

5.5 Energy State Evolution and Myopic Policy Optimization

In EH-CSS, energy states of SUs evolve over time such that energy state in the next timeslot depends on the energy state and action taken (i.e., duration of energy harvesting, spectrum sensing, and transmitting) in the current timeslot. We define the maximum time spent for harvesting+sensing for HDS/FDS in (5.7)/(5.8), the net gained energy during Θ^{hd}/Θ^{fd} in (5.9)/(5.10), harvested energy from RF source for HDS/FDS in (5.11)/(5.12), and the total harvested energy from renewable source for FDS in (5.13) as follows

$$\Theta^{hd} = \max\left(\varrho_n T + S_n \tau_s\right) \tag{5.7}$$

$$\Theta^{fd} = \max\left(S_n \tau_s\right) \tag{5.8}$$

$$\Delta_n^{hd} = \lambda_n^t \zeta_n \left(\Theta^{hd} - S_n \tau_s\right) - S_n E_s \tag{5.9}$$

$$\Delta_n^{fd} = \lambda_n^t \left[\zeta_n^1 \varrho_n T + \zeta_n^2 [\Theta - \varrho_n T]^+\right] - S_n E_s \tag{5.10}$$

$$\Delta_n^{rf,hd} = \lambda_n^{rf,t} \left(T - \Theta^{hd}\right) \tag{5.11}$$

$$\Delta_n^{rf,fd} = \lambda_n^{rf,t} \left(T - \Theta^{fd}\right) \tag{5.12}$$

$$\Upsilon_n = \lambda_n^t \left[\zeta_n^1 \varrho_n + \zeta_n^2 \left(1 - \varrho_n\right)\right] T \tag{5.13}$$

where τ_s is the sensing duration per sample, E_s is the sensing energy expenditure per sample, $[x]^+ = \max(0, x)$, $E_n^{tx} = \min\left(E_n, B_n^{t-1} + \Delta_n\right)$ is the transmission energy where $0 \leq E_n \leq B_n$ is the allocated transmission energy for SU_n. By setting $E_n = B_n^{t-1} + \Delta_n$, SUs exhaust all available residual energy for secondary data transmission, otherwise residual energy of SUs for the next timeslot will be B_n^t which is shown for all four cases in Table 5.1.

Table 5.1: Energy States at the beginning of timeslot t, B_n^t.

HDS	**Global Decision:** $\mathcal{H}_0$	**Global Decision:** $\mathcal{H}_1$
π_0	$\min\left(B_n, B_n^{t-1} + \Delta_n^{hd} - E_n^{tx}\right)$	$\min\left(B_n,\ B_n^{t-1} + \Delta_n^{hd} + \lambda_n^t \left(T - \Theta^{hd}\right)\right)$
π_1	$\min\left(B_n, B_n^{t-1} + \Delta_n^{hd} - E_n^{tx}\right)$	$\min\left(B_n,\ B_n^{t-1} + \Delta_n^{hd} + \lambda_n^t \left(T - \Theta^{hd}\right) + \Delta_n^{rf,hd}\right)$
FDS	**Global Decision:** $\mathcal{H}_0$	**Global Decision:** $\mathcal{H}_1$
π_0	$\min\left(B_n, B_n^{t-1} + \Upsilon_n - S_n E_s - E_n^{tx}\right)$	$\min\left(B_n, B_n^{t-1} + \Upsilon_n - S_n E_s\right)$
π_1	$\min\left(B_n, B_n^{t-1} + \Upsilon_n - S_n E_s - E_n^{tx}\right)$	$\min\left(B_n, B_n^{t-1} + \Upsilon_n - S_n E_s + \Delta_n^{rf.fd}\right)$

For any taken action $a_n = \{\varrho_n, S_n, \varepsilon_n, \kappa\}$, $\forall n$, there are four possible outcomes:

1. *Idle State Detection with probability* $\pi_0 \left(1 - Q_f\right)$: In this case, SUs correctly detect the absence of the PU while it is indeed absent. Hence, by exhausting E_n^{tx} amount of energy, SUs obtain expected achievable throughput of CSS in HDS and FDS as

$$R^{hd} = \pi_0 \left(1 - Q_f\right) R_{00}^{hd} = \pi_0 \left(1 - Q_f\right) \sum_n \frac{T - \Theta^{hd}}{T} \log_2 \left[1 + \frac{E_n^{tx}}{T - \Theta^{hd}}\right] \tag{5.14}$$

$$R^{fd} = \pi_0 \left(1 - Q_f\right) R_{00}^{fd} = \pi_0 \left(1 - Q_f\right) \sum_n \frac{T - \Theta^{fd}}{T} \log_2 \left[1 + \frac{E_n^{tx}}{T - \Theta^{fd}}\right] \tag{5.15}$$

   where R_{00}^{hd} and R_{00}^{fd} are sum of the achievable throughput of HDS and FDS for a normalized noise power at a given timeslot, respectively.

2. *False alarm with probability* $\pi_0 Q_f$: PU is absent while the channel is detected to be busy. The SUs decided to harvest from both renewable source and RF energy instead of utilizing the channel but only renewable source is harvested.

3. *Miss-Detection with probability* $\pi_1 (1 - Q_d)$: PU is present while the sensing result is incorrect. SUs decided to transmit but transmission was unsuccessful due to the collision with PUs.

4. *True-Detection with probability* $\pi_1 Q_d$: PU is present while the sensing result is correct. The SUs decided to harvest from both renewable source and RF energy instead of utilizing the channel.

Based on these outcomes and energy state evolution of SUs, an optimal design for energy harvesting and sensing strategy can be formulated as an MDP with an uncountable and continuous state and action space. Hence, a myopic policy is considered to only focus on the current timeslot by ignoring its effects on future rewards. It has been shown that a myopic policy is very close to the optimal policy with greatly reduced computational cost [111].

$$
\begin{aligned}
\mathbf{P\ 5.1}: \max_{\boldsymbol{\varrho},\boldsymbol{S},\boldsymbol{\varepsilon},k} \quad & \log_2(\pi_0) + \log_2(1 - Q_f) + \log_2\left(R_{00}^{hd}\right) \\
1: \quad \text{s.t.} \quad & \log\left(Q_{th}^{d}\right) \leq \log(Q_d) \\
2: \quad & 0.5 \leq P_n^d, \ \forall n \\
3: \quad & P_n^f \leq 0.5, \ \forall n \\
4: \quad & 0 \leq T - \Theta^{hd} \\
5: \quad & 0 \leq B_n^{t-1} + \Delta_n^{hd}, \ \forall n \\
6: \quad & 0 \leq \varrho_n \leq \min\left(B_n - B_n^{t-1}, 1\right), \ \forall n \\
7: \quad & 30 \leq S_n \leq T/\tau_s, \ \forall n \\
8: \quad & k \in \mathbb{N}^+, \ S_n \in \mathbb{R}^+, \ \varepsilon \in \mathbb{R}, \ \forall n
\end{aligned}
$$

Accordingly, problem of maximizing the average achievable throughput for HDS can be formulated as in **P 5.1** where we take the logarithm of (5.14) to put the objective in a convex form. **P 5.1** is an MINLP problem whose mixed-integer nature is due to the variables S_n and κ. It is a practical approach to relax the problem by unintegerizing S_n. After obtaining the optimal reel valued solution, one can obtain the closest upper integer value, which does not negatively effect the system performance since $S_n >> 1$ and $\tau_s,\ E_s << 1$. However, **P 5.1**

is still an MINLP problem due to the decision rule, $1 \leq \kappa \leq N$ and its optimal value can be found by the branch-and-bound algorithm. For the rest of this chapter, we will employ the majority voting rule, $\kappa = \lceil N/2 \rceil$ where $\lceil \cdot \rceil$ denotes the ceiling operation, which has already been shown to be the optimal voting rule for required minimum SNR (i.e. required minimum sensing energy cost) of CSS [13]. Therefore, the following convexity analysis is based on the unintegerization of S_n for $\kappa = \lceil N/2 \rceil$.

The first term of the objective function is a constant and out of the consideration. The second term is a concave function since Q_f/Q_d are log-concave functions of $\tilde{P}_n^f/\tilde{P}_n^d$ in both Binomial and Poisson-Binomial distribution cases. It is also non-decreasing in each term $\tilde{P}_n^f/\tilde{P}_n^d$ since Q_f/Q_d intuitively increases as SUs report with more confidence. P_n^f/P_n^d are expressed in the form of $\mathcal{Q}$ function in (2.9)/(2.10) which is convex and concave for values $\mathcal{Q}(\cdot) \leq 0.5$ and $\mathcal{Q}(\cdot) \geq 0.5$, respectively. Indeed, constraining local detection probabilities to be higher than 0.5 and false alarm probabilities to be lower than 0.5 are not against the practical point of interests. Reported local probabilities $\tilde{P}_n^f/\tilde{P}_n^d$, on the other hand, are non-negative weighted sums of the reporting error in (5.2)/(5.3) and still preserve the concavity and convexity at the CH side. Furthermore, exploiting the convex composition mechanics [34], the concavity of the $\log(1 - Q_f)$ and the first constraint, $\log(Q_d) > Q_{th}^d$ is given in Appendix A.1.2.

The last term in the objective is the logarithm of R_{00}^{hd} which is a function of Θ^{hd} in (5.7). Θ^{hd} is a piece-wise maximum of functions $f_n(\varrho_n, S_n) = \varrho_n T + S_n \tau_s$ which is a linear function of ϱ_n, S_n and constant for $\varrho_{n'}, S_{n'}$, $\forall n' \neq n \in [1, N]$. Since piece-wise maximization preserves the convexity and $f_n(\varrho_n, S_n), \forall n$ is linear, Θ^{hd} is a convex function of $\varrho_n, S_n, \forall n$, which is again followed from the convex composition rules. On the other hand, since $g(x) = \log(1 + x)$ is concave and monotonically non-decreasing for non-negative x and perspective operation preserves concavity [34], the inner part of last term can be considered as the perspective function of Θ^{hd}. Thus, the last term of the objective is also concave following from the convex composition rules. Constraint 4, $\Theta^{hd} \leq T$, defines the upper-bound of the maximum harvesting+sensing time as the timeslot duration. Constraint 5 enforces the system to have enough storage to execute the sensing operation for $S_n E_s$ amount of energy. Constraint 6 limits the harvesting rate since harvesting and storing energy up to a fully charged battery does not provide any additional

energy. Then, number of samples, S_n in constraint 7, is lower-bounded to evoke the CLT and upper-bounded to maximum permissible number of samples within a timeslot duration. For FDS, **P 5.1** can be modified to become **P 5.2** as follows

$$\mathbf{P\ 5.2}: \max_{\boldsymbol{\varrho},\boldsymbol{S},\boldsymbol{\varepsilon},k} \quad \log_2(\pi_0) + \log_2(1-Q_f) + \log_2\left(R_{00}^{fd}\right)$$

$$\text{1:} \quad \text{s.t.} \quad \log\left(Q_{th}^{d}\right) \leq \log(Q_d)$$

$$\text{2:} \quad 0.5 \leq P_n^d,\ \forall n$$

$$\text{3:} \quad P_n^f \leq 0.5,\ \forall n$$

$$\text{4:} \quad 0 \leq T - \Theta^{fd}$$

$$\text{5:} \quad 0 \leq B_n^{1,t-1} + B_n^{2,t-1} + \Delta_n^{fd},\ \forall n$$

$$\text{6:} \quad 0 \leq B_n^{1,t-1} + \lambda_n^t \zeta_n^1 \varrho_n T \leq B_n^1,\ \forall n$$

$$\text{7:} \quad 0 \leq B_n^{2,t-1} + \lambda_n^t \zeta_n^2 (1-\varrho_n) T \leq B_n^2,\ \forall n$$

$$\text{8:} \quad 30 \leq S_n \leq T/\tau_s,\ \forall n$$

$$\text{9:} \quad k \in \mathbb{N}^+,\ S_n \in \mathbb{R}^+,\ \varepsilon \in \mathbb{R},\ \forall n$$

where constraints 5, 6 and 7 is adapted for FDS to apply the same reasoning given above. Even though the convexity analysis of **P 5.2** follows the same spirit of **P 5.1**, it is worth indicating that the objective function of **P 5.2** is free of ϱ_n. Unlike in HDS, this is because of the FDS feature that the entire timeslot is accessible for both harvesting and sensing + transmitting. SUs can spend the harvested energy in the beginning of a timeslot within the same timeslot, which requires joint optimization of all variables. Hence, if SUs are allowed to expend only the residual energy from the previous timeslot, variables ϱ_n and (S_n, ε_n, κ) can be separated inherently. Such a policy can be formulated as

$$\mathbf{P\ 5.3}: \max_{\varrho_n} \quad \Upsilon_n = \lambda_n^t \left[\zeta_n^1 \varrho_n + \zeta_n^2 (1-\varrho_n)\right] T$$

$$\text{1:} \quad \text{s.t.} \quad 0 \leq B_n^{1,t-1} + \lambda_n^t \zeta_n^1 \varrho_n T \leq B_n^1,\ \forall n$$

$$\text{2:} \quad 0 \leq B_n^{2,t-1} + \lambda_n^t \zeta_n^2 (1-\varrho_n) T \leq B_n^2,\ \forall n$$

where the objective is the total harvested energy during the entire timeslot and harvesting ratios are limited to the PB and SB capacity in lines 1 and 2, respectively, so that, once one

of them is fully charged, the other one starts to harvest energy in order to avoid wasting the energy arrivals. **P 5.3** can equivalently be written as

$$\mathbf{P\ 5.4}: \max_{\varrho_n} \ \varrho_n \lambda_n^t \left(\zeta_n^1 - \zeta_n^2\right) T$$

$$\text{s.t.} \quad \max\left(0, -\frac{B_n^{1,t-1}}{\lambda_n^t \zeta_n^1 T}, 1 - \frac{B_n^2 - B_n^{2,t-1}}{\lambda_n^t \zeta_n^2 T}\right) \leq \varrho_n \leq \min\left(1, \frac{B_n^1 - B_n^{1,t-1}}{\lambda_n^t \zeta_n^1 T}, 1 + \frac{B_n^{2,t-1}}{\lambda_n^t \zeta_n^2 T}\right)$$

Based on **P 5.4**, finding the optimal harvesting policy of FDS is trivial and can be analyzed in three different cases:

1. $\zeta_n^1 = \zeta_n^2$: In this case, the PB and SB have identical harvesting efficiency and any ϱ_n within the feasible region is optimal.

2. $\zeta_n^1 > \zeta_n^2$: In this case, optimal harvesting ratio is attained at the upper bound.

3. $\zeta_n^1 < \zeta_n^2$: In this case, optimal harvesting ratio is attained at the lower bound.

Please note that the optimal policy is independent from the storage capacities, B_n^1 and B_n^2.

5.6 Results and Analysis

Even though the proposed work is adaptable to more general scenarios, throughout the simulations, we deliberately enforce HDS and FDS to have identical total storage capacity and storing efficiency to establish a fair comparison between them. Energy arrival intensity is assumed to follow Gamma distribution with shape and scale parameters 1 and 0.75, respectively. To clearly show the impacts of heterogeneous SNR levels, cooperation of 5 SUs is considered with -5, -10, -15, -20, -25 SNRs in dB. Unless it is explicitly stated otherwise, the parameters given in Table 5.2 is exploited through the results.

Table 5.2: Default parameters used for obtaining results

Par.	Value	Par.	Value	Par.	Value	Par.	Value
B_n	30 J	B_n^1	15 J	B_n^2	15 J	σ_n^2	1
ζ_n	0.99	ζ_n^1	0.99	ζ_n^2	0.99	ζ_n^{rf}	0.6
W_n	1 MHz	T	2 s	τ_s	1 μs	π_0	0.4, 0.8
Q_{th}^d	0.99	E_n	2 J	E_s	1 μJ	θ	2

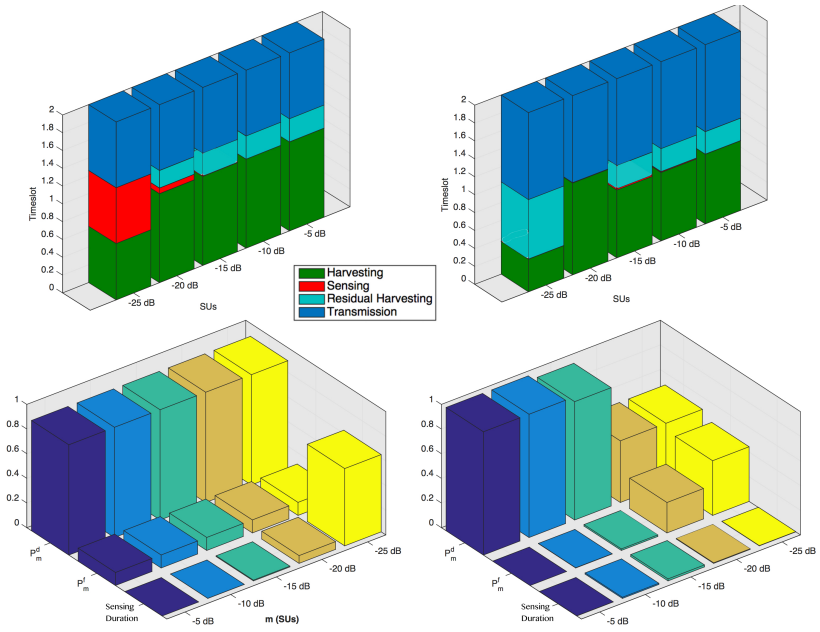

Figure 5.3: Comparison of Binomial and Poisson-Binomial based fusion rules: Optimal timeslots for Binomial (a) and (b) Poisson-Binomial, number of samples, detection and false alarm probabilities for Binomial (c) and (d) Poisson-Binomial.

Figure 5.3 compares the optimal values of traditional binomial and the Poisson-Binomial based majority voting rule, $\kappa = \lceil N/2 \rceil$, for an HDS with an empty storage. As can be observed from (a) and (c), the SU with the lowest SNR has to expend its all harvested energy to sense for a long duration in order to achieve 0.9/0.1 local P_d/P_f target. For Poisson-Binomial case, on the other hand, while SUs with relatively low SNRs are relaxed to have low local detection performances (around 0.5), SUs with relatively high SNRs are enforced to have nearly perfect local detection performances. Therefore, by exploiting the SNR diversity of SUs, Poisson-Binomial approach reduced the required sensing energy, which leaves more room in a timeslot for harvesting and secondary transmission. Even though SUs with high SNRs harvest more energy in HDS, utilization of this energy in terms of the achievable throughput is negatively affected by the unnecessarily long sensing duration of the slowest SU. Overall, considering the sensing and reporting channel heterogeneity of SUs by assigning different local false alarm and detection probabilities is more efficient and balanced in terms of harvesting, sensing, and throughput efficiency.

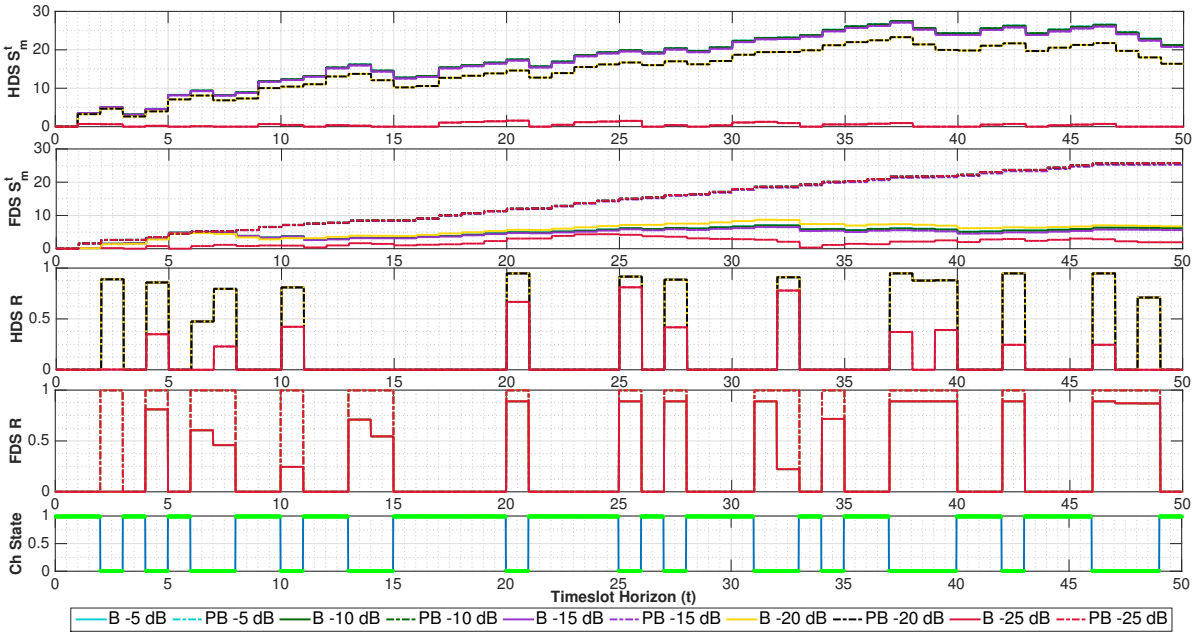

Figure 5.4: Horizontal energy levels and throughput for $\pi_0 = 0.4$.

Figure 5.4 demonstrates the above discussion for a finite horizon of size 50 where apriori probability of being idle for the channel is 0.4. The bottom plot shows the energy levels at the beginning of the timeslots, and the middle plots show the corresponding achieved data rate corresponding to the actual channel state shown at the bottom. Since the primary channel is mostly busy, which is detected with at lest $Q_{th}^d = 0.99$ probability, both HDS and FDS accumulate energy due to the lack of chance to spend it for transmission. It is clear that, the SU with the lowest SNR does not experience energy accumulation in both HDS and FDS under the traditional binomial case. However, its negative nature is mitigated in Poisson-Binomial approach and it behaves similar to other SUs. Poisson-Binomial case in HDS have superior performance than the traditional one in terms of the throughput. When it comes to FDS, both Poisson-Binomial and Binomial approach have a better performance than the HDS. Among all combinations, It is clear that the combining the FDS with the Poisson-Binomial is the best solution.

Similar observations can be made for Figure 5.5 where the apriori probability of being idle for the channel is 0.8. In this case, the PU is mostly absent and SUs take advantage of this by

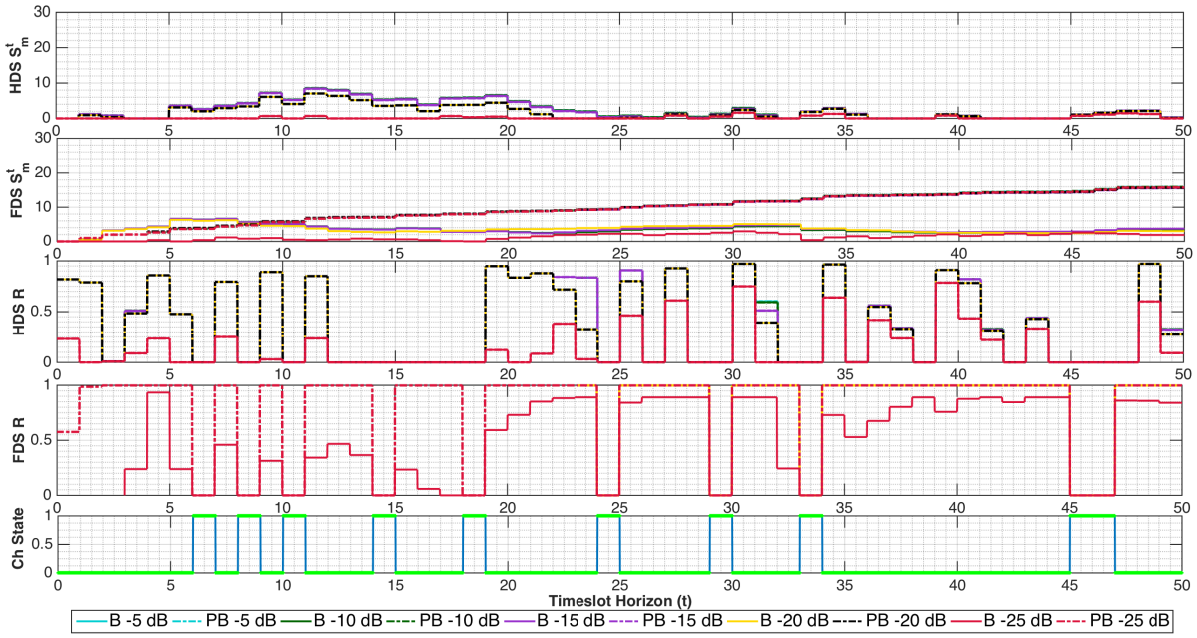

Figure 5.5: Horizontal energy levels and throughput for $\pi_0 = 0.8$

utilizing the channel instead of not transmitting and saving the harvested energy. It is worth noting that if the energy arrival intensity increases, the slope of the energy accumulation will also increase, or vice versa.

5.7 Chapter Summary

In this chapter, the performance of half-duplex and full-duplex energy harvesting systems are investigated under the heterogeneous sensing and reporting channel characteristics of SUs. The results show that exploiting the hybrid full-duplex EH system gives a superior performance since the whole timeslot is available for both EH and sensing-reporting-transmitting tasks. Moreover, instead of using a traditional Binomially distributed voting rule which enforces SUs to see identical local detection performances at the CH, exploitation of Poisson-Binomially distributed voting rule allowed the capitalization the SU heterogeneity, which has yielded less energy cost and more time left for secondary data transmission. Finally, it is shown that the combination of the full-duplex EH with the Poisson-Binomially distributed voting rule gives

the best result in terms of in terms of sensing energy cost reduction, achievable throughput maximization and harvested energy accumulation under the network heterogeneity.

CHAPTER 6. CONCLUSIONS AND FUTURE WORK

6.1 Conclusions and Summary of Contributions

EEH-CRNs have potential of self-sustaining its spectrum and energy demands in an opportunistic and non-intrusive manner such that it keeps its harm to the primary network and the environment at a negligible level. To alleviate the shortcomings of individual SUs, CSS is primarily exploited to obtain cooperative gain by taking benefits from spatiotemporal diversity of individual observations. However, such a gain is not free of energy, delay, and communications overhead in real life scenarios. If the minimization of the energy cost along with the maximization of the obtained opportunity is the main concern of the system design and a designer is obligated to obey a collision constraint to protect primary network activity, there exists many tradeoffs to be dealt with as repeatedly pointed out through the thesis. In a heterogeneous CRN scenario, on the other hand, the complexity of the design increases since every single SU is required to be considered by its own sensing and reporting characteristics. Combinatorial nature of the problem is another major issue when there exists multiple PCs offering different levels of QoS. In such a case, one needs to determine the optimal set of PCs to be scheduled for sensing along with the optimal set of SUs and their optimal sensing parameters to sense those PCs. Since the PU protection is a non-linear constraint, the system design becomes an MINLP problem which is known to be NP-hard and requires impractical time complexity even for moderate sizes of CRNs. In addition to the collision constraint, EH restricts the system design to another fundamental limit, namely, the energy causality constraint which is a result of random nature of the energy arrivals. In this thesis, all research efforts have focused on achieving a green CRN by satisfying these fundamental limits and taking the practical con-

cerns into account. In the sequel, a brief summary of the main contributions of the thesis is outlined.

1. In Chapter 3, partitioning of a heterogeneous CRN into clusters was addressed such that each cluster is responsible for sensing a PC and an SU can join at most one cluster at a time. The set of PCs to be sensed was given and SUs were required to sense all of them. This problem was formulated as a multi-objective MINLP problem with the following objectives: 1) Intra-cluster energy minimization of each cluster, 2) Intra-cluster throughput maximization of each cluster, and 3) Inter-cluster energy and throughput fairness. A two tier solution strategy is developed from macro and micro perspectives. While the macro perspective was dealing with the selection of SUs into cluster, the micro perspective was a sub-routine to evaluate the fitness of candidate solutions generated by the macro perspective using a multi-objective genetic algorithm. In the micro perspective, a generalized CH selection procedure was developed to find the best CH with the minimum reporting error and the optimal routing paths from cluster members to the best CH. Numerical results have shown that the performance of multihop diversity is superior to traditional single hop approach and it is robust against the BEP wall phenomenon after which there is no reliable CSS [13]. Given the best CH and optimal routing paths, a novel HDF based CSS scheme was developed in a convex framework by taking the heterogeneity of the sensing quality of SUs into consideration. Using the same spirit, a WSST is proposed for quantized SDF based CSS by assigning weighted sample size proportional to SUs' sensing quality. A significant performance increase was observed with respect to the CSS schemes which assumes the homogeneity of SUs and treats them equally.

2. Unlike Chapter 3, Chapter 4 considered the case when the number of PCs is very large such that they cannot be sensed at the same time. A PC may provide very low QoS due to its high probability of being busy and/or it may require very high energy consumption since SUs have very low sensing quality to reliably sense this PC. If both of these cases happen at the same time, a poor QoS will be obtained even though a large amount of

energy is expended. Therefore, determination of the set of PCs to be sensed was focused in Chapter 4. On the other hand, restricting SUs to join at most one cluster at a time may not be the best strategy if the SU has high SNR on different PCs. That is, it can sense multiple PCs at a given timeslot for a very low energy cost. However, an SU needs to reconfigure its radio and sensing parameters to sense multiple PCs. This naturally requires an additional energy cost of channel switching and time delay. Defining the opportunity as the achievable total data rate and its cost as the total energy consumption as a result of sensing, reporting and channel switching operations, an CSSS problem was formulated to minimize the cost per obtained opportunity subject to collision and spectrum utilization constraints. An optimal CSSS is required to determine the following: 1) The optimal subset of PCs to be scheduled for sensing, 2) The SU assignment set for each scheduled PC, and 3) Optimal sensing parameters of SUs for each PC. Assuming 1 and 2 are given, a convex framework of the sub-problem is established. After that, a closed-form expression for the homogeneity assumption was derived for obtaining a more tractable approach and for comparison purposes. Exploiting this sub-problem, a prioritized ordering heuristic was developed to order PCs under the spectrum, energy and spectrum-energy limited regimes. After that, a scheduling and assignment heuristic is proposed and is shown to have a performance that is very close to the exhaustive optimal solution. Finally, the behavior of the CRN is numerically analyzed under these three regimes with respect to various numbers of SUs, PCs and mean SNR levels.

3. In addition to the collision constraint, energy causality is another fundamental constraint to be satisfied by EH-CRNs. This is mainly because of the random and intermittent arrivals of the energy. Due to the half-duplex EH constraint which does not allow simultaneous charging and discharging of the ultra-capacitors, harvesting duration emerges as an additional tradeoff and a timeslot is required to be shared among harvesting, sensing and secondary transmission. In Chapter 5, a full duplex hybrid EH-CR module is proposed to solve the half-duplex EH limitation and to harvest from both renewable source and ambient RF signals. After demonstrating the differences in the timeslotted opera-

tion of SUs for a single PC, the energy state evolution of half and full duplex systems are derived under stochastic energy arrivals. To find an optimal myopic EH policy, a convex optimization framework is then developed to jointly obtain the optimal harvesting ratio, sensing duration and detection threshold of each SU which maximizes the sum of the achievable throughput of cooperating SUs subject to collision and energy-causality constraints. Obtained results demonstrated that the combination of proposed full-duplex EH system with the consideration of heterogeneity provide the best result in terms of sensing energy cost reduction, achievable throughput maximization and harvested energy accumulation.

6.2 Future Work

Some of the possible future research directions can be given as follows:

- Proposed multihop reporting based CH and route selection had the goal of achieving the minimum total reporting error. From a delay sensitive approach, however, proposed method could be adopted to minimize the total time delay, hence, increasing PC availabilities.

- Although various HDF and SDF based CSS schemes were investigated and compared with respect to their energy efficiency performance, a generalized policy might be beneficial to decide on which scheme to employ according to sensing and reporting quality of SUs. As an illustration, an optimal policy may be developed to decide on the number of reported bits by each SU, which would assign various quantization resolutions for each SU.

- In Chapters 3 and 4, assignment of SUs into clusters were mostly studied to minimize the total energy cost. However, another practical concern should also take the spatiotemporal correlation of SUs on the same PC during the SU assignment.

- Finally, Chapter 5 enforced all SUs to be involved in sensing in a greedy manner. However, an optimal action policy would provide a higher performance gain if SUs wisely decide to cooperate for sensing or keep silent based on their battery levels and energy

arrival rates. Similar to different energy and spectrum availability regimes in Chapter 4, developing different action policies could be very useful. Another practical approach would be generalizing the proposed methods along with the aforementioned future works to CRNs with multiple PCs.

APPENDIX A. CHAPTER 3 PROOFS

A.1 Convexity Analysis of Hard Decision Case

The convexity analysis of **P 3.1-LLP** and **P 3.1-ULP** are handled in two subsections: A) After showing that **P 3.1** is not a convex problem, the parameterized concavity / convexity of $P^d_{m,n}(S^n_m, \varepsilon^n_m, \rho^n_m)$ / $P^f_{m,n}(S^n_m, \varepsilon^n_m)$ is proven. B) Based on part A, it is shown that the global detection / false alarm probability $Q^d_m(\tilde{P}^d_{m,n}(S^n_m, \varepsilon^n_m, \rho^n_m))$ / $Q^f_m(\tilde{P}^f_{m,n}(S^n_m, \varepsilon^n_m))$ is a log-concave function of $\tilde{P}^d_{m,n}(S^n_m, \varepsilon^n_m, \rho^n_m)$ / $\tilde{P}^f_{m,n}(S^n_m, \varepsilon^n_m)$, so that line 2 in **P 3.1-LLP** and lines 2-3 in **P 3.1-ULP** are both convex constraints.

Throughout this appendix, cluster and SU indices (i.e, m and n) are omitted for the sake of notational convenience without loss of generality. To distinguish from each other, the inside expressions of erfc$(\cdot)$ in (2.15-2.16) are denoted as follows

$$f(S,\varepsilon) = \frac{A\varepsilon}{\sqrt{S}} + B\sqrt{S}$$
$$g(S,\varepsilon,\rho) = \frac{1}{1-\rho^2}\left(\frac{A\varepsilon}{\sqrt{S}} + (B-\rho)\sqrt{S}\right)$$

where $A = \frac{1-\rho^2}{2\rho}$ and $B = A\log(1-\rho^2) + \rho$. Since convex composition rules is extensively exploited in this section, it is better to remind the readers of these rules as follows

Remark A.1: *For* $b : \boldsymbol{R}^k \to \boldsymbol{R}$, $c : \boldsymbol{R}^n \to \boldsymbol{R}^k$, $a = b \circ c : \boldsymbol{R}^n \to \boldsymbol{R}$ *is defined by* $a(\boldsymbol{x}) = b(c(\boldsymbol{x})) = b(c_1(\boldsymbol{x}), \ldots, c_k(\boldsymbol{x}))$ *for* $\boldsymbol{x} \in \boldsymbol{R}^n$.

1. *a is convex if b is convex and non-increasing in each argument, and c_i is concave in $\boldsymbol{x}$, $\forall i$.*

2. *a is concave if b is concave and non-increasing in each argument, and c_i is convex in $\boldsymbol{x}$, $\forall i$.*

A.1.1 Concavity / convexity of $P^d_{m,n}(S^n_m, \varepsilon^n_m, \rho^n_m)$ / $P^f_{m,n}(S^n_m, \varepsilon^n_m)$

Local false alarm and detection probabilities are given in (2.15-2.16), where ρ is a given parameter, thus, it is not considered to be an optimization variable taken into account in the convexity analysis.

Lemma A.1: *$P^d(S, \varepsilon, \rho)$ and $P^f(S, \varepsilon)$ are neither convex nor concave functions of (S, ε), and neither are $Q^d_m(\tilde{P}^d(S, \varepsilon, \rho))$ and $Q^f_m(\tilde{P}^f(S, \varepsilon))$. Hence, **P 3.1** is not a convex optimization problem.*

Proof. This is the scalar case of the composition rule given in Remark A.1 with $k = 1$, $n = 2$, b : erfc$(\cdot)$, and c : $f(S, \varepsilon)$. Although erfc$(\cdot)$ is a non-increasing convex and concave function for cases erfc$(\cdot) \leq 0.5$ and erfc$(\cdot) \geq 0.5$, respectively, to meet the composition requirements erfc$(f(S, \varepsilon))$ / erfc$(g(S, \varepsilon, \rho))$, $f(S, \varepsilon)$ / $g(S, \varepsilon, \rho)$ must be concave / convex in (S, ε). However, $f(S, \varepsilon)$ and $g(S, \varepsilon, \rho)$ are neither convex nor concave in $f(S, \varepsilon)$ since the Hessian matrix of $f(S, \varepsilon)$ in (A.1) and that of $g(S, \varepsilon, \rho)$ in (A.2) are neither positive nor negative semi-definite as follows

$$\nabla^2 f(S, \varepsilon) = S^{-3/2} \begin{bmatrix} \frac{3A\varepsilon}{4S} - \frac{B}{4} & -\frac{A}{2} \\ -\frac{A}{2} & 0 \end{bmatrix} \tag{A.1}$$

$$\nabla^2 g(S, \varepsilon, \rho) = \frac{S^{-3/2}}{1 - \rho^2} \begin{bmatrix} \frac{3A\varepsilon}{4S} - \frac{B-\rho}{4} & -\frac{A}{2} \\ -\frac{A}{2} & 0 \end{bmatrix} \tag{A.2}$$

Therefore, $P^f(S, \varepsilon)$ and $P^d(S, \varepsilon, \rho)$ are neither convex nor a concave function of (S, ε). Thus, this result directly affects the convexity / concavity of $Q^f_m(\tilde{P}^f(S, \varepsilon))$, $Q^d_m(\tilde{P}^d(S, \varepsilon, \rho))$, and **P 3.1**. □

Lemma A.2: *This Lemma provides the basis for convexity of parameterized approach used in bilevel optimization.*

1. *$f(S, \varepsilon)$ and $g(S, \varepsilon, \rho)$ are both linear functions of ε. Thus, $P^f(S, \varepsilon) \leq 0.5$ / $P^d(S, \varepsilon, \rho) \geq 0.5$ is a convex / concave function of ε.*

2. *For a parameterized ε, $f(S,\varepsilon)$ is a concave function of S if $S \geq {}^{3A\varepsilon}/_{B}$, and a convex function of S if $S \leq {}^{3A\varepsilon}/_{B-\rho}$. Thus, $P^f(S,\varepsilon) \leq 0.5$ / $P^d(S,\varepsilon,\rho) \geq 0.5$ is a convex / concave function of S for $\frac{3A\varepsilon}{B-\rho} \geq S \geq \frac{3A\varepsilon}{B}$.*

Proof. 1. Because of $\frac{\partial^2 f(S,\varepsilon)}{\partial \varepsilon^2} = \frac{\partial^2 g(S,\varepsilon,\rho)}{\partial \varepsilon^2} = 0$, f and g are both convex and concave functions of ε, i.e. linear. Since $\text{erfc}(\cdot) \leq 0.5$ is a non-increasing convex function of $f(S,\varepsilon)$ and $f(S,\varepsilon)$ is a concave function of ε, their composition $P^f(S,\varepsilon) \leq 0.5$ is also convex in ε. In a similar manner, since $\text{erfc}(\cdot) \geq 0.5$ is a non-increasing concave function of $g(S,\varepsilon,\rho)$ and $g(S,\varepsilon,\rho)$ is a convex function of ε, their composition $P^d(S,\varepsilon,\rho) \geq 0.5$ is also concave in ε.

2. By using the same composition rules in (a), for a parameterized $\bar{\varepsilon}$, $\frac{\partial^2 f(S,\bar{\varepsilon})}{\partial S^2} = \frac{S^{-3/2}}{4}\left(\frac{3A\bar{\varepsilon}}{S} - B\right) \leq 0$ is needed to assure the concavity of $f(S,\bar{\varepsilon})$ in S. Noting that the sensing duration cannot be negative (i.e. $S \geq 0$), this condition reduces to $S \geq \frac{3A\bar{\varepsilon}}{B}$. Likewise, $\frac{\partial^2 g(S,\bar{\varepsilon},\rho)}{\partial (S)^2} = \frac{S^{-3/2}}{4(1-\rho^2)}\left(\frac{3A\bar{\varepsilon}}{S} - (B-\rho)\right) \geq 0$ is required to assure the convexity of $g(S,\bar{\varepsilon},\rho)$. Due to $S \geq 0$, this condition reduces to $\frac{3A\bar{\varepsilon}}{B-\rho} \geq S$.

As a result, line 2 in **P 3.1-LLP** and lines 3-4 in **P 3.1-ULP** are convex constraints. □

Lemma A.3: *Convexity and concavity analysis in Lemma A.2 also hold for reported local probability of detection, $\tilde{P}^d(S,\varepsilon,\rho)$, and reported false alarm probability, $\tilde{P}^f(S,\varepsilon)$.*

Proof. In (3.10-3.11), $\tilde{P}^d(S,\varepsilon,\rho)$ and $\tilde{P}^f(S,\varepsilon)$ are expected values of $P^d(S,\varepsilon,\rho)$ and $P^f(S,\varepsilon)$ over the reporting channel error probabilities, respectively. Thus, Lemma A.3 is an immediate result of the fact that non-negative weighted summation preserves convexity and concavity. □

A.1.2 Log-concavity of $Q_m^d(\tilde{P}_{m,n}^d)$ and $Q_m^f(\tilde{P}_{m,n}^f)$

Sum of independent (but not necessarily identical) *Bernoulli* variables forms a log-concave random variable since log-concavity is closed under convolution [112]. Consequently, sum of local hard decision reports, $\mathcal{K}$ given in (3.12), is a summation of independent *Bernoulli* random variables and it is log-concave under both identical ($\mathcal{K} \sim \mathcal{B}(C,\tilde{P}^d)$) and nonidentical ($\mathcal{K} \sim \mathcal{PB}(C,\tilde{\boldsymbol{P}}^{\boldsymbol{d}})$) *Bernoulli* trial cases. Since log-concavity is preserved by integration [34],

cumulative distribution function (cdf), $\mathcal{P}(\mathcal{K} \leq \kappa)$, and survivability function (sf), $\mathcal{P}(\mathcal{K} \geq \kappa)$, of a log-concave random variable are also log-concave functions. However, this is true with respect to κ which is a parameter in our case. Therefore, it is necessary to analyze the log-concavity of these functions with respect to $\tilde{P}^d(S, \varepsilon, \rho)$ and $\tilde{P}^f(S, \varepsilon)$ to establish connection to concavity in (S, ε).

Lemma A.4: *Pmf of a Binomial random variable* $\mathcal{K} \sim \mathcal{B}(C, \tilde{P}^d)$ / $\mathcal{K} \sim \mathcal{B}(C, \tilde{P}^f)$ *is a log-concave function of* $\tilde{P}^d$ / $\tilde{P}^f$, *so are its cdf and sf.*

Proof. Without loss of generality, the proof for $\tilde{P}^d$ is shown and it can be repeated for $\tilde{P}^f$. The logarithm of *Binomial pmf* and its second derivative are given as

$$\log\left(P\left(\mathcal{K}=i\right)\right) = \log\left[\binom{C}{i}\right] + i\log(\tilde{P}^d) + (C-i)\log(1-\tilde{P}^d)$$

$$\frac{\partial^2 \log\left(P(\mathcal{K}=i)\right)}{\partial(\tilde{P}^d)^2} = -\frac{i}{(\tilde{P}^d)^2} - \frac{C-i}{(1-\tilde{P}^d)^2},\ 1 \leq i \leq C$$

where the second derivative is always non-positive since $C \geq i$, hence, $\log(P(\mathcal{K}=i))$ is a log-concave function of $\tilde{P}^d$.

Since log-concavity is preserved by integration as indicated above, cdf and sf of $\mathcal{K} \sim \mathcal{B}(C, \tilde{P}^d)$ are also log-concave functions of $\tilde{P}^d$. □

Lemma A.5: *Pmf of a Poisson-Binomial random variable* $\mathcal{K} \sim \mathcal{PB}(C, \tilde{\boldsymbol{P}}^{\boldsymbol{d}})$ / $\mathcal{K} \sim \mathcal{PB}(C, \tilde{\boldsymbol{P}}^{\boldsymbol{f}})$ *is a log-concave function of* $\tilde{\boldsymbol{P}}^{\boldsymbol{d}}$ / $\tilde{\boldsymbol{P}}^{\boldsymbol{f}}$, *so are its cdf and sf.*

Proof. The proof for $\tilde{P}^d$ is considered without loss of generality and the same steps can be repeated for $\tilde{P}^f$. Fernandez et. al. show that the distribution of *Poisson-Binomial* random variable is given by the following probability generating function [80]

$$A_0 + A_1 z + A_2 z^2 + \cdots + A_C z^C = \alpha(z - s_1)(z - s_2)\cdots(z - s_C)$$

where polynomial coefficients on the left hand side represent the *pmf* in terms of the real roots on the right hand side (i.e. $A_i = \mathcal{P}(\mathcal{K}=i),\ 1 \leq i \leq C$), $\alpha = \prod_{n=1}^{C} \tilde{P}_n^d$ and $s_n = -\frac{1-\tilde{P}_n^d}{\tilde{P}_n^d},\ 1 \leq n \leq C$.

The coefficients of a polynomial with real negative roots are log-concave functions of the roots [112], which is the case here since $s_n < 0,\ 1 \leq n \leq C$. Second, s_n is an increasing (non-decrasing) and strictly concave function of $\tilde{P}_n^d$ since

$$\frac{\partial^2 s_n}{\partial (\tilde{P}_n^d)^2} = -2(\tilde{P}_n^d)^{-3}$$

is always negative and s_n increases as $\tilde{P}_n^d$ increases. Contingent upon Lemma A.3 and Remark 1, s_n is a concave function of $\tilde{P}_n^d$. Third, α is obviously a linear function of $\tilde{P}_n^d$. Combining these three steps proves the log concavity of the *Poisson-Binomial pmf* with respect to $\tilde{P}_n^d$. Finally, log-concavity of *Poisson-Binomial cdf* and *sf* again follows from the integration property of log-concave functions. □

Lemma A.6: *[(a)]*

1. *Poisson-Binomial cdf / sf is an increasing / decreasing function of* $\tilde{P}_n^d$ *and* $\tilde{P}_n^f$.
2. *Binomial cdf / sf is an increasing / decreasing function of* $\tilde{P}_n^d$ *and* $\tilde{P}_n^f$.

Proof. [(a)]

In above polynomial, coefficient A_{C-k} is the sum of products of k roots such that

$$A_{C-k} = (-1)^k \sum_{1 \leq j_1, j_2, \ldots, j_k \leq C} s_{j_1} s_{j_2} \ldots s_{j_k}$$

where negative sign of roots are eliminated for both odd and even numbers of k, thus, coefficients are decreasing functions of $\tilde{P}_n^d$, so are *pmf*s. Based on this, *cdf* is a decreasing function of $\tilde{P}_n^d$, thus, tail *cdf* is an increasing function of $\tilde{P}_n^d$.

𝟚. This part is a special case of (a) such that $\tilde{P}_n^d = \tilde{P}^d$.

□

Consequently, based on Lemmas A.2 and A.3, constraints $-\boldsymbol{P_d}(\cdot) \preceq -0.5$ and $\boldsymbol{P_f}(\cdot) \preceq 0.5$ are convex. Furthermore, by use of Lemmas A.2-A.5 and Remark 1, $\log(Q_m^f(\tilde{P}_{m,n}^f(\cdot)))$ and $\log(Q_m^d(\tilde{P}_{m,n}^d(\cdot)))$ are concave functions, so does the constraint $-\log(Q_m^d(\tilde{\boldsymbol{P}}_{\boldsymbol{d}})) \leq -\log(\bar{Q}_m^d)$. Moreover, objective function of **P 3.1-LLP**, $|\log(\bar{Q}_m^f) - \log(Q_m^f(\tilde{\boldsymbol{P}}_{\boldsymbol{f}}))|$, is also a convex function since $-\log(Q_m^f(\tilde{\boldsymbol{P}}_{\boldsymbol{f}}))$ is convex.

APPENDIX B. CHAPTER 4 PROOFS

B.1 Convexity Analysis of CSSS

Throughout the appendices, we omit cluster and SU indices, m and n, for the sake of notational convenience without loss of generality. We simply consider the scalar case of the composition rule given in Remark A.1 with $K = 2$, $L = 1$, $b : \mathcal{Q}(g)$ / $b : \mathcal{Q}(h)$, and $c : g$ / $c : h$. $\mathcal{Q}(\cdot)$ is a non-increasing convex / concave function in the case of $\mathcal{Q}(\cdot) \leq 0.5$ / $\mathcal{Q}(\cdot) \geq 0.5$, respectively. This can be easily satisfied by constraining the detection threshold as

$$1 \leq \varepsilon \leq \gamma + 1, \ \forall m; \forall n \tag{B.1}$$

which follows from the fact that S is non-negative. To meet the composition requirements of $P^f = \mathcal{Q}(g)$ / $P^d = \mathcal{Q}(h)$ as in Remark A.1, g / h is still required to be jointly concave / convex in (S, ε). Unfortunately, this is not the case since the Hessian matrix of g in (B.2) and that of h in (B.3) are neither positive nor negative semi-definite as follows

$$\bigtriangledown^2 g(S,\varepsilon) = \begin{bmatrix} \frac{(1-\varepsilon)}{4S^{3/2}} & \frac{1}{2\sqrt{S}} \\ \frac{1}{2\sqrt{S}} & 0 \end{bmatrix} \tag{B.2}$$

$$\bigtriangledown^2 h(S,\varepsilon,\gamma) = \begin{bmatrix} \frac{(\gamma+1-\varepsilon)}{4S^{3/2}\sqrt{2\gamma+1}} & \frac{1}{2\sqrt{S(2\gamma+1)}} \\ \frac{1}{2\sqrt{S(2\gamma+1)}} & 0 \end{bmatrix} \tag{B.3}$$

Therefore, local probabilities $P^f(g)$ and $P^d(h)$ are neither convex nor a concave function of (S, ε). As a consequence, this result directly affects the convexity / concavity of $Q_m^f(\tilde{P}^f(\tau,\varepsilon))/Q_m^d(\tilde{P}^d(\tau,\varepsilon,\rho))$, and $\mathbf{CSSS}(\bar{\boldsymbol{y}},\bar{\boldsymbol{X}})$.

For a fixed (parameterized) feasible number of samples $\bar{S}$, however, g and h are both linear functions of ε due to the zero terms in (B.2) and (B.3). On the other hand, g / h is a concave

/ convex function of S for a parameterized feasible detection threshold $\bar{\varepsilon}$ since $\frac{(1-\varepsilon)}{4S^{3/2}} \leq 0$ / $\frac{(\gamma+1-\varepsilon)}{4S^{3/2}\sqrt{2\gamma+1}} \geq 0$ if (B.1) is satisfied. Therefore, $P^f(g)$ is a convex function of ε / S for a parameterized S / ε. Similarly, $P^d(h)$ is a concave function of ε / S for a parameterized S / ε. This parameterized convexity can be further applied to the received local probabilities $\tilde{P}^f$ / $\tilde{P}^d$ since (3.11) / (3.10) is nothing but the non-negative weighted sum of P^f / P^d.

B.2 Monotonicity and Convexity Analysis of η

We first note that the nominator of the objective function, E, is a linear function of number of samples since T_{sns} is the summation of S's while T_{sw} and T_r are both constant with respect to S. As a consequence, E increases as the S increases. Since the piece-wise maximization of convex functions is convex, T is a constant, and T_s is negated in $\frac{T-T_s}{T}$, R is a concave function.[1] For an increase in S, R either decreases, if the SU n is the slowest SU which determines the T_s, or stay unchanged. Therefore, η monotonically increases as S increases.

For the quasi-convexity of η, we simply consider a cooperation scheme comprising of SU_1 and SU_2 with real sensing durations $0 < a \leq T$ and $0 < b \leq T$, respectively, which can be easily generalized to other cases. For given $(\bar{\boldsymbol{y}},\bar{\boldsymbol{X}})$, the objective function can be simplified as

$$\eta(a,b) = \frac{a+b}{T - \max(a,b)} \tag{B.4}$$

where we omit the reporting and switching costs in the nominator and the sum rate in the denominator since they are constant with respect to a and b. To obtain the Hessian matrix elements of $\eta(a,b)$, we first define the derivatives of $\max(a,b)$ as follows

$$\frac{\partial}{\partial a}\max(a,b) = \begin{cases} 1, & a > b \\ 0, & \text{otherwise} \end{cases} \tag{B.5}$$

$$\frac{\partial}{\partial b}\max(a,b) = \begin{cases} 1, & a < b \\ 0, & \text{otherwise} \end{cases} \tag{B.6}$$

[1] We assume that the Q_m^f is constant since it is Q_{th}^f at the optimal point as explained in Corollary 4.1.

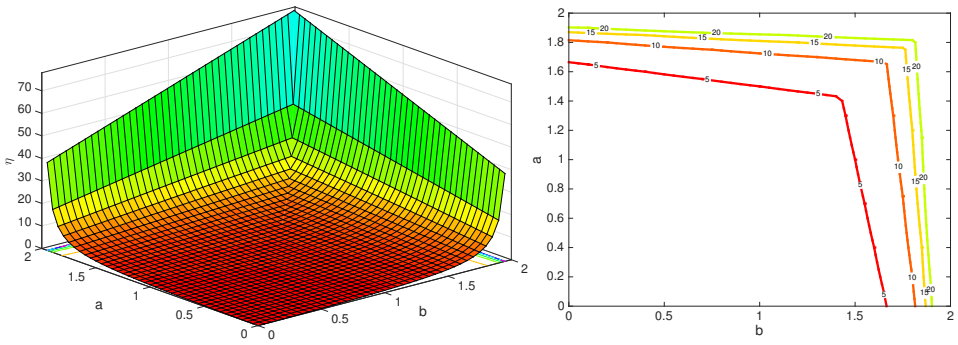

Figure B.1: η with respect to sensing durations a and b along with the contour plot under the three-dimensional shaded surface which shows the polyhedron shaped convex sub-level sets for $\alpha = 5, 10, 15, 20$.

The elements of the hessian matrix are then given as

$$\frac{\partial^2 \eta(a,b)}{\partial a^2} = \begin{cases} \frac{2}{(T-\max(a,b))^2}\left(\frac{a+b}{T-\max(a,b)}+1\right) & ,\text{if } a > b \\ 0 & ,\text{otherwise} \end{cases}$$

$$\frac{\partial^2 \eta(a,b)}{\partial b^2} = \begin{cases} \frac{2}{(T-\max(a,b))^2}\left(\frac{a+b}{T-\max(a,b)}+1\right) & ,\text{if } a < b \\ 0 & ,\text{otherwise} \end{cases}$$

$$\frac{\partial^2 \eta(a,b)}{\partial a \partial b} = \frac{2\,(a+b)\,\frac{\partial \max(a,b)}{\partial a}\frac{\partial \max(a,b)}{\partial b}}{(T-\max(a,b))^3} + \frac{\frac{\partial \max(a,b)}{\partial a}}{(T-\max(a,b))^2} + \frac{\frac{\partial \max(a,b)}{\partial b}}{(T-\max(a,b))^2} = \frac{1}{(T-\max(a,b))^2}$$

all of which is non-negative due to (B.5), (B.6), $0 < a \leq T$ and $0 < b \leq T$. Since $\frac{\partial^2 \eta(a,b)}{\partial a^2}\frac{\partial^2 \eta(a,b)}{\partial b^2}$ is always zero in either cases of $a > b$ and $a < b$, η has a non-definite hessian matrix with respect to a and b. However, it is a quasi-convex function since its sub-level sets $\mathcal{S}_\alpha \{a, b \in \mathbb{R}^+ | \eta(a,b) \leq \alpha\}$ for $\alpha \in \mathbb{R}$ is a convex set as can be seen in Figure B.1.

BIBLIOGRAPHY

[1] J. G. Andrews, S. Buzzi, W. Choi, S. V. Hanly, A. Lozano, A. C. Soong, and J. C. Zhang, "What will 5g be?," *IEEE Journal on Selected Areas in Communications*, vol. 32, no. 6, pp. 1065–1082, 2014.

[2] S. Pollin *et al.*, "Meera: Cross-layer methodology for energy efficient resource allocation in wireless networks," *IEEE Transactions on Wireless Communications*, vol. 7, no. 1, pp. 98–109, 2008.

[3] A. P. Bianzino, C. Chaudet, D. Rossi, and J.-L. Rougier, "A survey of green networking research," *IEEE Communications Surveys & Tutorials*, vol. 14, no. 1, pp. 3–20, 2012.

[4] F. C. Commission *et al.*, "Spectrum policy task force report, fcc 02-155," 2002.

[5] I. F. Akyildiz, W.-Y. Lee, M. C. Vuran, and S. Mohanty, "Next generation/dynamic spectrum access/cognitive radio wireless networks: a survey," *Computer Networks*, vol. 50, no. 13, pp. 2127–2159, 2006.

[6] Q. Zhao and B. M. Sadler, "A survey of dynamic spectrum access," *IEEE Signal Processing Magazine*, vol. 24, no. 3, pp. 79–89, 2007.

[7] J. Mitola III *et al.*, "Cognitive radio: making software radios more personal," *IEEE Personal Communications*, vol. 6, no. 4, pp. 13–18, 1999.

[8] J. Mitola, "Cognitive radio: An integrated agent architecture for software defined radio," *Doctor of Technology*, 2000.

[9] S. Haykin, "Cognitive radio: brain-empowered wireless communications," *IEEE Journal on Selected Areas in Communications*, vol. 23, no. 2, pp. 201–220, 2005.

[10] A. Ghasemi and E. S. Sousa, "Collaborative spectrum sensing for opportunistic access in fading environments," in *Proc. First IEEE International Symposium on New Frontiers in Dynamic Spectrum Access Networks*, pp. 131–136, IEEE, 2005.

[11] G. Ganesan and Y. Li, "Cooperative spectrum sensing in cognitive radio networks," in *Proc. First IEEE International Symposium on New Frontiers in Dynamic Spectrum Access Networks*, pp. 137–143, IEEE, 2005.

[12] I. F. Akyildiz, B. F. Lo, and R. Balakrishnan, "Cooperative spectrum sensing in cognitive radio networks: A survey," *Physical communication*, vol. 4, no. 1, pp. 40–62, 2011.

[13] S. Chaudhari, J. Lunden, V. Koivunen, and H. V. Poor, "Cooperative sensing with imperfect reporting channels: Hard decisions or soft decisions?," *IEEE Transactions on Signal Processing*, vol. 60, no. 1, pp. 18–28, 2012.

[14] C. Sun, W. Zhang, and K. Ben, "Cluster-based cooperative spectrum sensing in cognitive radio systems," in *Proc. IEEE International Conference on Communications*, pp. 2511–2515, IEEE, 2007.

[15] G. Gur and F. Alagoz, "Green wireless communications via cognitive dimension: an overview," *IEEE Network*, vol. 25, no. 2, pp. 50–56, 2011.

[16] M. Webb *et al.*, "Smart 2020: Enabling the low carbon economy in the information age," *The Climate Group, London*, vol. 1, no. 1, pp. 1–1, 2008.

[17] O. Ozel, K. Tutuncuoglu, S. Ulukus, and A. Yener, "Fundamental limits of energy harvesting communications," *IEEE Communications Magazine*, vol. 53, no. 4, pp. 126–132, 2015.

[18] X. Lu, P. Wang, D. Niyato, and E. Hossain, "Dynamic spectrum access in cognitive radio networks with rf energy harvesting," *IEEE Wireless Communications*, vol. 21, no. 3, pp. 102–110, 2014.

[19] R. Zhang and C. K. Ho, "Mimo broadcasting for simultaneous wireless information and power transfer," *IEEE Transactions on Wireless Communications*, vol. 12, no. 5, pp. 1989–2001, 2013.

[20] S. Luo, R. Zhang, and T. J. Lim, "Optimal save-then-transmit protocol for energy harvesting wireless transmitters," *IEEE Transactions on Wireless Communications*, vol. 12, no. 3, pp. 1196–1207, 2013.

[21] S. Bayhan and F. Alagoz, "Scheduling in centralized cognitive radio networks for energy efficiency," *IEEE Transactions on Vehicular Technology*, vol. 62, no. 2, pp. 582–595, 2013.

[22] D. Gozupek, S. Buhari, and F. Alagoz, "A spectrum switching delay-aware scheduling algorithm for centralized cognitive radio networks," *IEEE Transactions on Mobile Computing*, vol. 12, no. 7, pp. 1270–1280, 2013.

[23] A. Ghasemi and E. S. Sousa, "Spectrum sensing in cognitive radio networks: requirements, challenges and design trade-offs," *IEEE Communications Magazine*, vol. 46, no. 4, pp. 32–39, 2008.

[24] T. Yucek and H. Arslan, "A survey of spectrum sensing algorithms for cognitive radio applications," *IEEE Communications Surveys & Tutorials*, vol. 11, no. 1, pp. 116–130, 2009.

[25] A. Sonnenschein and P. M. Fishman, "Radiometric detection of spread-spectrum signals in noise of uncertain power," *IEEE Transactions on Aerospace and Electronic Systems*, vol. 28, no. 3, pp. 654–660, 1992.

[26] R. Tandra and A. Sahai, "Snr walls for signal detection," *IEEE Journal of Selected Topics in Signal Processing*, vol. 2, no. 1, pp. 4–17, 2008.

[27] A. Goldsmith, *Wireless communications*. Cambridge university press, 2005.

[28] J. Ma, G. Y. Li, and B. H. Juang, "Signal processing in cognitive radio," *Proceedings of The IEEE*, vol. 97, no. 5, pp. 805–823, 2009.

[29] B. Wang and K. R. Liu, "Advances in cognitive radio networks: A survey," *IEEE Journal of Selected Topics in Signal Processing*, vol. 5, no. 1, pp. 5–23, 2011.

[30] E. Axell, G. Leus, E. G. Larsson, and H. V. Poor, "Spectrum sensing for cognitive radio: State-of-the-art and recent advances," *IEEE Signal Processing Magazine*, vol. 29, no. 3, pp. 101–116, 2012.

[31] H. Urkowitz, "Energy detection of unknown deterministic signals," *Proceedings of The IEEE*, vol. 55, no. 4, pp. 523–531, 1967.

[32] F. F. Digham, M.-S. Alouini, and M. K. Simon, "On the energy detection of unknown signals over fading channels," in *Proc. IEEE International Conference on Communications*, vol. 5, pp. 3575–3579, IEEE, 2003.

[33] F. F. Digham, M.-S. Alouini, and M. K. Simon, "On the energy detection of unknown signals over fading channels," *IEEE transactions on communications*, vol. 55, no. 1, pp. 21–24, 2007.

[34] S. Boyd and L. Vandenberghe, *Convex optimization*. Cambridge university press, 2004.

[35] Y. C. Liang, Y. Zeng, E. C. Peh, and A. T. Hoang, "Sensing-throughput tradeoff for cognitive radio networks," *IEEE Transactions on Wireless Communications*, vol. 7, no. 4, pp. 1326–1337, 2008.

[36] S. Chaudhari, V. Koivunen, and H. V. Poor, "Autocorrelation-based decentralized sequential detection of ofdm signals in cognitive radios," *IEEE Transactions on Signal Processing*, vol. 57, no. 7, pp. 2690–2700, 2009.

[37] E. Axell and E. G. Larsson, "Optimal and sub-optimal spectrum sensing of ofdm signals in known and unknown noise variance," *IEEE Journal on Selected Areas in Communications*, vol. 29, no. 2, pp. 290–304, 2011.

[38] J. G. Proakis, "Digital communications, 2001."

[39] A. Sahai, R. Tandra, S. M. Mishra, and N. Hoven, "Fundamental design tradeoffs in cognitive radio systems," in *Proc. of The 1st International Workshop on Technology and Policy for Accessing Spectrum*, p. 2, ACM, 2006.

[40] D. Cabric, S. M. Mishra, and R. W. Brodersen, "Implementation issues in spectrum sensing for cognitive radios," in *Proc. of The 38th Asilomar Conference on Signals, Systems and Computers*, vol. 1, pp. 772–776, IEEE, 2004.

[41] N. Han, S. Shon, J. H. Chung, and J. M. Kim, "Spectral correlation based signal detection method for spectrum sensing in ieee 802.22 wran systems," in *Proc. of The 8th International Conference Advanced Communication Technology*, vol. 3, pp. 6–pp, IEEE, 2006.

[42] M. Ghozzi, F. Marx, M. Dohler, and J. Palicot, "Cyclostatilonarilty-based test for detection of vacant frequency bands," in *Proc. of 1st International Conference on Cognitive Radio Oriented Wireless Networks and Communications*, pp. 1–5, IEEE, 2006.

[43] N. Khambekar, L. Dong, and V. Chaudhary, "Utilizing ofdm guard interval for spectrum sensing," in *Proc. of Wireless Communications and Networking Conference*, pp. 38–42, IEEE, 2007.

[44] K. Kim, I. Akbar, K. Bae, J.-S. Um, C. Spooner, and J. Reed, "Cyclostationary approaches to signal detection and classification in cognitive radio," in *Proc. of 2nd IEEE International Symposium on New Frontiers in Dynamic Spectrum Access Networks*, pp. 212–215, IEEE, 2007.

[45] J. Lunden, V. Koivunen, A. Huttunen, and H. V. Poor, "Spectrum sensing in cognitive radios based on multiple cyclic frequencies," in *Proc. of 2nd International Conference on Cognitive Radio Oriented Wireless Networks and Communications*, pp. 37–43, IEEE, 2007.

[46] D. Cabric and R. W. Brodersen, "Physical layer design issues unique to cognitive radio systems," in *Proc. of IEEE 16th International Symposium on Personal, Indoor and Mobile Radio Communications*, vol. 2, pp. 759–763, IEEE, 2005.

[47] W. A. Gardner, "Exploitation of spectral redundancy in cyclostationary signals," *IEEE Signal Processing Magazine*, vol. 8, no. 2, pp. 14–36, 1991.

[48] A. V. Dandawate and G. B. Giannakis, "Statistical tests for presence of cyclostationarity," *IEEE Transactions on Signal Processing*, vol. 42, no. 9, pp. 2355–2369, 1994.

[49] Y. Zeng and Y.-C. Liang, "Eigenvalue-based spectrum sensing algorithms for cognitive radio," *IEEE Transactions on Communications*, vol. 57, no. 6, pp. 1784–1793, 2009.

[50] Y. Zeng and Y.-C. Liang, "Spectrum-sensing algorithms for cognitive radio based on statistical covariances," *IEEE Transactions on Vehicular Technology*, vol. 58, no. 4, pp. 1804–1815, 2009.

[51] Y. Zeng and Y.-C. Liang, "Maximum-minimum eigenvalue detection for cognitive radio," in *Proc. of IEEE PIMRC*, vol. 7, pp. 1–5, 2007.

[52] F. Penna, R. Garello, and M. A. Spirito, "Cooperative spectrum sensing based on the limiting eigenvalue ratio distribution in wishart matrices," *IEEE Communications Letters*, vol. 13, no. 7, pp. 507–509, 2009.

[53] Z. Quan, S. Cui, A. H. Sayed, and H. V. Poor, "Optimal multiband joint detection for spectrum sensing in cognitive radio networks," *IEEE Transactions on Signal Processing*, vol. 57, no. 3, pp. 1128–1140, 2009.

[54] R. Fan, H. Jiang, Q. Guo, and Z. Zhang, "Joint optimal cooperative sensing and resource allocation in multichannel cognitive radio networks," *IEEE Transactions on Vehicular Technology*, vol. 60, no. 2, pp. 722–729, 2011.

[55] Z. Tian and G. B. Giannakis, "Compressed sensing for wideband cognitive radios," in *Proc. of IEEE International Conference on Acoustics, Speech and Signal Processing*, vol. 4, pp. IV–1357, IEEE, 2007.

[56] Z. Tian, "Compressed wideband sensing in cooperative cognitive radio networks," in *Proc. of IEEE Global Telecommunications Conference*, pp. 1–5, IEEE, 2008.

[57] Y. Wang, A. Pandharipande, Y. L. Polo, and G. Leus, "Distributed compressive wideband spectrum sensing," in *Proc. of Information Theory and Applications Workshop*, pp. 178–183, IEEE, 2009.

[58] Z. Fanzi, C. Li, and Z. Tian, "Distributed compressive spectrum sensing in cooperative multihop cognitive networks," *IEEE Journal of Selected Topics in Signal Processing*, vol. 5, no. 1, pp. 37–48, 2011.

[59] S. M. Mishra, A. Sahai, and R. W. Brodersen, "Cooperative sensing among cognitive radios," in *Proc. IEEE International Conference on Communications*, vol. 4, pp. 1658–1663, IEEE, 2006.

[60] A. Ghasemi and E. S. Sousa, "Opportunistic spectrum access in fading channels through collaborative sensing," *Journal of communications*, vol. 2, no. 2, pp. 71–82, 2007.

[61] J. Unnikrishnan and V. V. Veeravalli, "Cooperative sensing for primary detection in cognitive radio," *IEEE Journal of Selected Topics in Signal Processing*, vol. 2, no. 1, pp. 18–27, 2008.

[62] Z. Li, F. R. Yu, and M. Huang, "A distributed consensus-based cooperative spectrum-sensing scheme in cognitive radios," *IEEE Transactions on Vehicular Technology*, vol. 59, no. 1, pp. 383–393, 2010.

[63] W. Zhang and K. B. Letaief, "Cooperative spectrum sensing with transmit and relay diversity in cognitive radio networks-[transaction letters]," *IEEE Transactions on Wireless Communications*, vol. 7, no. 12, pp. 4761–4766, 2008.

[64] Z. Chair and P. K. Varshney, "Optimal data fusion in multiple sensor detection systems," *IEEE Transactions on Aerospace and Electronic Systems*, no. 1, pp. 98–101, 1986.

[65] J. Ma, G. Zhao, and Y. Li, "Soft combination and detection for cooperative spectrum sensing in cognitive radio networks," *IEEE Transactions on Wireless Communications*, vol. 7, no. 11, pp. 4502–4507, 2008.

[66] N. Nguyen-Thanh and I. Koo, "Log-likelihood ratio optimal quantizer for cooperative spectrum sensing in cognitive radio," *IEEE Communications Letters*, vol. 15, no. 3, pp. 317–319, 2011.

[67] S. Huang, H. Chen, Y. Zhang, and F. Zhao, "Energy-efficient cooperative spectrum sensing with amplify-and-forward relaying," *IEEE Communications Letters*, vol. 16, no. 4, pp. 450–453, 2012.

[68] R. Deng, J. Chen, C. Yuen, P. Cheng, and Y. Sun, "Energy-efficient cooperative spectrum sensing by optimal scheduling in sensor-aided cognitive radio networks," *IEEE Transactions on Vehicular Technology*, vol. 61, no. 2, pp. 716–725, 2012.

[69] S. Wang, Y. Wang, J. P. Coon, and A. Doufexi, "Energy-efficient spectrum sensing and access for cognitive radio networks," *IEEE Transactions on Vehicular Technology*, vol. 61, no. 2, pp. 906–912, 2012.

[70] D. Huang, G. Kang, B. Wang, and H. Tian, "Energy-efficient spectrum sensing strategy in cognitive radio networks," *IEEE Communications Letters*, vol. 17, no. 5, pp. 928–931, 2013.

[71] A. E. et. al., "Sensor selection and optimal energy detection threshold for efficient cooperative spectrum sensing," *IEEE Transactions on Vehicular Technology*, vol. 64, no. 4, pp. 1565–1577, 2015.

[72] C. Mousavifar, S.A. ; Leung, "Energy efficient collaborative spectrum sensing based on trust management in cognitive radio networks," *IEEE Transactions on Wireless Communications*, vol. 14, no. 4, pp. 1927–1939, 2015.

[73] C.-h. Lee and W. Wolf, "Energy efficient techniques for cooperative spectrum sensing in cognitive radios," in *Proc. IEEE 5th Consumer Communications and Networking Conference*, pp. 968–972, IEEE, 2008.

[74] C. Guo, T. Peng, S. Xu, H. Wang, and W. Wang, "Cooperative spectrum sensing with cluster-based architecture in cognitive radio networks," in *Proc. IEEE 69th Vehicular Technology Conference*, pp. 1–5, IEEE, 2009.

[75] W. Xia, S. Wang, W. Liu, and W. Chen, "Cluster-based energy efficient cooperative spectrum sensing in cognitive radios," in *Proc. 5th International Conference on Wireless Communications, Networking and Mobile Computing*, pp. 1–4, IEEE, 2009.

[76] N. Nguyen-Thanh and I. Koo, "A cluster-based selective cooperative spectrum sensing scheme in cognitive radio," *EURASIP Journal on Wireless Communications and Networking*, vol. 2013, no. 1, pp. 1–9, 2013.

[77] A. S. Kozal, M. Merabti, and F. Bouhafs, "Spectrum sensing-energy tradeoff in multi-hop cluster based cooperative cognitive radio networks," in *Proc. IEEE Conference on Computer Communications Workshops*, pp. 765–770, IEEE, 2014.

[78] A. Celik and A. E. Kamal, "Multi-objective clustering optimization for multi-channel cooperative sensing in crns," in *Proc. IEEE Global Communications Conference*, pp. 3441–3446, IEEE, 2014.

[79] Y. H. Wang, "On the number of successes in independent trials," *Statistica Sinica*, vol. 3, no. 2, pp. 295–312, 1993.

[80] M. Fernandez and S. Williams, "Closed-form expression for the poisson-binomial probability density function," *IEEE Transactions on Aerospace and Electronic Systems*, vol. 46, no. 2, pp. 803–817, 2010.

[81] C. Jiang, H. Zhang, Y. Ren, and H.-H. Chen, "Energy-efficient non-cooperative cognitive radio networks: micro, meso, and macro views," *IEEE Communications Magazine*, vol. 52, no. 7, pp. 14–20, 2014.

[82] G. Casella and R. L. Berger, *Statistical inference*, vol. 2. Duxbury Pacific Grove, CA, 2002.

[83] V. Pareto, "Manual of political economy," 1971.

[84] R. T. Marler and J. S. Arora, "Survey of multi-objective optimization methods for engineering," *Structural and multidisciplinary optimization*, vol. 26, no. 6, pp. 369–395, 2004.

[85] K. Deb, A. Pratap, S. Agarwal, and T. Meyarivan, "A fast and elitist multiobjective genetic algorithm: Nsga-ii," *IEEE Transactions on Evolutionary Computation*, vol. 6, no. 2, pp. 182–197, 2002.

[86] S. Chaudhari and V. Koivunen, "Effect of quantization and channel errors on collaborative spectrum sensing," in *Proc. 43th Asilomar Conference on Signals, Systems and Computers*, pp. 528–533, IEEE, 2009.

[87] T. Zhang and D. H. Tsang, "Optimal cooperative sensing scheduling for energy-efficient cognitive radio networks," in *Proc. INFOCOM*, pp. 2723–2731, IEEE, 2011.

[88] X. Sun and D. H. Tsang, "Energy-efficient cooperative sensing scheduling for multiband cognitive radio networks," *IEEE Transactions on Wireless Communications*, vol. 12, no. 10, pp. 4943–4955, 2013.

[89] S. Eryigit, S. Bayhan, and T. Tugcu, "Energy-efficient multichannel cooperative sensing scheduling with heterogeneous channel conditions for cognitive radio networks," *IEEE Transactions on Vehicular Technology*, vol. 62, no. 6, pp. 2690–2699, 2013.

[90] T. Zhang and D. H. Tsang, "Cooperative sensing scheduling for energy-efficient cognitive radio networks," *IEEE Transactions on Vehicular Technology*, vol. 64, no. 6, pp. 2648 – 2662, 2015.

[91] A. Celik and A. E. Kamal, "Multi-objective clustering optimization for multi-channel cooperative spectrum sensing in heterogeneous green crns," *IEEE Transactions on Cognitive Communications and Networking (under revision)*, 2016.

[92] S. Eryigit, S. Bayhan, and T. Tugcu, "Channel switching cost aware and energy-efficient cooperative sensing scheduling for cognitive radio networks," in *Communications (ICC), 2013 IEEE International Conference on*, pp. 2633–2638, IEEE, 2013.

[93] A. Celik and A. E. Kamal, "More spectrum for less energy: Green cooperative sensing scheduling in crns," in *IEEE International Conference on Communications*, pp. 62–67, IEEE, 2015.

[94] D. P. Palomar and M. Chiang, "A tutorial on decomposition methods for network utility maximization," *IEEE Journal on Selected Areas in Communications*, vol. 24, no. 8, pp. 1439–1451, 2006.

[95] V. Raghunathan *et al.*, "Emerging techniques for long lived wireless sensor networks," *IEEE Communications Magazine*, vol. 44, no. 4, pp. 108–114, Apr. 2006.

[96] A. Kansal, J. Hsu, S. Zahedi, and M. B. Srivastava, "Power management in energy harvesting sensor networks," *ACM Transactions on Embedded Computing Systems*, vol. 6, no. 4, p. 32, 2007.

[97] D. Gunduz, K. Stamatiou, N. Michelusi, and M. Zorzi, "Designing intelligent energy harvesting communication systems," *IEEE Communications Magazine*, vol. 52, no. 1, pp. 210–216, 2014.

[98] S. Yin, Z. Qu, and S. Li, "Achievable throughput optimization in energy harvesting cognitive radio systems," *IEEE Journal on Selected Areas in Communications*, vol. 33, no. 3, pp. 407–422, 2015.

[99] S. Lee, R. Zhang, and K. Huang, "Opportunistic wireless energy harvesting in cognitive radio networks," *IEEE Transactions on Wireless Communications*, vol. 12, no. 9, pp. 4788–4799, 2013.

[100] A. Sultan, "Sensing and transmit energy optimization for an energy harvesting cognitive radio," *IEEE Wireless Communications Letters*, vol. 1, no. 5, pp. 500–503, 2012.

[101] E. C. Y. Peh, Y.-C. Liang, Y. L. Guan, and Y. Zeng, "Optimization of cooperative sensing in cognitive radio networks: a sensing-throughput tradeoff view," *IEEE Transactions on Vehicular Technology*, vol. 58, no. 9, pp. 5294–5299, 2009.

[102] S. Park *et al.*, "Cognitive radio networks with energy harvesting," *IEEE Transactions on Wireless Communications*, vol. 12, no. 3, pp. 1386–1397, 2013.

[103] S. Park and D. Hong, "Optimal spectrum access for energy harvesting cognitive radio networks," *IEEE Transactions on Wireless Communications*, vol. 12, no. 12, pp. 6166–6179, 2013.

[104] S. Park and D. Hong, "Achievable throughput of energy harvesting cognitive radio networks," *IEEE Transactions on Wireless Communications*, vol. 13, no. 2, pp. 1010–1022, 2014.

[105] J. Jeya Pradha, S. S. Kalamkar, and A. Banerjee, "Energy harvesting cognitive radio with channel-aware sensing strategy," *IEEE Communications Letters*, vol. 18, no. 7, pp. 1171–1174, 2014.

[106] M. Usman and I. Koo, "Access strategy for hybrid underlay-overlay cognitive radios with energy harvesting," *IEEE Sensors Journal*, vol. 14, no. 9, pp. 3164–3173, 2014.

[107] W. Chung, S. Park, S. Lim, and D. Hong, "Spectrum sensing optimization for energy-harvesting cognitive radio systems," *IEEE Transactions on Wireless Communications*, vol. 13, no. 5, pp. 2601–2613, 2014.

[108] S. Yin, E. Zhang, Z. Qu, L. Yin, and S. Li, "Optimal cooperation strategy in cognitive radio systems with energy harvesting," *IEEE Transactions on Wireless Communications*, vol. 13, no. 9, pp. 4693–4707, 2014.

[109] D. T. Hoang, D. Niyato, P. Wang, and D. I. Kim, "Performance optimization for cooperative multiuser cognitive radio networks with rf energy harvesting capability," *IEEE Transactions on Wireless Communications*, vol. 14, no. 7, pp. 3614–3629, 2015.

[110] J. Yang, X. Wu, and J. Wu, "Optimal scheduling of collaborative sensing in energy harvesting sensor networks," *IEEE Journal on Selected Areas in Communications*, vol. 33, no. 3, pp. 512–523, 2015.

[111] Q. Zhao *et al.*, "On myopic sensing for multi-channel opportunistic access: structure, optimality, and performance," *IEEE Transactions on Wireless Communications*, vol. 7, no. 12, pp. 5431–5440, 2008.

[112] O. Johnson and C. Goldschmidt, "Preservation of log-concavity on summation," *ESAIM: Probability and Statistics*, vol. 10, pp. 206–215, 2006.